



## A review for the peripheral nerve interface designer

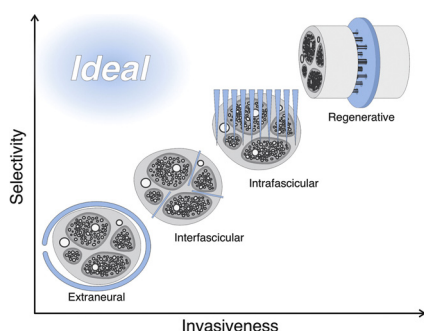
Christopher E. Larson<sup>a</sup>, Ellis Meng<sup>a,b,\*</sup>

<sup>a</sup> Department of Biomedical Engineering, University of Southern California, Los Angeles, CA, 90089, USA

<sup>b</sup> Ming Hsieh Department of Electrical and Computer Engineering, University of Southern California, Los Angeles, CA, 90089, USA



### GRAPHICAL ABSTRACT



### ARTICLE INFO

#### Keywords:

Peripheral nerve interface  
Neural prosthesis  
Bioelectronic medicine  
Vagus nerve stimulation  
Functional electrical stimulation  
Brain machine interface

### ABSTRACT

Informational density and relative accessibility of the peripheral nervous system make it an attractive site for therapeutic intervention. Electrode-based electrophysiological interfaces with peripheral nerves have been under development since the 1960s and, for several applications, have seen widespread clinical implementation. However, many applications require a combination of neural target resolution and stability which has thus far eluded existing peripheral nerve interfaces (PNIs). With the goal of aiding PNI designers in development of devices that meet the demands of next-generation applications, this review seeks to collect and present practical considerations and best practices which emerge from the literature, including both lessons learned during early PNI development and recent ideas. Fundamental and practical principles guiding PNI design are reviewed, followed by an updated and critical account of existing PNI designs and strategies. Finally, a brief survey of *in vitro* and *in vivo* PNI characterization methods is presented.

**Abbreviations:** AP, action potential; BMI, brain machine interface; CAP, compound action potential; CE, counter electrode; CNS, central nervous system; CSC<sub>c</sub>, cathodal charge storage capacity; CV, cyclic voltammetry; ECH, electrically-conductive hydrogel; EIS, electrochemical impedance spectroscopy; EMG, electromyography; ENG, electroneurography; ESA, electrochemical surface area; FES, functional electrical stimulation; FFC, flat flexible cable; FINE, flat interface nerve electrode; GSA, geometric surface area; hd-USEA, high-density Utah slanted electrode array; LIFE, longitudinal intrafascicular electrode; MPM, multiphoton microscopy; OCT, optical coherence tomography; PBS, phosphate-buffered saline; PCB, printed circuit board; PEEK, polyether ether ketone; PNI, peripheral nerve interface; PNS, peripheral nervous system; PTFE, polytetrafluoroethylene; RE, reference electrode; REMI, regenerative multielectrode interface; RSE, regenerative scaffold electrode; SCE, saturated calomel electrode; SHG, second harmonic generation; SI, selectivity index; SNR, signal-to-noise ratio; TEENI, tissue-engineered electronic nerve interface; TIME, transverse intrafascicular multichannel electrode; UEA, Utah electrode array; USEA, Utah slanted electrode array; VNS, vagus nerve stimulation; WE, working electrode; ZIF, zero-insertion-force connector

\* Corresponding author.

E-mail addresses: [larsone@usc.edu](mailto:larsone@usc.edu) (C.E. Larson), [ellis.meng@usc.edu](mailto:ellis.meng@usc.edu) (E. Meng).

<https://doi.org/10.1016/j.jneumeth.2019.108523>

Received 7 June 2019; Received in revised form 14 November 2019; Accepted 15 November 2019

Available online 16 November 2019

0165-0270/ © 2019 Elsevier B.V. All rights reserved.

## 1. Introduction

The peripheral nervous system (PNS) carries control (efferent) and informational (afferent) signals between the central nervous system and other parts of the body. In cases of neurological or other dysfunction due to injury or disease, the informational density and relative accessibility of the peripheral nervous system presents an attractive target for therapeutic intervention. To this end, a wide variety of implantable peripheral nerve interfaces (PNIs) have been developed to enable monitoring and modulation of peripheral nerve signals.

Clinical implementation of implanted PNIs was first achieved in the 1960s. The first applications included diaphragmatic pacing (Judson, 1968) and treatment of urinary incontinence (Alexander and Rowan, 1968). Though these early devices were merely looped wires, they were sufficient to produce the desired muscle contractions. The 1970s and 80s saw refinement of devices and methods for these same applications (Brindley, 1977; Brindley et al., 1986, 1982; Glenn and Phelps, 1985; Schmidt et al., 1978) and further exploration of functional electrical stimulation (FES) via PNIs, including chronic pain management (Avery and Wepsic, 1973; Picaza et al., 1977) and lower limb activation for walking and standing assistance in cases of paralysis (Brindley et al., 1979; McNeal and Bowman, 1985; Waters et al., 1975). Similar methods were later applied to upper body control in spinal cord injury patients (Popovic et al., 2002). FES applications of PNIs continue to be an important area of development. For example, a recently approved commercial FES system stimulates the hypoglossal nerve overnight, maintaining a slight contraction of the tongue muscle to treat obstructive sleep apnea (Eastwood et al., 2011; FDA Approves Inspire Upper Airway Stimulation Therapy for Obstructive Sleep Apnea, 2014; Schwartz et al., 2001)

Concurrent with advances in robotics and computing, a new focus of PNI application beginning in the late 1990s, though anticipated much earlier (Hoffer and Loeb, 1980; Stein et al., 1975), was that of hybrid bionic systems, or brain-machine interfaces (BMI) (Micera et al., 2006; Navarro et al., 2005; Wright et al., 2016). BMIs aim to directly link the nervous system with a computer or robotic prosthesis, ideally utilizing two-way communication of sensory and control signals and thereby enabling possibilities such as neurally-controlled prosthetic limbs for amputees (Ciancio et al., 2017; Lebedev and Nicolelis, 2006; Lu et al., 2012; Micera et al., 2010; Pasluosta et al., 2018; Schultz and Kuiken, 2011). While many BMIs directly interface with the cerebral cortex, the PNS may be an attractive alternative in cases where the target nerve is intact due to lower surgical risk and greater isolation of the desired neural targets.

There are also a range of non-motor applications of PNIs. The vagus nerve, which carries autonomic signals between visceral organs and the brain stem, was targeted for therapeutic stimulation as early as the late 1800s (Guiraud et al., 2016). Vagus nerve stimulation (VNS) was first shown to offer reduction of epileptic seizures in 1985 (Zabara, 1985), and since 1988, VNS systems have been implanted in more than 168,000 patients around the world (VNS Therapy, 2019). Because of the vagus nerve's innervation of visceral organs, it is a potential site of intervention for many disorders that would otherwise be treated with limited success by medications, including depression (Rush et al., 2000), hypertension (Plachta et al., 2014), obesity (Banni et al., 2012; Cork et al., 2018; Guiraud et al., 2016), heart failure (Guiraud et al., 2016), and autoimmune or inflammatory diseases such as rheumatoid arthritis (Koopman et al., 2016; Payne et al., 2019; Zitnik, 2011). The use of peripheral nerve recording and stimulation, especially of the vagus nerve and its branches, for such applications is often called bioelectronic medicine, or "electroceuticals" (Birmingham et al., 2014; Giagka and Serdijn, 2018). While bioelectronic medicine has largely focused on use of pre-programmed or "open-loop" stimulation schedules, recent approaches not only modulate organ function *via* stimulation, but also monitor organ status *via* recording of vagus nerve signals with the aim of eventually closing the feedback loop to

autonomously maintain healthy organ function (Ganzer and Sharma, 2019; Plachta et al., 2014; Sun and Morrell, 2014; Zanos, 2019).

Despite five decades of development and multiple instances of clinical translation, each of the PNI application areas described above remain highly active areas of research. Successful clinical applications have largely been limited to those that rely only on non-specific stimulation. Chronically stable, high-resolution PNIs for ambitious applications such as neurally-integrated prosthetic limbs and closed-loop organ modulation have not yet been realized. From the late 1990s to present, the variety of PNI designs being investigated at the research level has expanded dramatically thanks to new technologies from fields such as biomedical microelectromechanical systems (bioMEMS) and microelectronics. Development continues to expand as PNI designers strive for devices that can record and stimulate with increased resolution and maintain performance in the body for decades.

Previous reviews have covered, in varying detail, particular PNI applications, fundamental concepts of PNI function, and anecdotal examples from the most prominent types of PNI designs (del Valle and Navarro, 2013; Giagka and Serdijn, 2018; Grill et al., 2009; Heiduschka and Thanos, 1998; Kim and Romero-Ortega, 2012; Micera and Navarro, 2009; Mortimer and Bhadra, 2004; Navarro et al., 2005; Ortiz-Catalan et al., 2012; Russell et al., 2019; Rutten, 2002; Saal and Bensmaia, 2015; Schultz and Kuiken, 2011; Tyler, 2018). This review presents an updated, comprehensive survey that closely examines critical design choices, strategies, and best practices that can inform next generation PNI designs. This review purposefully encompasses a broad range of work to counteract symptoms of recency-bias. Much of the foundational knowledge and practical wisdom regarding PNI design and use was ascertained in the 1960s to 1990s. Lastly, there is a need to collect, in one place, the methods and best practices to guide *in vitro* and *in vivo* characterization of a PNI towards the goal of clinical impact. In sum, the present review aims to aid the PNI designer in development of next-generation devices by reviewing principles guiding PNI design, examining different PNI design strategies that have been explored, and surveying methods of PNI characterization.

## 2. Guiding principles for peripheral nerve interface design

### 2.1. Peripheral nerve anatomy

PN fibers are extensions of neurons which have their cell body in or near the central nervous system (CNS). Their ability to function as neural conductors is dependent on the support of complex, composite tissue structures which provide nutrition and protection (Lundborg, 2004). Coarsely described, the anatomical structure of a PN trunk is "a bundle of bundles" (Fig. 1). Myelinated and unmyelinated nerve fibers of varying diameter and function (e.g. motor and sensory) are tightly packed together in fascicles. A specialized sheath-like structure called the perineurium forms the outer boundary of each fascicle. The perineurium is the primary source of mechanical strength for the nerve trunk and is comprised of up to 15 dense layers of cells and collagen (Lundborg, 2004). Analogous to the crucial blood-brain barrier of the CNS, the perineurium additionally serves as a blood-nerve barrier to maintain the privileged microenvironment of the enclosed endoneurial space. In addition to nerve fibers, the endoneurium consists of Schwann cells, immune cells, capillaries, and a matrix of collagen and other connective tissue fibers (Grill et al., 2009; Lundborg, 2004). Finally, holding multiple fascicles together to form the outer bundle of a compound nerve trunk is the epineurium. The epineurium is a relatively loose matrix of collagen, fat, elastin fibers and blood vessels, which, besides holding the bundle together, also serves to cushion the fascicles from compressive forces (Sunderland, 1965). Blood vessels, being crucial to nerve fiber health and function, form a dense intraneural network along the entire length of the nerve trunk, as shown in Fig. 2b (Rydevik et al., 1990; Sunderland, 1978). "Extrinsic" vessels running alongside the nerve are connected to intraneural vessels *via* frequent

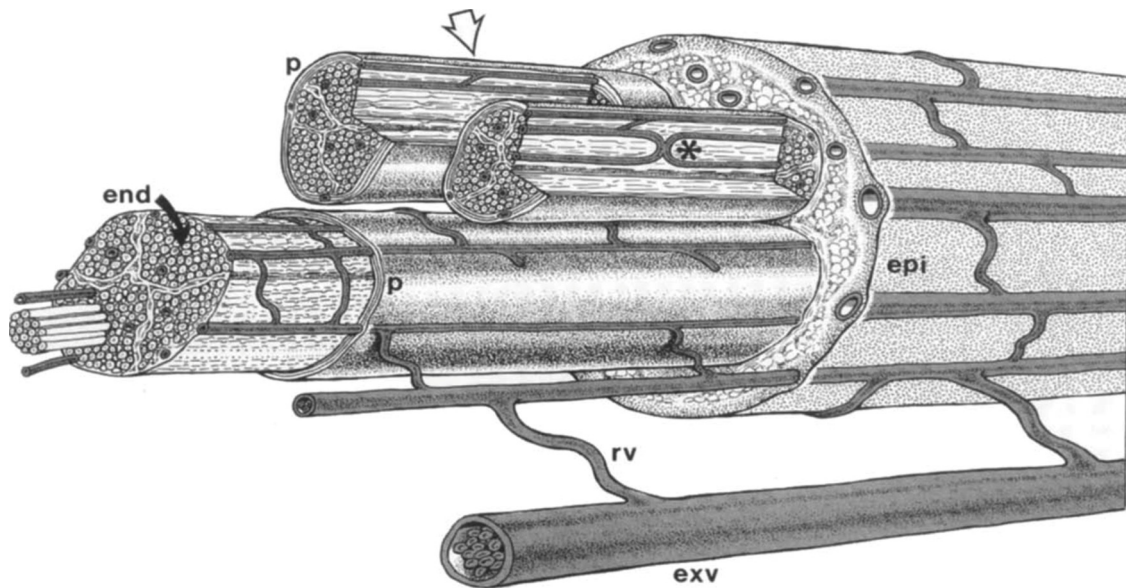


**Fig. 1.** Illustration of nerve trunk anatomy, highlighting the epineurium (epi), fascicles (arrow), perineurium (p), and endoneurium (end). Also shown is the network of extrinsic (exv) and regional (rv) blood vessels and internal vascular structures (\*). Reprinted from (Lundborg, 2004) with permission from Elsevier.

“regional” vessels which obliquely penetrate into the nerve trunk’s connective tissue layers (Fig. 1, Lundborg, 2004). The smallest endoneurial capillaries are 6–10  $\mu\text{m}$  in diameter and possess looping and coiling forms which help accommodate motion (Lundborg, 2004).

Nerves vary widely in terms of size, fascicle count, and fiber count across species, nerve types, and proximal to distal positions within the same nerve. The number of fascicles in a nerve trunk ranges from 1 to 100, and the number of individual fibers ranges from hundreds to tens of thousands (Sunderland, 1990). To give a sense of the numbers in a common model for PNI study, the rat sciatic nerve has four fascicles comprised of approximately 8,000 myelinated fibers and 19,000 unmyelinated fibers in total. The number of myelinated and unmyelinated fibers in each fascicle ranges from 300 to 5,000 and 2,000 to 9,000, respectively (Schmalbruch, 1986). The cross-section of a PN trunk is

generally presumed to be circular or ovoid, though the gradual separation and eventual branching of fascicles at more distal locations produces a more flattened or irregular shape, as evident in Fig. 3 (Schmalbruch, 1986).

A remarkable feature of PN anatomy, especially in the extremities, is its accommodation of relative motion among nerve components and surrounding tissues. Peripheral nerves in high-motion areas such as limbs, and especially joints, are served by a loose, fatty, lubricating layer of paraneural connective tissue to facilitate gliding in the nerve groove (Millesi et al., 1995). Within the nerve, the epineurium is only loosely connected to perineurium so that individual fascicles can slide past one another and rearrange under transverse compression (Lundborg, 2004; Millesi et al., 1995; Sunderland, 1990). Undulated patterns are found throughout the microanatomy of the nerve in its

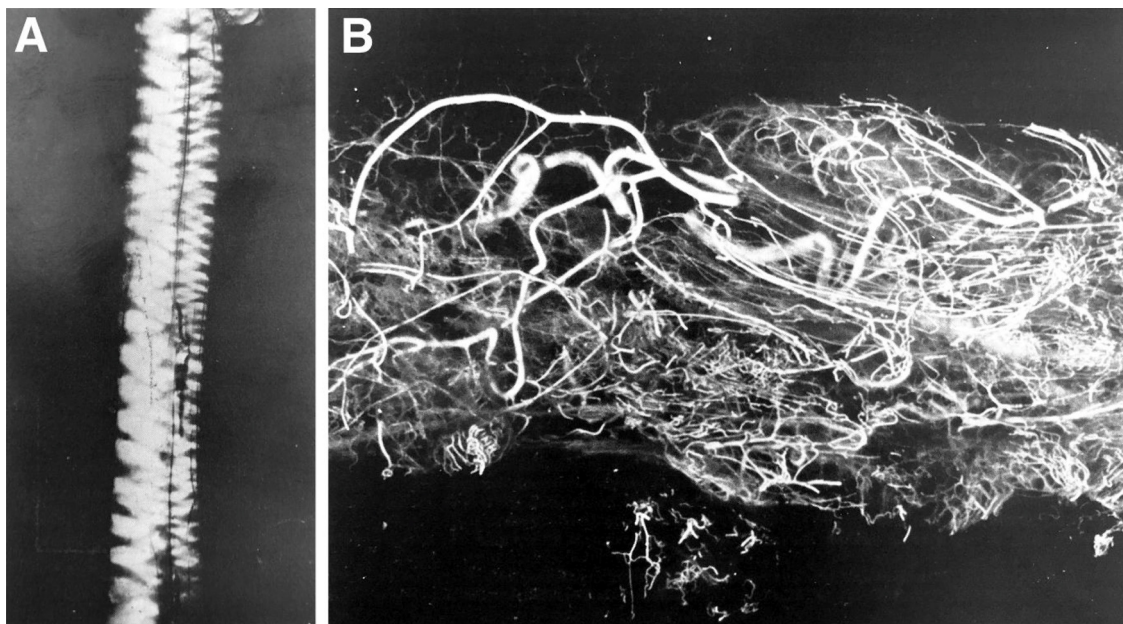


**Fig. 2.** A) A photograph of an unstretched nerve shows bands of Fontana caused by the undulating pattern of the tissue structure. These bands reversibly disappear when the nerve is stretched. B) An injected and cleared sample of a peripheral nerve trunk shows the dense microvascular network. Reprinted from (Sunderland, 1978) with permission from Elsevier.

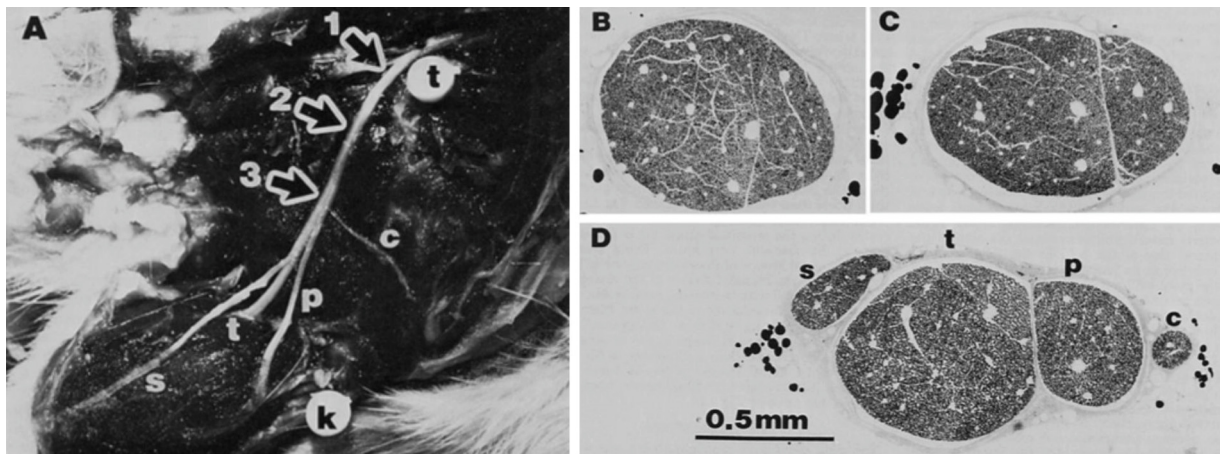


**Fig. 3.** A) Surgically exposed rat sciatic nerve, with the trochanter (t) and knee (k) marked by pins. B), C), and D) show cross-sections of the nerve at positions 1, 2, and 3, respectively. The cross-section becomes flatter as the sural (s), tibial (t), peroneal (p), and cutaneous (c) fascicles separate and eventually branch off. Reprinted from (Schmalbruch, 1986) with permission from Wiley.

unstretched state, such as the wavy shape of nerve fibers within a fascicle and the arrangement of collagen fibers in the epi- and endoneurium (Millesi et al., 1995; Stolinski, 1995; Sunderland, 1978). The nerve trunk and fascicles default to a wavy form when unstretched (Sunderland, 1978). Visible striations, known as bands of Fontana (Fig. 2a), reversibly disappear when the nerve is stretched, attesting to their role in allowing dynamic elongation and shortening (Sunderland, 1978). During length changes, volume of a PN trunk is conserved; the diameter decreases when elongated and increases when shortened (Millesi et al., 1995).

In summary, the structural and dynamic features of PN anatomy have profound implications for PNI design.

## 2.2. Electrodes

From an extracellular perspective, the inward rush of sodium ions during the rising phase of an action potential is a strong current sink, accompanied by adjacent current sources: ahead, a weak source arising from the initial discharging of the membrane; behind, a strong source arising from the efflux of potassium ions. Given the current sources and sinks occurring at any instant during an action potential, there are necessarily currents passing between them in the extracellular space. It is these extracellular currents that may be measured by the electrodes of a PNI (Loeb and Gans, 1986; Stein and Oğuztöreli, 1978).

While charge in neural signalling is carried by ions, in metallic conductors it is carried by electrons. Thus, at the metal-saline interface of an implanted PNI electrode, there is necessarily some translation between the two. The flow of charge across this interface can occur by two types of mechanisms: capacitive and faradaic. Water molecules orient themselves on the electrode surface, forming what is known as the *double layer* and collectively act as a dielectric between ionic charges in the saline and electronic charges in the metal. Up to about  $20 \mu\text{C}/\text{cm}^2$ , the transfer of charge occurs only by Columbic attraction and repulsion across this layer, with no charge-carrying species crossing the interface (*capacitive*, Robblee and Rose, 1990). Above this limit, the double layer breaks down and both reversible and irreversible *faradaic* reactions can occur. In *reversible* faradaic processes, also called *pseudocapacitive*, charge carriers cross the boundary and new chemical species are created in oxidation and reduction (redox) reactions, however they do not leave the electrode surface and are readily reversed by a flow of charge in the opposite direction. *Irreversible* faradaic processes produce new chemical species that are not bound to the electrode surface. They lead to corrosion or dissolution of the electrode, release of toxic products into the surrounding fluid and tissue, potentially harmful shifts in pH, and gas formation from electrolysis of water. The regime in

which an electrode operates depends on a variety of factors such as electrode size, location, and stimulation protocol. Methods for characterizing PNI electrodes and finding the limits between charge injection regimes are discussed in Section 4.1.1.

Several surface modification strategies exist to increase the amount of charge that an electrode can capacitively and pseudocapacitively deliver. The charge injection required by PNIs is usually beyond the capacitive limit of common noble metal electrodes (namely, platinum and platinum-iridium alloys) so these electrodes predominantly operate in the pseudocapacitive regime (Robblee and Rose, 1990). However, an electrode's capacitive limit can be increased to a usable range by coating it with a thin dielectric layer which imparts a higher dielectric strength and prevents transfer of charge carriers; these are known as capacitive electrodes (Howell and Grill, 2015). Assuming the electrode-dielectric-electrolyte system exhibits parallel plate capacitor behavior, the electrode's capacitance is  $C = \epsilon_0 \epsilon_r A_e / d$  where  $\epsilon_0$  is the permittivity of free space,  $\epsilon_r$  is the relative permittivity of the dielectric,  $A_e$  is the electrode's electrochemical surface area, and  $d$  is the thickness of the dielectric. An effective dielectric coating for an electrode provides increased  $\epsilon_r$  while minimizing  $d$  (Howell and Grill, 2015). Electrode capacitance can be further enhanced by increasing the electrochemical or "real" surface area (ESA). Surface roughness increases ESA without increase of the geometric surface area (GSA). Titanium nitride is often selected for its electrical conductivity, amenability to thin film deposition, and surface roughness when deposited by sputtering (Cogan, 2008).

In some cases, such as with small electrodes (tens of  $\mu\text{m}$ ), not even pseudocapacitive mechanisms may provide enough charge transfer with unmodified Pt or Pt-Ir electrodes (Cogan, 2008; Robblee and Rose, 1990). One method to increase the reversible charge transfer limit is application of *faradaic electric coatings*, also called *valence change oxides* (Howell and Grill, 2015; Robblee and Rose, 1990). Iridium oxide films are the most common example; these possess two oxidative states and readily accept or donate electrons during pulsing of the electrode. Another method is to roughen the surface by etching, abrading, or coating for increased ESA (Cogan, 2008; Geddes and Roeder, 2003; Lee et al., 2016a; Ordonez et al., 2014; Robblee and Rose, 1990; Weremfo et al., 2015). The advantages of surface roughening may reach a limit when significant roughness or porosity increases the so-called *pore resistance*. As the conductive path through solution reaches deeper into the roughened electrode surface, a time constant may be added to the electrode's response, and the deep surfaces of the electrode may not be utilized (Cogan, 2008; Robblee and Rose, 1990). Rough electrode surfaces may also be less mechanically robust and more prone to bio-fouling by protein adhesion (Cogan, 2008; Straka et al., 2018; Wellman

et al., 2018).

Low electrode impedance yields improved stimulation efficiency and noise reduction. Depending on the design, placement, and application of a PNI, geometric dimensions of the electrodes on the order of hundreds of  $\mu\text{m}$  or even single mm may be appropriate and can achieve low impedance (tens of  $\text{k}\Omega$  at 1 kHz) without any further modification to a platinum surface. For smaller dimensions, faradaic coatings and increased ESA also decrease electrode impedance (Howell and Grill, 2015).

### 2.2.1. Stimulation

PN stimulation initiates an action potential by depolarization of the axonal membrane to the threshold potential. This is accomplished by injecting negative charge (*i.e.* a cathodic pulse) into the tissue, which, as it approaches the membrane, locally cancels the net positive charge outside the cell and repels negative charges on the inside of the cell. Though without any physical transfer of ions in or out of the cell, the spatial shifting of charges produces a local outward current and discharging of the membrane, thereby activating the sodium channels of that region and initiating the action potential (Mortimer and Bhadra, 2018). The goals of PN stimulation are to accomplish this activation safely and efficiently while ideally affecting only the targeted nerve fibers.

As for safety, general recommendations are to avoid irreversible faradaic reactions and combinations of high charge density and charge per phase. A long-established technique for the former is to use charge-balanced biphasic pulses. The second phase of opposite polarity reverses any surface-bound faradaic products that result from the initial pulse, thereby avoiding charge accumulation on the electrode or in the tissue after repeated cycles and keeping the electrode potential within a safe range (Cogan, 2008; Donaldson and Donaldson, 1986). A general guide for safe charge density, though it does not account for all relevant factors (Cogan et al., 2016), is the Shannon limit, given by  $\log(D) = k - \log(Q)$  where  $Q$  is the charge per phase or time integral of the current,  $D = Q/A$  is the charge density or charge per phase divided by the geometric area of the electrode, and  $k$  is a constant usually set at 1.85, or 1.5 for a more conservative guideline (Shannon, 1992). Any combination of parameters above this limit is expected to induce tissue damage. While these guidelines may serve as a starting point, tissue damage resulting from stimulation is a complex topic and the reader is referred to a number of other reviews and studies (Agnew et al., 1999, 1990; Agnew and McCreery, 1990; Cogan et al., 2018; Günter et al., 2019; McCreery et al., 1995, 1990; Pasluosta et al., 2018).

Stimulation efficiency is concerned with the amount of electrical energy needed to achieve the desired neural activation, or, equivalently, the time integral of electrical power, which is the product of current and voltage. Therefore, efficiency is increased by minimizing the current, voltage, or duration of stimulation waveforms. Low electrode impedance contributes to efficiency by decreasing the voltage required to deliver a given current. Another tactic is to shape the extracellular potential such that greater activation is achieved for the same amount of current. Activation is proportional to the second spatial difference in the longitudinal direction of the potential on the surface of an axon (Howell and Grill, 2015; Rattay, 1986). Positioning two return electrodes longitudinally on either side of a central cathode, known as a tripolar configuration, can achieve a greater second spatial difference for the same amount of current as compared with a single (monopolar) electrode with distant return (Howell and Grill, 2015). PNIs may also take advantage of insulative materials and other electrode arrangements to shape the electric field and “steer” the current for more efficiency and localization to the targeted nerve fibers (Tarler and Mortimer, 2004, 2003).

How best to limit activation to only the targeted nerve fibers is one of the prevailing considerations of PNI development. The most straightforward approach is to position small electrodes as close as possible to the nerve fibers, taking advantage of activation that

decreases sharply with distance. However, this tactic involves other crucial compromises in PNI performance. Other strategies that have been explored include current steering and differential activation based on fiber size. These and other examples of design strategies for improved stimulation performance will be discussed in Section 3.

Stimulation with varied parameters can also be used for the purpose of blocking, rather than activating neural activity, as discussed by Bhadra and Kilgore (2018). Several reviews provide further discussion regarding strategic parameters and waveforms for enhanced stimulation (Cogan et al., 2016; Grill, 2018; Mortimer, 1990; Mortimer and Bhadra, 2004; Pasluosta et al., 2018).

### 2.2.2. Recording

A crucial consideration for peripheral nerve recording is the relative amplitudes of extracellular neural signals and noise sources. Electric fields produced by nerve fibers are about three orders of magnitude smaller than the electromyographic (EMG) fields produced by nearby muscles (*i.e.* microvolts versus millivolts). Hoffer and Kallesøe (2001) draw an analogy by equating the signal amplitudes to audio decibels, in which case recording a PN signal in the body is like listening to a quiet voice while a loud horn is sounding one meter away.

The simplest recording arrangement is a monopolar electrode placed near the nerve and a distant electrode used as reference. However, this arrangement is highly susceptible to EMG noise sources. Differential or bipolar recording is effective in cancelling some of this noise by subtracting the signals of two electrodes placed near the nerve and outputting their difference. Bipolar electrodes should be oriented along the length of the nerve, ideally spaced to match the distance between source and sink of a propagating action potential which will maximize the amplitude of the measured differential signal. This distance can be approximated by multiplying the nerve fiber's conduction velocity and the time between maximum inward and outward currents, or about half the period of an action potential. As a rule of thumb, myelinated fiber conduction velocity, in m/s, is approximately six times the fiber diameter in  $\mu\text{m}$ ; for unmyelinated fibers it is a factor of two (Kandel, 2013). A “medium” diameter myelinated nerve fiber of 10  $\mu\text{m}$ , for example, has a conduction velocity of  $\sim 60$  m/s. Combined with the nominal 1 ms duration of an action potential, we can estimate an ideal (though not necessarily practical) electrode spacing of 30 mm. The most effective electrode arrangement for rejecting noise is the tripolar configuration in which a central electrode is measured differentially with respect to electrodes on either side. The tripolar electrode configuration and its variations, along with other strategies for enhanced PN recording, are discussed in Section 3.1.1.1.

A general principle for optimal recording of neural signals is to position the electrode(s) as close as possible to the signal source, which for PNIs is the axonal membrane exposed at nodes of Ranvier. As distance between the signal source and electrode increases, more current is shunted away through the tissue and the signal is attenuated. Another factor affecting recording quality is tissue impedance. Differential recording of a nerve, perhaps counterintuitively, can gain increased signal amplitude from increased tissue impedance between the electrodes, assuming the source-to-electrode distance remains the same. To flow from current source to sink, extracellular currents must flow parallel to nerve fiber and the bipolar electrode alignment. Thus, increased impedance of this path yields an increased voltage difference between the electrodes.

### 2.3. Invasiveness versus selectivity

As described above, for optimal stimulation and recording performance it is desirable to position electrodes close to the targeted nerve fibers. However, the layered, bundled, densely-vascularized anatomical structure of PN conflicts with this goal. Directly inserting electrodes into nerve fibers may allow high stimulation and recording selectivity, but breaching the blood-nerve barrier and inducing other injuries to

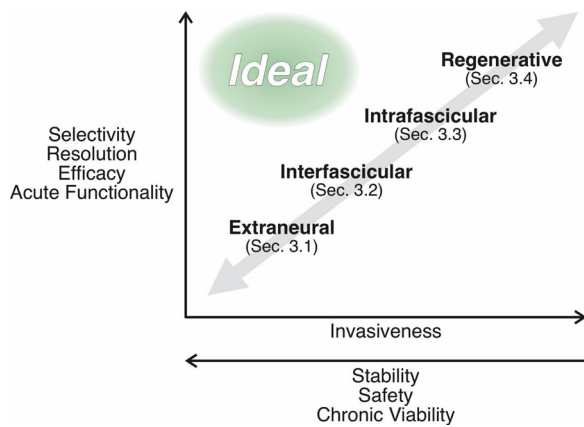


**Fig. 4.** Plot illustrating the strategic tradeoff between invasiveness to the nerve and selectivity. Existing PNI types generally lie on the diagonal, while a variety of strategies attempt to enhance performance toward the “ideal” region of the plot. Categories omitted from the plot are optical PNIs (Sec. 3.5) and hybrid approaches (Sec. 3.6).

nerve tissues may increase likelihood of interface failure in the long-term. On the other hand, positioning electrodes outside of the nerve is more likely to maintain long-term interface stability but suffers from poor selectivity and signal discrimination. Such trade-offs can be described in multiple ways: invasiveness *versus* selectivity; stability *versus* resolution; safety *versus* efficacy; chronic viability *versus* acute functionality (Fig. 4). Section 3 will highlight approaches that balance or circumvent trade-offs towards the combined goal of selectivity and long-term performance.

#### 2.4. Host response

Implantation of any object triggers an immune reaction which is intended to facilitate healing by destroying, removing, or containing the intruding object, clearing debris from the area, and increasing local fluid for migration of repair cells (Coleman et al., 1974). This “foreign body response” generally involves, at a minimum, immediate blood clotting around the implantation site, acute inflammation, and ensuing encapsulation of the implant in fibrotic tissue (Stroncek and Reichert, 2008). If the implant continues to have some injurious effect other than its presence, such as chemical or mechanical irritation, the response may intensify and include worse effects such as extreme inflammation, edema, hemorrhage, or necrosis (Naples et al., 1990). Therefore, a PNI implementation should minimize or tailor host response to maximize its operational lifetime.

Naples et al. (1990) provide a useful framework to summarize the multiple aspects of biocompatibility that the PNI designer should consider in order to minimize the host response: chemical, mechanical, and geometric. It is important to note that in and among these properties, which are mostly intrinsic to the device, there are also a number of extrinsic considerations such as implant site and stimulation characteristics.

Chemical biocompatibility is chiefly a material issue. The interface between tissue and the implant surface is the target of chemical reactions that will progress until an equilibrium is reached. In the process, the implant may degrade and release noxious products into the body. Therefore, inert or near-inert materials are preferred (Naples et al., 1990). Furthermore, the materials should remain inert and intact when subjected to prolonged electrical stimulation (White and Gross, 1974).

Mechanically, an implant should ideally possess similar properties to the nerve and also accommodate relative motion, either by moving with the tissue or avoiding friction at the interface (Naples et al., 1990). Accordingly, the chosen implantation site may play a large role in the apparent mechanical biocompatibility of a device; the same device

implanted at different locations (e.g. extremity *versus* core) may incite vastly different host responses due to different degrees of nerve movement (Naples et al., 1990).

Geometry also plays an important role in biocompatibility. While macroscale geometry of PNIs will be discussed in Section 3, a general recommendation provided here is to avoid sharp edges and bulky masses. Surface geometry may be adjusted to achieve a desired effect depending on the application. A smooth surface minimizes tissue adhesion and facilitates device mobility. A porous or perforated surface will encourage tissue ingrowth, which may be desirable for anchoring to the nerve and in some cases for increasing recorded signal amplitude, but will make future removal of the device difficult (Hoffer and Kallesøe, 2001; Marks and Loeb, 1976; Naples et al., 1990; Stein and Öğuztöreli, 1978).

In addition to the generalized host response discussed here, other potential agents of neural damage must be considered in all aspects of PNI design, including surgical implantation and connection methods (Sections 2.6 and 2.7). Furthermore, different types of PNI designs come with their own considerations of implicit nerve damage, as discussed in Section 3.

#### 2.5. Material selection

Based on the multiple facets of biocompatibility discussed above, there exists no list of universally-accepted materials for use in PNIs. Rather, material selection must account for interplay of multiple aspects of the design and application. Materials commonly used in PNIs include silicone, polyimide, and Parylene C as insulation and platinum and iridium as conductors. Among these, only silicone, platinum, and platinum-iridium have been clinically implemented in PNIs on a large scale. Parylene is known for its biological inertness and use in many approved medical devices and has seen success in neural interfaces used in research (Hara et al., 2016; Lecomte et al., 2017; Scholten and Meng, 2015; Sohal et al., 2016). Polyimide has seen similar success in research applications but with limited historical use in approved medical devices (Hassler et al., 2011; Stieglitz et al., 2011, 2005). However, these polymer materials suffer from moisture permeation, delamination, and fabrication difficulties and limitations (Hassler et al., 2011; Ortigoza-Diaz et al., 2018; Rubehn and Stieglitz, 2010; Srinivasan et al., 2016). When inserted into the endoneurium, Parylene and polyimide can provoke growth of a significant encapsulation layer (de la Oliva et al., 2018a,c; del Valle et al., 2015; Wurth et al., 2017). Silicone elastomer may eventually degrade in the body (Garrido et al., 1993). According to the physician’s manual for a commercially distributed PNI, the integrity of silicone is not guaranteed after about 25 years (Finetech-Brindley Sacral Anterior Root Stimulator (CPC2): Notes for Surgeons and Physicians, 2016). Even platinum, with its reputation for robustness and excellent characteristics, cannot completely avoid dissolution under chronic stimulation (Robblee and Rose, 1990; Wellman et al., 2018).

New materials being explored for PNIs include hydrogels, liquid crystal polymer, SU-8, conductive polymers, carbon fiber, graphene, carbon nanotubes, and even collagen (Fattahi et al., 2014; Green and Abidian, 2015; Kim and Romero-Ortega, 2012; Tian et al., 2018; Wellman et al., 2018; Woloszko et al., 1998). If clinical translation of devices using exploratory materials is desired, the associated regulatory obstacles should be evaluated. Materials selected may impact a device’s safety profile which is determined following a rigorous battery of biocompatibility tests, such as those outlined by the widely accepted standard ISO 10993-1, “Biological evaluation of medical devices” (Standards and Guidances for Neurological Devices, 2018). As Wellman et al. (2018) pointed out, beyond *in vitro* and animal demonstrations of safety, any “new” material will also need substantial historical data to warrant the financial risk of a clinical trial (which typically exceeds \$100 million). Overall strategy should not be limited to optimization of one or several material variables such as softness or conductivity, but

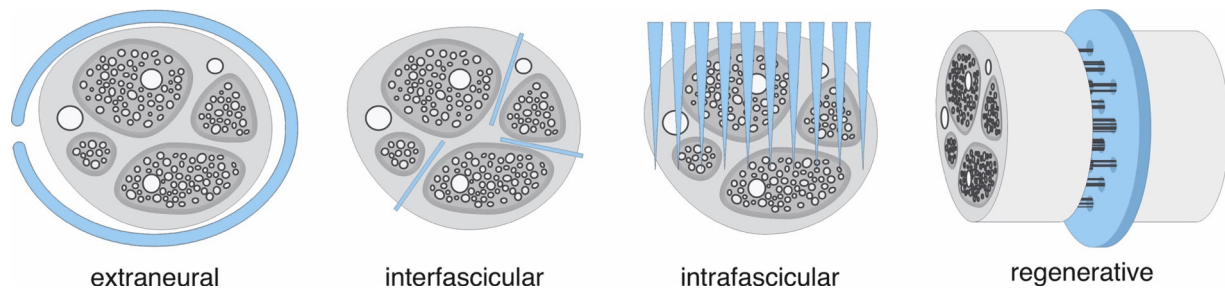


**Fig. 5.** Illustrations of common forms (blue) representing the main PNI categories. The PNI forms contain both the electrode, insulation, and any additional supporting structure.

entail a careful balance of numerous interdependent trade-offs across all material-related design factors.

### 2.6. Surgical implantation

PNI design should incorporate the entire scope of a device's use, including handling and surgical implantation (Mortimer et al., 1995). Devices should be robust and the handling instructions straightforward. Some designs may benefit from auxiliary features, such as tabs, loops, or handles that solely serve as a grasping point during device preparation and installation (Payne et al., 2019; VNS Therapy System Epilepsy Physician's Manual (US), 2018). Such features can be designed for easy *in situ* removal after installation.

The implantation process itself should be made as efficient and failproof as possible. Something as simple as an “up” label on an otherwise transparent polymer device can help avoid the easy but terminal mistake of installing it inside-out (Cobo et al., 2019). Chances of accidental damage to the nerve during the installation process should be minimized, such as pinching trauma resulting from premature closure of a nerve cuff. Several groups have devised special tools to facilitate installation of the PNI, such as a syringe-like electrode injector (Yim et al., 2018), or purpose-made forceps for opening, positioning, and closing a helical or spiral electrode (Bakula and Mortimer, 2000; Bullara, 1990; Rise and Klepinski, 1992). It is a prudent choice to make these tools in forms that are already familiar to surgeons. Others have incorporated installation mechanisms into the device itself, such as an eyelet for leading the device around or through the nerve with a suture (Boretius et al., 2010; Cobo et al., 2019; Yoshida et al., 2000).

### 2.7. Packaging

Another crucial aspect of any PNI is the series of supporting components which facilitate connection to the interface from outside the body, frequently referred to as packaging. In practice, packaging has many more potential points of failure than the interface itself (Mortimer et al., 1995). Most PNI packaging is concerned with electrical connections, but newer devices may also include fluidic connections for drug delivery.

Usually, the minimum arrangement of components consists of the interface connected to either a telemetry and control module for clinical and long-term use, or a percutaneous connector for shorter-term studies. The main principles of successful packaging for PNIs are to avoid any transfer of tension from the leads to the interface, protect the leads from breakage, and ensure sealing of any components that should remain isolated from tissues and fluids (Naples et al., 1990).

The standard practice of accessing each of a PNI's electrodes *via* its own lead wire with a percutaneous connection is not scalable to high channel counts (dozens or more); increased channel counts are inevitable as advanced PNIs seek more degrees of freedom. To reduce the number of electronic connections, a number of groups have integrated amplifying and multiplexing electronics into the device or the cable (Ballini et al., 2017; Lancashire et al., 2018, 2019; Lertmanorat et al.,

2009; Ramachandran et al., 2006; Schuettler et al., 2000; Wodlinger et al., 2015) and others have replaced the cable entirely with wireless approaches (Larson and Towe, 2011; Lee et al., 2018a,b; Park et al., 2015a,b; SetPoint Medical, 2019; Sharma et al., 2011).

A recently proposed packaging solution involves routing the remaining nerve ending of an amputated limb into the interior of the bone, which offers a protected space for housing the interface and other components, and also a convenient site for direct connection to a robotic prosthesis (Israel et al., 2018).

Section 4.2.1.2 will cover packaging in more detail with specific considerations for implementation in animal studies. Though some of the same principles apply to clinical use of PNIs in humans, packaging of implantable devices for human use is a highly specialized topic in the medical device industry and will not be specifically covered.

## 3. Types of peripheral nerve interfaces

This section surveys the different PNI approaches that have been explored. The categorized approaches (Fig. 5) are presented along with design considerations and best practices that have emerged. Particular attention is given to strategies for optimizing efficacy and safety, and, where available, *in vivo* longevity of the interface is reported.

### 3.1. Extraneural

Extraneural PNIs are situated outside the nerve; this placement can preserve nerve health at the cost of greater distance to individual fibers. However, extraneural PNIs may injure the nerve by constriction which prevents crucial nutritional and metabolic transport through neural blood vessels and the axons (Ju et al., 2006; Krarup et al., 1989). Ju et al. (2006) observed a decrease in blood perfusion beginning at 30.5 mmHg of nerve constriction. Constriction may inadvertently arise when a circumneural electrode is fitted too closely around a nerve trunk. The ensuing acute inflammation that follows implantation temporarily increases the nerve diameter and after the swelling subsides, a layer of fibrotic encapsulation invariably forms between the nerve and the interface, effectively increasing its diameter (Hoffer and Kallesøe, 2001). Nerve diameter will also change with motion since volume is conserved during changes in length, though the literature does not specify if this change is significant enough to be affected by PNIs.

The anatomical groove in which a nerve trunk resides may induce lateral compression as it attempts to accommodate the extra bulk of an extraneural PNI. Mechanical pressure from adjacent tissues can be transmitted through the compliant material of an extraneural PNI to the nerve. Rydevik et al. (1981) observed blood flow in a nerve to be affected starting at 20 mmHg of lateral compression and complete occlusion at 60 mmHg.

Relative motion between the PNI and the nerve can also be a source of damage. Cabling connected to the PNI can apply tension, creating irregular pressure points on the nerve *via* lateral pulling or torquing (Hoffer and Kallesøe, 2001; Restaino et al., 2014). Before fibrotic encapsulation anchors a PNI to the nerve, there may be motion between

them, causing abrasion and an aggravated response (Naples et al., 1990). If fibrotic tissue on the outside of the PNI anchors it in place relative to the surrounding tissues, the nerve may also become anchored and experience damaging levels of tension (Hoffer and Kallesøe, 2001; Sunderland, 1990).

The following explores extraneural PNI strategies, highlighting best practices for mitigating nerve damage and enhancing recording and stimulation.

### 3.1.1. Cuff

Extraneural cuffs are the most widely used and studied of PNIs. Their general form is an insulative tube wrapped around the nerve containing exposed metal sites on its inner wall. In 1948, Sarnoff et al. described a method of looping wires around the phrenic nerve and wrapping the assembly with a piece of polyethylene sheeting. Sarnoff explains: "In this way the phrenic nerve could not escape contact with the electrode but was not compressed by it and the latter could not deliver an impulse to any other structure" (Sarnoff et al., 1948). A more standardized cuff design emerged consisting of wires sewn into the wall of a section of silicone tubing with a longitudinal slit across its length (Loeb and Peck, 1996; Stein et al., 1977). New fabrication technologies enabled greater dimensional precision, design flexibility, and a wider choice of material properties. Hoffer and Kallesøe (2001) provide a thorough and practical review on the design and use of nerve cuffs using traditional fabrication techniques.

**3.1.1.1. Strategies for enhanced recording with extraneural cuffs.** The goals of neural recording are rejection of noise from extraneural sources (namely, EMG) and discrimination of signals from different nerve fibers.

**3.1.1.1.1. Noise rejection.** An effective and widely used method to reject large extraneural noise sources in cuffs is the tripolar electrode configuration: a central electrode is connected to one input of a differential amplifier and two equidistant surrounding electrodes are shorted together and connected to the other input (Stein et al., 1975). The external EMG source can only access the cuff electrodes by entering one end and leaving the other; the resultant voltage gradient is linearly dependent on distance. The two shorted electrodes effectively measure the average potential between them, and therefore any EMG voltage picked up by them is equivalent to the potential at their midpoint. Consequently, the EMG signal measured by the amplifier is the difference between the central electrode and a virtual electrode at that same point, which is zero. Meanwhile, signals generated within the cuff, i.e. the electroneurogram (ENG), are not spatially linear and are not cancelled. Mathematically, the measured ENG is the second spatial difference of the voltage across the length of the cuff (Stein et al., 1977).

Stein et al. (1977) provided a demonstration of EMG cancellation with a tripolar cuff, shown in Fig. 6. Monopolar, bipolar, and tripolar cuff recordings were recorded in the presence of EMG and only revealed following denervation, while the tripolar recording captures the major features albeit with some EMG contamination.

Several conditions must be met in order for tripolar cancellation of extraneural noise to be effective (Loeb and Gans, 1986). First, the impedance of the two end electrodes must be as similar as possible. Second, the middle electrode must be equidistant between the two ends. Third, the impedance of the amplifier inputs should be similar, accounting for the fact that one input is coming from a single electrode and the other input is coming from two electrodes. Fourth, the voltage gradient is slightly nonlinear at the entrance and exit of the cuff, so the end electrodes should be positioned away from the cuff ends (generally by a few mm) (Rahal et al., 2000a). Finally, the cuff must be well-sealed and insulated to ensure a constant voltage gradient from one end to the

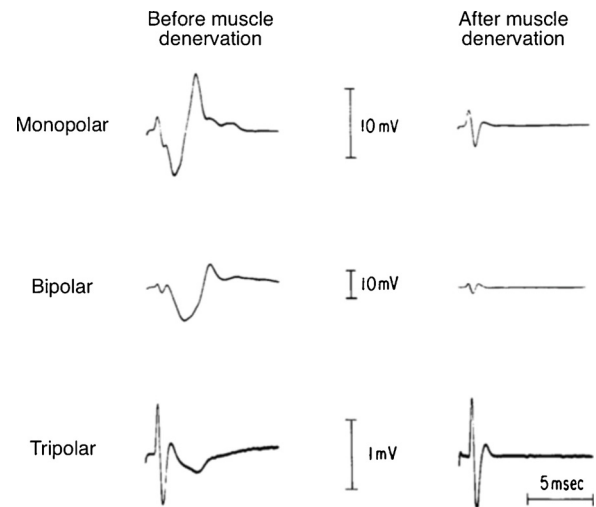


**Fig. 6.** Demonstration of EMG rejection using a tripolar electrode configuration. In monopolar and bipolar recordings, the neural signal is dominated by EMG and only evident after muscle denervation. In the tripolar recording the neural signal is clearly seen in the presence of EMG. Reprinted from (Stein et al., 1977) with permission from Elsevier.

other. The first four requirements are readily met by leveraging the precision and layout flexibility of microfabrication techniques. The latter requirement has bearing on design of the cuff's closure mechanism which will be discussed in more detail below.

Several improvements to this historical *quasi-tripolar* configuration have been explored to further enhance its noise cancellation abilities (Fig. 7). Fibrotic tissue growth over time may affect the impedance balance between the two end electrodes or the linearity of the voltage gradient inside the cuff. To compensate for this, Struijk and Thomsen (1995) connected the two end electrodes with a potentiometer, allowing for adaptive balancing of the asymmetric tissue effects. This *adaptive tripolar* configuration decreased the EMG artifact by 30 % while only decreasing the ENG by 3 %. Pflaum et al. (1997) amplified the central electrode with respect to each end electrode separately then added the two outputs in a configuration called *true tripolar*. This resolved the dissimilar impedance between one and two-electrode inputs and yielded a 10 % improvement in signal-to-noise ratio (SNR). Plachta et al. (2014) later used the *true tripolar* configuration to perform adaptive balancing by making adjustments to the first amplification stage. In a *revised quasi-tripolar* configuration, Chu et al. (2012) achieved an 11 % improvement in SNR by replacing the central electrode with a pair of shorted electrodes separated by a strategic distance. The mechanism by which this improvement is achieved is subtle: as the separation distance between the center electrodes increases from zero (i.e. a single electrode), the EMG signal decreases linearly while the ENG decreases non-linearly, remaining near its maximum value at short separation distances. Therefore, the ratio ENG/EMG is maximized with a short separation between a pair of central electrodes (Chu et al., 2012; Lee et al., 2016a).

Other strategies for noise rejection include passive shunting or shielding features. The *screened tripole* devised by Rahal et al. consists of two additional electrodes which are shorted together and positioned outside the end electrodes. They serve to provide a low-resistance path for shunting the external signal around the lumen of the cuff rather than through it. The effect is a shallower voltage gradient through the cuff so that the recording is less affected by asymmetries in the tripole, similar to what would be achieved by a longer cuff (Rahal et al., 2000b). Another approach is to include a conductive shield layer covering the entire outside of the cuff. Modelling by Sadeghlo (2013) estimated a 70 % reduction in noise using this technique, and Sabetian et al. (2017) found it reduced stimulus artifacts by 63 %.

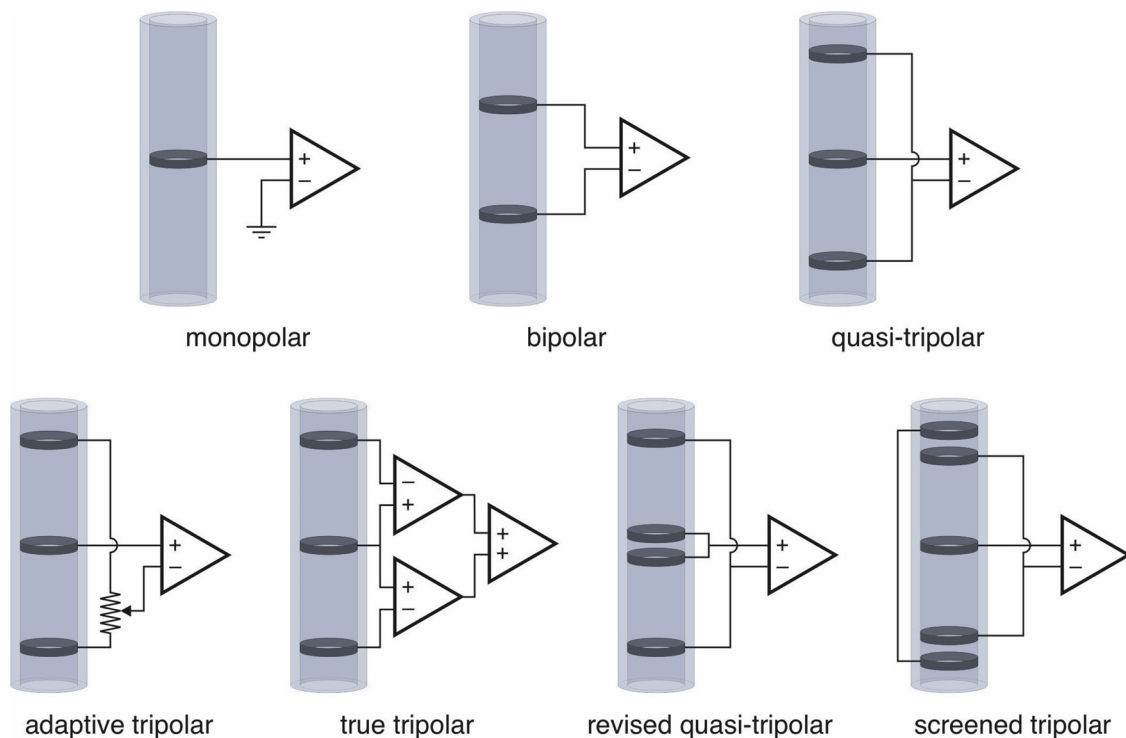


Fig. 7. Electrode configurations for recording with extraneural cuffs.

Finally, filtering can further improve noise rejection. ENG generally occupies the range of 100–5000 Hz with most of its power between 1 and 3 kHz, while EMG is 1–500 Hz with most of its power between 100 and 300 Hz (Tyler, 2018). A notch filter around 60 Hz is also usually necessary to reject room noise.

**3.1.1.1.2. Signal discrimination.** The signals recorded by a cuff are a summation of all the signals from the nerve fibers it encircles, which often number in the thousands. The use of small electrodes may enhance the ability to localize signals coming from fascicles near the surface of the nerve. However, arraying small electrodes around the inner wall of a cuff may only yield modest improvements due to extracellular currents' spreading throughout the cuff lumen (Hoffer and Kallesøe, 2001; Lichtenberg and De Luca, 1979; Sahin and Durand, 1997; Struijk et al., 1997). Such a strategy is most effective when combined with distal placement on the nerve where there is greater separation among fascicles as they near branching points (Silveira et al., 2018).

Discrimination of signals based on location in the nerve may be helped by modification of the cuff's inner wall, as proposed by Hoffer et al. (Hoffer et al., 1998; Hoffer and Kallesøe, 2001). The multi-chambered cuff has parallel ridges on the inside wall which are intended to contact the surface of the nerve and form isolated extraneural chambers, each with its own tripolar set of electrodes. This would potentially limit the spreading of extracellular currents that would otherwise be picked up on multiple electrodes around the circumference.

One long-established method for isolating a signal is coherent averaging, also called spike-triggered averaging (Hoffer et al., 1981; Mendell and Henneman, 1971). A signal which is too small to distinguish in one recording may emerge after tens or hundreds of the recordings are averaged. Coherent averaging requires a repeated signal that is time-coupled to some other detectable signal such as a stimulus or biological signal. Plachta et al. (2014), for example, averaged recordings of baroreceptor signals in the vagus nerve using the rising edge of the electrocardiogram as a trigger.

Discrimination between efferent and afferent signals may be possible given the reversal of the recorded signal shape. However, a

tripolar configuration may make it more difficult to distinguish because of the symmetric electrode arrangement. It is possible to maintain directionality with the use of multiple tripoles in a single cuff, perhaps interleaved or sharing electrodes in each set (Hoffer et al., 1981).

Extending the idea of using multiple electrodes to distinguish signal direction, Taylor and co-workers demonstrated the ability to discriminate signal sources by conduction velocity (Al-Shueli et al., 2014; Donaldson et al., 2008; Metcalfe et al., 2018, 2014; Schuettler et al., 2013; Taylor et al., 2004). Conduction velocity of a fiber correlates to its size, and different sized fibers generally correlate to different types of signals within the nerve. For example, pain signals are carried by small, slow fibers while proprioceptive signals are carried by large, fast fibers. Velocity-selective recording is based on a “delay-and-add” process using a cuff with about ten electrodes longitudinally arranged with even spacing. A delay, corresponding to position in the row of electrodes, is added to the output of each overlapping tripole before the signals of all tripoles are summed. The result is that a neural signal propagating at a particular velocity will end up being summed constructively with itself in all of the outputs. The resulting peak reveals the propagation velocity of the signal and its amplitude is multiplied by the number of electrodes (Taylor et al., 2015). An extension of this method may be used to extract the amount of activity occurring in a nerve at each velocity, called the “velocity spectral density” (Metcalfe et al., 2014). These methods have recently been demonstrated to capture distinct physiological neural signals from the vagus nerve of a pig, discriminated by direction and velocity (Metcalfe et al., 2018).

An emerging technique for recordings of higher spatial resolution is fast neural electrical impedance tomography (EIT) (Aristovich et al., 2018). In this technique, the impedance changes among an array of extraneural electrodes are measured while a constant current is passed between any two of them. The measurements are used to reconstruct tomographic “images” of the nerve cross-section using a process similar to inverse source analysis for electroencephalography. The changes in membrane conductivity as ion channels open and close are captured in the image and thereby give an indication of neural activity. Fast neural EIT has been demonstrated to localize compound action potentials to a particular fascicle in rat sciatic nerve with temporal resolution of 0.3 ms

and spatial resolution of 100  $\mu\text{m}$ . This technique currently requires averaging over tens of seconds or minutes (Aristovich et al., 2018). Relatedly, a more direct adaptation of inverse source analysis techniques was investigated by Zariffa et al. (2011) though with limited success. Wodlinger and Durand (2010, 2009) also present a source-localization technique utilizing spatial filters determined by the interface geometry and demonstrated localization of activity in two fascicles.

**3.1.1.2. Strategies for enhanced stimulation with extraneural cuffs.** Goals of neural stimulation are efficiency and selectivity. Extraneural cuffs derive their efficiency from the insulative wall which confines stimulation currents. A well-sealed cuff is not as crucial for stimulation as it is for recording, but prevents wasteful spill-over of current which may cause unwanted side effects (Hoffer and Kallesøe, 2001). A tripolar electrode configuration with return electrodes near the cuff ends helps confine current and also shapes the generated field to have a higher second spatial difference for the same amount of current (as compared with a monopole) thereby more efficiently initiating action potentials (Howell and Grill, 2015).

To achieve selectivity, it is straightforward to install cuffs at distal locations after branch points (Payne et al., 2019). However, this approach is often undesirable because the branched nerves are smaller, more fragile, and less accessible. It also requires multiple implantations, cables, and connectors if multiple degrees of freedom are required. It is preferable to implant a single PNI on a larger compound nerve trunk.

The primary mechanisms for differential activation of nerve fibers are spatial selectivity and fiber size selectivity. Grill (1995) provided an in-depth review of selective stimulation strategies using cuffs. A summary is provided here along with recent advancements.

Spatial selectivity is based on the increase in a fiber's stimulus threshold as distance from the electrode increases. A given stimulus pulse can activate fibers within a certain radius. Spatial selectivity may be improved by arraying and positioning electrodes around the cuff with reference to the fascicle positions in the nerve trunk. Furthermore, the spatial pattern of activated fibers can be shaped via electrode arrangement. A tripolar arrangement is generally used with the cathode at center and anodes at the ends, though Tarler and Mortimer found a monopolar arrangement to be nearly as selective (Tarler et al., 1995; Tarler and Mortimer, 2003). A transverse anode, *i.e.* on the other side of the cuff, may also be used to "steer" the current depending on the amplitude of the anodal pulse (Grill et al., 1991; Sweeney et al., 1990; Veraart et al., 1993). Grill and Mortimer (1996a) found the use of shortened pulses can exaggerate the effect of spatial selectivity, increasing the difference in stimulation threshold for fibers at different distances from the electrode. An inversion of the distance-threshold relationship can be achieved by use of sub-threshold depolarizing pre-pulses before the main stimulation pulse. These pre-pulses deactivate the sodium channels in nearby fibers while those farther away are unaffected. In such a manner, fibers at the center can be activated without activating those near the surface (Grill and Mortimer, 1997). Other waveforms for blocking can also be used for this purpose (Vuckovic et al., 2008).

Beyond these guidelines, spatially selective activation of fascicles with cuffs is a case-by-case practice. A period of characterization and "tuning" after implantation will generally be required to find the electrode combinations that achieve the desired effects. Tarler and Mortimer (2004) demonstrated selective activation of each of four fascicles in cat sciatic nerve using only four monopolar electrodes in combination with anodic and cathodic steering currents. Veraart et al. (1998) implanted a cuff on a human optic nerve and with four electrodes elicited a range of percepts roughly corresponding to four quadrants in the visual field. Good selectivity was achieved in human upper extremity using a combination of monopolar electrodes and current steering (Polasek et al., 2009). Plachta et al. (2014), with a tripolar configuration, achieved activation of baroreceptors in rat vagus nerve that was at least selective enough to avoid cardiac and respiratory

side effects.

Fiber size selectivity is based on the fact that larger diameter fibers have a lower stimulation threshold. Gorman and Mortimer (1983) found that shortened pulse durations exaggerate the effect as they do for spatial selectivity, by increasing the differences in threshold for different fiber sizes. Notably, the tendency to recruit large fibers before small fibers is opposite to the physiological recruitment order for voluntary muscle contractions which begins with low-force, fatigue-resistant motor units and progresses to high-force, quickly-fatiguing motor units. Consequently, graded stimulation levels intended to reproduce natural-like motor control will instead produce poor gradation of force and quick onset of fatigue. This is evident in the steep slope of most recruitment curves (plots of a muscle's contraction force *versus* stimulation amplitude) found in the literature. Sub-threshold depolarizing pre-pulses before the main pulse, as with the distance-threshold relationship, have been found to invert the diameter-threshold relationship, which can be used to achieve a more natural recruitment order (Sassen and Zimmermann, 1973).

Lertmanorat and Durand (2006; 2004) proposed an extraneural method to recruit small myelinated fibers before large ones that does not rely on use of a long pre-pulse and large amounts of charge injection, but instead strategically shapes the extracellular voltage profile using an array of electrodes. This technique is based on the proportionality of fiber excitation to the second spatial difference of the voltage profile along the nerve, and internodal spacing to fiber diameter. The electrode configuration is an evenly spaced array of 5–11 alternating anodes and cathodes. A fiber whose internodal spacing approximately matches the spacing between cathodes will see a more uniform voltage profile and thus a drastically diminished second spatial difference. Meanwhile, fibers with smaller internodal spacing, especially those matching the cathode-anode spacing, will have a larger second spatial difference and thus can be activated independently of the larger fibers. This technique was demonstrated to be effective at preferentially recruiting smaller myelinated fibers in both simulations and experiments and decreased the slope of recruitment curves by at least a factor of four as compared to a tripolar cuff (Lertmanorat et al., 2006).

**3.1.1.3. Cuff closure mechanisms.** Cuffs are largely differentiated from each other by the mechanisms by which they close around a nerve. Closure mechanism design should consider sealing, sizing, and ease of installation. As previously mentioned, complete sealing along the entire length of the cuff is crucial for maximal recording quality. The seal should also deny the aggressive ingrowth of fibrotic tissue at any point other than the ends of the cuff. The host immune response will breach and expand even the tiniest gap or crack in the seal by packing it with fibrotic tissue, which then provides a path for internal signals to leak out and for external noise to invade (Hoffer and Kallesøe, 2001; Loeb and Gans, 1986; Loeb and Peck, 1996; Naples et al., 1990).

Sizing of a cuff's diameter must balance several factors. A fit that is too tight will compromise nerve health by constriction during post-operative swelling, tissue encapsulation, and motion. If it is too loose, the recording and stimulation performance will be impaired. The prevailing convention for cuff sizing is to use an inner diameter that is 1.2–1.5 times the nerve diameter. Hoffer and Kallesøe (2001) note that a looser fit may increase nerve damage because it has a tendency to allow misalignment of the cuff's and nerve's axes, resulting in sharp pressure points at either end of the cuff. Likewise, Naples et al. (1990) suggested that a closer fit may improve stabilization of the cuff on the nerve, and that the greater cause of damage is incongruous motion between the two. Naples' review found a variety of confounding factors in reports of health or harm caused by various cuff diameters, including various implantation sites subject to different amounts of motion and different cabling qualities that may serve to either aggravate or stabilize the interface. From these discussions, when selecting a fixed cuff diameter, it seems prudent to aim for 1.2–1.3 times the nerve diameter.

**3.1.1.3.1. Split cuffs.** Split cuffs possess a simple design and were

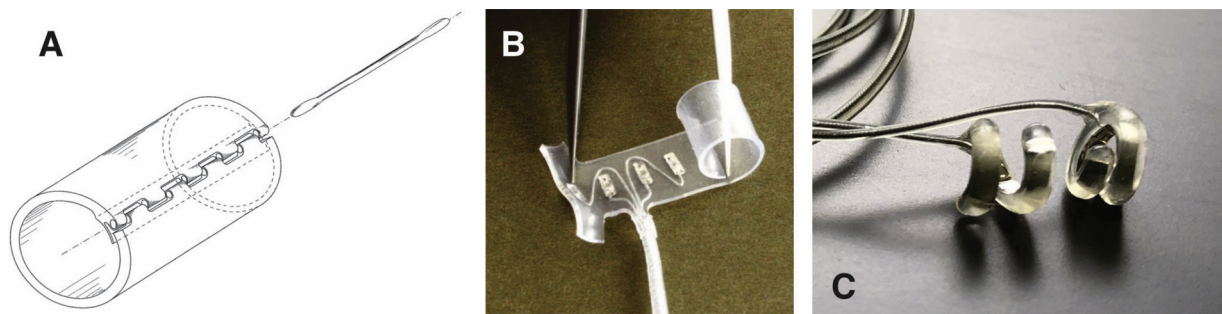


**Fig. 8.** Extraneural electrodes. A) Cuff with “piano hinge” closure mechanism (Kallesøe et al., 1996). B) Silicone spiral cuff. Image reproduced courtesy of Ardiem Medical, Inc (Neural Cuff | Ardiem Medical, 2019). C) Two-electrode helical array (McCreery, 2004).

preferred throughout the first two decades of PNI research. They consist of a sheet of insulation folded around the nerve or a piece of tubing with a longitudinal end-to-end slit. To close and seal split cuffs, sutures and/or silicone can be applied and the silicone cured *in situ*. This method is still widely used for its simplicity (Avery and Wepsic, 1973; Caravaca et al., 2017; González-González et al., 2018; Hoffer and Kallesøe, 2001; Loeb and Peck, 1996; Stein et al., 1977; Tian et al., 2018). However, the obvious drawbacks are imprecision and inconsistency. Sutures on the exterior of a cuff may cause problematic adhesion to surrounding tissues (Hoffer and Kallesøe, 2001).

Alternatively, an outer shell can be applied which gives form to the flexible inner cuff, holding it closed *via* spring force (Micro-Leads Research Products, 2019). A double-layered cuff design used an outer split cuff wrapped around the inner cuff with its longitudinal slit positioned on the opposite side of the nerve, which was then sealed with silicone (Loeb and Peck, 1996). This design is particularly resistant to tissue ingrowth but at the expense of a bulkier profile.

Kallesøe et al. presented a split cuff having inter-locking teeth that are aligned and linked by inserting a single nylon suture (Fig. 8a), much like the hinge of a piano lid (Hoffer and Kallesøe, 2001; Kallesøe et al., 1996).

A few examples in literature have bendable metal skeletons, or armatures, embedded inside the cuff wall, giving it a formable structure. An armature cuff intended for acute experiments by Földes et al. (2011) is simply pinched closed to hold it in place around the nerve. A design by Crampon et al. (1999) used a temperature sensitive shape-memory alloy which can maintain an open state for easy installation around the nerve, followed by automatic closing once it warms to body temperature.

**3.1.1.3.2. Spiral cuffs.** Unlike split cuffs that require additional closure mechanisms to achieve appropriate fitting around a nerve, spiral cuffs were introduced that could “self-size” (Naples et al., 1988, 1986). Spiral cuffs (Fig. 8b) have a dynamically adapting diameter and can be installed with a snug fit (a resting diameter of about 0.9 times the nerve diameter), keeping electrodes in contact with the surface of the epineurium while accommodating swelling, fibrosis, and motion. The accommodating fit can minimize abrasion of the nerve before tissue encapsulation can anchor it (Naples et al., 1990).

Models showed that a spiral cuff could accommodate a 21 % expansion of the nerve diameter before reaching the 20 mmHg pressure safety threshold Rydevik observed as the starting point of effects on blood flow (Naples et al., 1988). Later, *in vitro* measurements by Cuoco and Durand (2000) revised this limit to at least 33 % expansion of the nerve. A seven-month implantation on cat sciatic nerves showed morphological changes only attributed to cabling issues while a subsequent four-month implantation showed no significant morphological differences as compared with controls (Grill and Mortimer, 2000; Romero et al., 2001). The majority of investigations on cuff-based stimulation by Mortimer and co-workers at Case Western Reserve University in the 1990s and 2000s were also performed using spiral cuffs (Grill et al., 1991; Grill and Mortimer, 1998, 1997, 1996b, 1996a; Tarler et al.,

1995; Tarler and Mortimer, 2004, 2003; Veraart et al., 1998, 1993). Spiral cuff implantations in humans have seen stable function without adverse effects up to 11 years in limbs (Christie et al., 2017; Fisher et al., 2009; Polasek et al., 2009), and up to 7 years on an optic nerve (Brelén et al., 2005).

Most spiral cuffs have been made from silicone and platinum foil, like the example shown in Fig. 8b. It is desirable to minimize the thickness of the cuff in order to avoid a bulky discontinuity in the lumen where the inner edge of the spiral ends. For this purpose, and to take advantage of the other benefits of microfabrication, several groups have microfabricated spiral cuffs from the thin-film polymers polyimide and Parylene (Kang et al., 2015; Lee et al., 2016a; Plachta et al., 2014; Rodríguez et al., 2000; Schuettler et al., 2000).

**3.1.1.3.3. Other closure mechanisms.** Several other cuff closure mechanisms can be found in literature. Ratchet or zip-tie inspired mechanisms presented by Yu et al. (2014) and Cobo et al. (2019) involve microfabricated teeth on the edge of a tab which is passed around the nerve and through a slit, the edges of which lock the teeth into place. The tooth spacing offers a set of discrete, though fixed, sizes from which a precise fit can be selected. Chronic experiments have not yet shown if the longitudinal slit in these designs may compromise the integrity of the cuff seal.

Another interesting closure mechanism is the hook-and-loop fastener proposed by Seki et al. (2017). Made from Parylene, one end of this cuff is patterned with three-dimensional microscale loops that project from the surface, while the other is patterned with hooks. After wrapping the device around the nerve, the two ends are pressed together and the arrays of hooks and loops become entangled. It is unclear how the design will fare in chronic studies as the cuff does not seal and the microstructures may irritate the nerve.

**3.1.1.4. Cuff length.** To optimize a tripolar cuff for recording purposes, its length would ideally match the wavelength of action potentials in the fibers of interest. For a medium-sized myelinated fiber of 10  $\mu\text{m}$  diameter, this can be estimated to be about 60 mm, and for the largest fibers it would be twice that. This excessive cuff length is not practical, however making the cuff as long as possible given anatomical and surgical constraints can aid in maximizing the recorded signal (Marks and Loeb, 1976; Rahal et al., 2000a).

Andreasen and Struijk (2002) estimate that single-fiber action potential amplitude begins to saturate when about 22 nodes of Ranvier are included within the ends of the tripole. Internodal spacing is 100 times the fiber diameter (Hursh, 1939), so the tripole length to maximally record from a 10  $\mu\text{m}$  fiber is about 22 mm. Short of maximal recordings, Tyler (2018) gives the rule of thumb that the tripole should cover *at least* 10 nodes of Ranvier, which, by the same calculation, would yield about 10 mm. In other words, a minimum cuff length for recording might be estimated by simply transliterating the targeted fiber diameter from  $\mu\text{m}$  to mm and adding a few mm to account for the non-linearities at the ends of the cuff, as discussed in Section 3.1.1.1.

Hoffer and Kallesøe (2001) state that adequate recording during

behavioural tasks in animals is achieved using a cuff length that is 10 times its diameter. However, longer cuffs yield better recordings. If even a few mm can be added, [Andreasen and Struijk \(2002\)](#) state that the extra length may have a significant impact on the RMS value of the ENG.

For the purposes of stimulation, cuff length is much less important and has not received special treatment in literature. A longer cuff will improve efficiency and current containment, and otherwise it is the desired electrode arrangements and field shaping capabilities that will dictate length ([Hoffer and Kallesøe, 2001](#)). For stimulation with a tri-polar configuration, length comparable to a short recording cuff, as described above, should be sufficient.

**3.1.1.5. Cuffs for small nerves.** Sizing extraneural cuffs for use on small, fragile nerves 500  $\mu\text{m}$  in diameter and smaller introduces additional challenges. Cuffs having thin walls and constructed from soft, compliant materials are necessary. Soft, thin-film polymer substrates may offer significant advantages in this case. A 30  $\mu\text{m}$ -thick cuff was microfabricated from shape memory polymer and used to acutely record from the pelvic nerve of rat, which has a diameter of 200  $\mu\text{m}$  ([González-González et al., 2018](#)). The shape memory polymer can form a very thin cuff wall that also softens upon implantation, in contrast to other commonly used materials like silicone, polyimide, and Parylene that do not have this combined feature set.

Smaller nerves require cuffs capable of tighter bending radius. The metal conductors used in larger cuffs may not accommodate small bending radii without significant stress. One strategy to address this is use of microfabrication methods to pattern thin metal layers (approximately 200 nm thick) as opposed to methods that involve metal foils (25  $\mu\text{m}$  thick). [Ordonez et al.](#) decreased the stress in a circumneural metal electrode for a 350  $\mu\text{m}$  diameter cuff by longitudinally dividing the electrode into two sections and reconnecting them with a serpentine metal trace (2014).

### 3.1.2. Book

Book electrodes, introduced by [Brindley \(1972\)](#), consist of deep grooves in a silicone block with platinum foil electrodes in each groove, where nerves are to be placed ([Brindley, 1977, 1972](#)). The flaps separating each groove are reminiscent of the pages of a book, thus the name. After placing the nerves, a silicone cover is placed and sealed with silicone adhesive. This device was designed for implantation on the sacral nerve roots near the spine for bladder control in spinal cord injury patients. Book electrodes were first commercially introduced in 1982 by Finetech Medical and have been implanted in thousands of patients ([About us – Finetech Medical, 2019](#)). The manufacturer states that longevity of the device is expected to be 20–25 years, limited by degradation of the silicone rubber, though it has not been observed ([Finetech-Brindley Sacral Anterior Root Stimulator \(CPC2\): Notes for Surgeons and Physicians, 2016](#)). In a 2018 survey of 33 patients who were implanted with the Brindley stimulator at one hospital, the average time since implant was 16 years and overall satisfaction with the device was 87.5 % ([Deberge et al., 2018](#)). A large advantage of the device is its stable implant location, which avoids complications of the relatively bulky geometry. Owing to the selectivity problem, installation of the device unfortunately includes cutting some of the afferent dorsal sacral roots so that reflex circuits do not interrupt function, which also eliminates other reflexes such as gastric emptying and sexual functions ([Navarro et al., 2005](#)).

### 3.1.3. Helical

The helical or helicoidal PNI, shown in [Fig. 8c](#), is another extraneural design that has been successfully commercialized. It was originally developed at Huntington Medical Research Institute by Agnew and co-workers in the 1980s, and nowadays is found in stimulation systems by LivaNova (previously Cyberonics) ([Agnew et al., 1989; Bullara, 1986; Naples et al., 1990; VNS Therapy, 2019](#)). The design

consists of a silicone substrate formed into an open-matrix helix with platinum foil electrodes. Like the spiral cuff, helical electrodes offer an adaptive fit to the nerve, accommodating changes in diameter. They have been widely successful for clinical non-selective stimulation of the vagus nerve, however the open-matrix form is not suited for sensitive ENG recording. Multiple design iterations have included a bidirectional helix with separate sections turning in opposite directions to prevent travel along the nerve, and “finger-like” gripping forms that resemble the open matrix of the helix but allow for easier implantation by obviating the need to completely wrap behind the nerve ([Baker, 1993; Bullara, 1990; Rise and Klepinski, 1992; Weinberg, 1993](#)).

At least one thin-film polyimide version of a helical electrode was proposed, though it has not been specifically compared with the traditional silicone helix ([Xiang et al., 2016](#)).

### 3.1.4. Flat interface neural electrode (FINE)

The flat interface neural electrode (FINE), introduced by [Tyler and Durand \(1997a\)](#), offers a powerful strategy for increasing extraneural access to individual fascicles in a nerve trunk. The concept is that the nerve will tolerate atraumatic rearrangement of the fascicles under limited transverse compression. The FINE aims to gently flatten the nerve, thereby bringing all fascicles closer to the nerve’s surface and increasing the cross-sectional perimeter while maintaining cross-sectional area. In addition to spreading out the fascicles to improve access to them, the increased perimeter allows for a greater number of electrode sites to contact the nerve ([Tyler, 2018](#)).

Individual fascicle selectivity and independent addressability of the FINE on cat sciatic nerve was demonstrated in acute studies ([Tyler and Durand, 2002](#)). A study of the four-week response to varying degrees of reshaping forces (*via* varying wall thickness) on rat sciatic nerve found that the low forces exerted by a 0.4 mm silicone wall were best-tolerated and still capable of achieving the desired reshaping ([Tyler and Durand, 2003](#)). Three-month studies of FINE on cat sciatic nerve demonstrated stable selectivity and no significant histological evidence of nerve damage in FINES with low or medium degrees of reshaping ([Leventhal et al., 2006; Leventhal and Durand, 2004](#)). Modelling by [Leventhal and Durand \(2003\)](#) suggests that selectivity is maximized by designing FINES to particularly match the dimensions of the targeted nerve, and that doing so may yield sub-fascicle selectivity.

Later, a FINE was designed, modelled, and intraoperatively tested on human femoral nerve with the aim of eventual use in a neuro-prosthesis for standing and walking. At least four of the six targeted leg muscles were selectively and independently activated in each of the seven subjects tested, and all six muscles in one subject ([Schiefer et al., 2010, 2008](#)). Similar studies were performed on other lower-limb nerves ([Schiefer et al., 2013, 2012](#)). Stable and selective sensory percepts were stimulated in upper arm amputees for up to two years using FINE ([Tan et al., 2015](#)).

Several variations of the initial FINE have been produced. A liquid crystal polymer version was designed to take advantage of micro-fabrication ([Hess et al., 2007](#)). A FINE was designed to close more slowly for more gradual reshaping of the nerve by integration of a biodegradable polymer, allowing a tuneable reshaping period ranging from 12 h to 16 days ([Caparso et al., 2009](#)). The latest generation of FINE is designed with regionally specific stiffness such that the flattening effect is still possible but with greater flexibility in the longitudinal direction to accommodate bending of the nerve. Stiffness was modulated by a strip of PEEK embedded in the center of the silicone wall ([Freeberg et al., 2017](#)). This composite-FINE was implanted in human trans-tibial amputees and stably elicited multiple sensory percepts in the missing limb over a period of seven months ([Charkhkar et al., 2018](#)).

### 3.1.5. Other extraneural PNIs

Other notable extraneural PNI designs are introduced here. A micro-scale, printable “nanoclip” was designed for nerves as small as 50  $\mu\text{m}$

(Lissandrello et al., 2017). The clip itself does not offer insulation but serves to hold the electrodes near the nerve. It features a “trap-door” closure for ease of installation. Non-active clips were installed on zebra finch tracheal syringeal nerve for 74 days and changes in bird song were monitored as an indicator of nerve health. Bird song deviated similarly to a nerve crush injury after implantation, but recovered to baseline after about 10–20 days while the clip was still present. While further characterization and optimization of this design are likely needed, the 200 nm-resolution 3D printing technique may provide a simple solution for interfacing with small nerves.

The split-ring polyimide PNI proposed by Lee et al. (2017) prioritizes ease of fabrication and installation. No subsequent fabrication steps are required after removing the microfabricated device from its carrier wafer, and the flexible split ring shape is intended to easily slip around the nerve and apply minimal pressure while keeping the electrodes in contact with the nerve. A drawback of this design is the transverse positioning of electrodes around the perimeter which is not optimal for either recording or stimulation. Furthermore, the sharp edges of the thin film are oriented normal to the nerve and the adjacent tissues and are likely to cause injury when implanted chronically.

A paperclip-inspired polyimide PNI is similarly flat and requires little manipulation after microfabrication (Lee et al., 2018a,b). This design is intended for use on small nerves, as it was implanted on rat pelvic nerves of 250–300  $\mu\text{m}$  diameter and used to initiate bladder voiding in acute experiments. The fixture mechanism depends on applying constant pressure to slightly kink the nerve, and the long-term safety of this remains to be seen in chronic experiments.

Ong et al. (2018) presented a sticky hydrogel-based PNI with mechanical compliance more similar to nerve tissue than most PNI materials. Embedded in the hydrogel substrate, platinum electrodes are insulated by Parylene, and SU-8 structures provide a gradual change in mechanical stiffness between the connection end and the interface end.

Another intriguing hydrogel-based PNI presented by Liu et al. (2019) uses micropatterned electrically-conductive hydrogel (ECH) in place of the metal electrodes and traces, insulated by a layer of stretchable insulative polymer and embedded in a hydrogel sheet. The ECH possesses excellent electrical characteristics and showed minimal host response when implanted around sciatic nerves of mice for six weeks. While the mechanical characteristics of hydrogels are near optimal for PNIs, a hydrogel PNI in a cuff-like form will not provide the same noise rejection and current containment as a cuff made from traditional insulative materials, and so a method to combine the merits of both material types remains to be explored.

### 3.2. Interfascicular

Interfascicular PNIs penetrate into the epineurium, however they do not breach the blood-nerve barrier. Modelling has shown that electrodes placed closer to fascicles may preferentially activate nerve fibers within the fascicle but not other fibers in the nerve trunk; this effect is

more pronounced for electrodes placed directly adjacent to the perineurium (Tyler et al., 2011). Intrafascicular electrodes discussed in the next section are situated within a fascicle. When comparing their stimulation windows, intrafascicular electrodes have a narrower window of stimulation amplitudes that achieve 100 % activation before spilling-over into other fascicles.

According to Sunderland (1978), disruption or removal of the epineurium, as in the medical removal of neural scar tissue known as neurolysis, has no harmful effects as long as the perineurium is not damaged. Unfortunately, there are not many examples of interfascicular PNIs in literature from which to learn. One example is the multigroove interfascicular PNI, proposed by Koole et al. (1997). This PNI takes inspiration from Brindley’s book electrodes, except instead of placing entire nerves between the pages of a “book,” the epineurium is surgically dissected and each fascicle is placed in its own groove. It is not clear whether *in vivo* studies were ever performed with this device.

Another example is the slowly-penetrating interfascicular nerve electrode (SPINE) (Tyler and Durand, 1997b). This device consists of a silicone cuff that has four partial longitudinal slits at one end, producing “beams” around the circumference which project fin-like elements toward the center of the nerve. As the name suggests, these elements are intended to slowly penetrate into the epineurium, allowing gradual rearrangement of the nerve trunk’s organization as the electrodes settle into position between the fascicles. 24-h implantations on cat sciatic nerve yielded promising results, demonstrating improved selectivity as compared to extraneural cuffs and no acute injury to the perineurium (Tyler and Durand, 1997b). Nielsen et al. (2014, 2012) introduced a roughly-constructed fin-like device with two electrodes on each side, led by a suture to be placed in between the tibial and peroneal fascicles of sciatic nerve in rabbits. Although acute results were promising for both interfascicular PNIs, no follow-up chronic experiments have been reported.

A device intended for intrafascicular interfacing was determined following histology to have instead an interfascicular interface with electrodes positioned between fascicles. Even so, the device could selectively stimulate five muscles (Kundu et al., 2014).

The few examples of interfascicular PNIs in literature suggest that the primary design concerns are the placement of electrodes among fascicles of irregular shape and size, electrical isolation between the fascicles, and the severity of host response under chronic use.

### 3.3. Intrafascicular

Despite the unavoidable damage to the nerve, much research has explored the use of intrafascicular PNIs (Fig. 9) which benefit from the insulating properties of the perineurium and may offer more efficient stimulation, sub-fascicular selectivity, and higher SNR and signal discrimination than other PNIs (Jung et al., 2018a,b).

The primary concern with intrafascicular PNIs is risk of damage to the nerve fibers and intraneural blood vessels and thus poor chronic

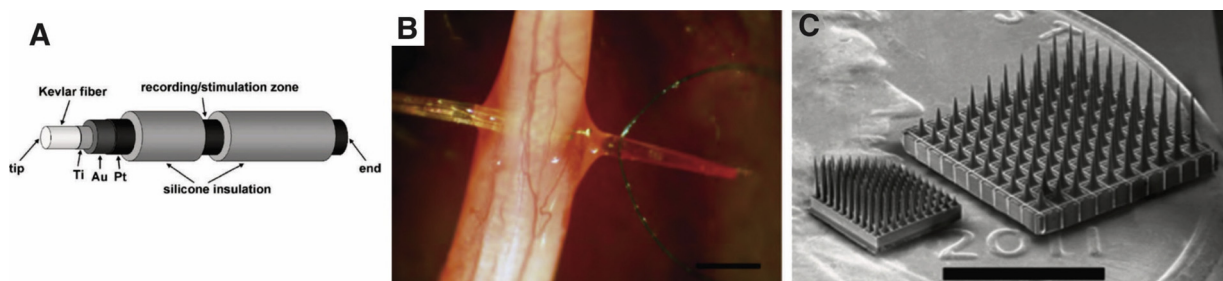


**Fig. 9.** Intrafascicular PNIs. A) Structural diagram of the poly-LIFE (not to scale). Reprinted from (Lawrence et al., 2003) with permission from Elsevier. B) Transverse intrafascicular multichannel electrode (TIME) implanted in a rat sciatic nerve. Scale bar = 1 mm. Reprinted from (Boretius et al., 2010) with permission from Elsevier. C) Right: Utah slant electrode array (USEA). Left: high-definition Utah slanted electrode array (hd-USEA). Reprinted from (Wark et al., 2013). Scale bar = 3 mm.

performance. The host response to an object in the sensitive endoneurial space may be especially consequential as there is no barrier to safeguarding the nerve fibers. Expected reactions are endoneurial edema and fibrosis, potentially leading to increased endoneurial pressure, compression of nerve fibers, and consequent neural damage including demyelination, decreased axon size, and degeneration of the fibers' distal portions (known as Wallerian degeneration) (Grill et al., 2009; Rydevik et al., 1990).

Despite these concerns, a variety of studies have shown fairly stable responses to intrafascicular electrodes, as reviewed by Yoshida et al. (2010) and Jung et al. (2018a,b). After a recovery period from the implantation (about one to four weeks), any functional deficits are often subtle and morphological changes in the nerve are limited, besides the usual significant fibrotic capsule surrounding the device. The intrafascicular PNIs that fare best tend to minimize the encapsulation and potential for re-injury by prioritizing small size and flexibility.

### 3.3.1. Longitudinal intrafascicular electrode (LIFE)

The longitudinal intrafascicular electrode (LIFE) is thread-like and implanted parallel to the nerve fibers. Installation is accomplished by attachment to an electro-sharpened tungsten needle which, after careful dissection of the epineurium, pierces into the perineurium, exits about 1 cm away, and is then pulled to position the electrode site inside the fascicle (Mortimer et al., 1995).

The first LIFE consisted of a 25  $\mu\text{m}$  diameter Pt-Ir wire insulated by Teflon, with about 1 mm of insulation removed at its midpoint to form the electrode site (Malagodi et al., 1989). The length of the site was intended to ensure positioning near a node of Ranvier. A bipolar version used a twisted pair of 5  $\mu\text{m}$  diameter carbon fibers instead of the Pt-Ir wire (Veltink et al., 1989). In another iteration, the polyLIFE utilized a 12  $\mu\text{m}$  diameter metallized Kevlar thread and silicone insulation for greater flexibility (Lawrence et al., 2003; McNaughton and Horch, 1996). An 11  $\mu\text{m}$ -thick thin-film version (tf-LIFE) was microfabricated from polyimide, enhancing precision, flexibility, and number of electrode sites (Lago et al., 2007b; Yoshida et al., 2000, 2006). The tf-LIFE is folded in half to position electrodes on opposite sides and also to provide a loop that can be led by suture into the fascicle. A further enhancement of the tf-LIFE was the integration of a shape-memory alloy that could be actuated *in situ* to achieve finer positioning and counteract positional drift (Bossi et al., 2007).

Early experiments demonstrated chronic stability of LIFE over six months in cats and the ability to record distinct signals from about 10 single fibers at a time, though the Pt-Ir wire was prone to drift within the fascicle and the population of fibers gradually changed (Goodall et al., 1991). Histology from a similar six-month experiment found significant encapsulation and a 40 % decrease in axon diameters at the implant site, but sections about 1 cm distal and proximal from the site showed no apparent changes (Lefurge et al., 1991). Implantation of the more flexible polyLIFE in rabbits for six months still showed encapsulation but no significant effects on axon count or diameter (Lawrence et al., 2002). A three-month evaluation of tf-LIFE in rats revealed a slight functional decline after one month which recovered at the two and three-month points and was attributed to recovery after the implantation procedure. Histology in this case showed encapsulation but no significant changes in axon count or diameter (Lago et al., 2007b; Navarro et al., 2007). In a two-week implantation in human amputees, polyLIFEs were able to stimulate sensory percepts and record volitional motor signals (Dhillon et al., 2005). In another human study, tf-LIFEs recorded output signals for four weeks and stimulated sensory percepts for 10 days, though stimulation ability decreased after that (Rossini et al., 2010).

A significant limitation of the LIFE design is low throughput in terms of the number of fibers accessed per implantation. The implantation process is relatively tedious and time consuming, and if multiple degrees of freedom are desired, multiple devices will need to be implanted. Thota et al. (2015) proposed a supporting system of

sheaths, leads, and connectors to facilitate handling and implantation of multiple LIFEs, which they call a distributed intrafascicular multi-electrode (DIME). LIFEs and other intrafascicular PNIs must address the problem of interfering EMG signals (Mortimer et al., 1995; Yoshida et al., 2010). Some groups have placed Faraday cages around the nerves, either in the form of a carbon fiber mesh, or a metal-and-insulator cuff (Djilas et al., 2007; Mortimer et al., 1995).

### 3.3.2. Transverse intrafascicular multichannel electrode (TIME)

The transverse intrafascicular multichannel electrode (TIME) takes a form similar to the tf-LIFE, except it is implanted perpendicularly through one or more fascicles so that multiple active sites gain access to a greater number of nerve fibers (Boretius et al., 2012, 2010). A 90-degree bend is positioned at the point where the TIME enters the nerve so that the insulated traces leading to the connector run longitudinally (Badia et al., 2011b).

Following two-month implantation through the three main fascicles of rat sciatic nerves, slight electrophysiological and functional deficits at one week, but recovery by one and two months were observed. There was also 30–60  $\mu\text{m}$  thick encapsulation and an 8–25 % decrease in myelinated fibers of the smaller fascicles. (Badia et al., 2011b). Though limited to monopolar electrode configurations by having all contacts at one longitudinal position, good selectivity in stimulation and recording were demonstrated in acute experiments in rats (Badia et al., 2016, 2011a).

TIMES have also been implanted into human amputees. Ranging from 4 to 12 months post-implantation, studies have demonstrated stimulation of sensory percepts, usually perceived as tingling, electricity, or vibration in a small region of the phantom limb (Rognini et al., 2018; Valle et al., 2018b, 2018a). Another study implanted the TIME for one month in the median nerve and, using an artificial fingertip with integrated microelectromechanical systems-based “tactile” sensors for mechano-transduction, the subject was able to distinguish between textures with 96 % accuracy (Oddo et al., 2016).

TIME is inserted through multiple fascicles, which anchors them together and disallows relative motion between them. This may explain the higher loss of myelinated fibers observed in the smaller fascicles, as the larger fascicle has an increased “hold” on the TIME due to increased area of interaction and the smaller fascicles must therefore endure more trauma to accommodate motion of the device. Also, the size of the device and its encapsulation are proportionally larger in the smaller fascicles, which may lead to greater impact on the nerve fibers there (Badia et al., 2011b). Another concern is that slight repositioning of the TIME by approximately 0.1 mm was found to significantly change its selectivity and its population of interfaced nerve fibers, which may be seen as an advantage for versatility but also a concern for the stability of input-output characteristics over the long term (Badia et al., 2016, 2011a).

A variation on the TIME design is the self-opening intrafascicular neural interface (SELINe) (Cutrone et al., 2015, 2013, 2011). Upon insertion into the nerve, SELINe is pulled back a short distance, which causes a set of “wings” on each side to spread from the plane of the device, helping to anchor it in place. Each of the four wings has a pair of electrodes on it, so another benefit is expanded access to reach additional nerve fibers which are not near the original insertion track. Three-month implantations in rats demonstrated selectivity and nerve health with the SELINe and also enhanced stability over the TIME (Cutrone et al., 2015). A thorough six-month characterization of the SELINe in rats found increasing stimulation thresholds and impedances during the first month corresponding to formation of a significant encapsulation layer, followed by stable thresholds and impedances over the final five months (Wurth et al., 2017). 60 % of the total channels were functional at three months post-implantation and 25 % at six-months, though the cause of lost channels was not specified. At six months, cross-sectional area of the nerve trunk near the implant was approximately doubled due to the fibrotic capsule. Despite the

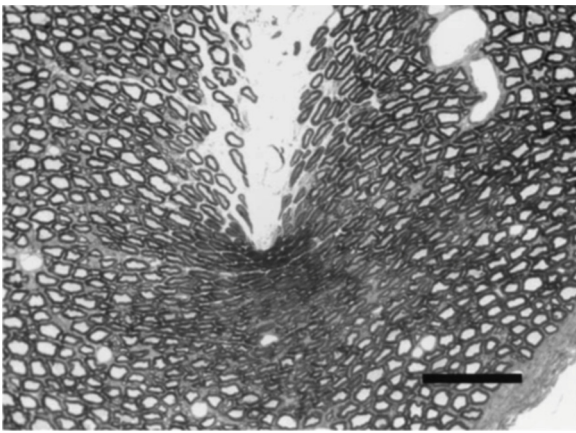


**Fig. 10.** Cross-section of the implant site at one shank of the Utah electrode array. Fibers were compressed under the tip and sheared adjacent to the insertion track. Reprinted from (Branner and Normann, 2000) with permission from Elsevier. Scale bar = 100  $\mu$ m.

significant encapsulation, selectivity over the experiment duration remained stable, as did the number of axons distal and proximal to the implant.

### 3.3.3. Utah slanted electrode array (USEA)

The Utah electrode array (UEA) was originally designed as an intracortical neural interface (Nordhausen et al., 1996). Its use in peripheral nerves was first explored by Branner and Normann (2000), who demonstrated its ability to record single-unit responses from mechanoreceptors and efficiently evoke twitches in individual digits during 36-h studies in felines. Histology of the implantation site showed a dramatic “compression wave” surrounding each shank, consisting of axonal cross-sections which were compressed under the tip and sheared adjacent to the insertion track, as shown in Fig. 10.

An adaptation of the intracortical UEA better suited to peripheral nerves is the Utah slanted electrode array (USEA) which has varied shank lengths so that a greater number of nerve fibers may be accessed, rather than only those that lie in a single plane (Branner et al., 2001). The shanks are spaced 400  $\mu$ m apart and range from 0.5 to 1.5 mm in length. Acute implantations of USEA in cats demonstrated four times broader recruitment curves and one tenth the required stimulus current as compared with extraneural cuffs (Branner et al., 2001).

A high-density version of the USEA (hd-USEA) was introduced by Wark et al. (2013) with a shank spacing of 200  $\mu$ m, yielding a density of 25 electrodes/mm<sup>2</sup> (compared with 6.25 electrodes/mm<sup>2</sup> for the USEA). Shank lengths of the hd-USEA range from 300 to 800  $\mu$ m. Acute experiments in rats and felines demonstrated single unit recording, selective stimulation of motor units, and histological confirmation of electrode placement in the fascicles (Wark et al., 2013). In another acute study, the hd-USEA was implanted in the feline pudendal nerve and was able to selectively record and distinguish among neural signals that corresponded to different genitourinary functions including bladder filling and distension-evoked contractions (Mathews et al., 2014b).

In contrast to the successful intrafascicular array demonstrations in acute studies, chronic experiments have yielded mixed results. USEAs implanted in felines for up to seven months resulted in limited functional deficits which recovered in most cases, inconsistent stimulation capabilities which seemed to depend on surgical technique, and poor recording capabilities which completely receded by one month (Branner et al., 2004). In some cases, histology showed that the shanks either did not penetrate the perineurium or were pushed out by connective tissue. In another study, USEAs were implanted in feline sciatic nerves for up to one year to study the foreign body reaction (Christensen et al., 2014). The reaction was poor, including persistent

activation of inflammatory cells at the implant site and a downward shift in distribution of fiber diameters.

Early on, an array similar to the UEA was implanted in the median nerve of a healthy human volunteer for 96 days (Gasson et al., 2004). Anecdotal stimulation and recordings were broadcast to and from a robotic hand, though only in a non-specific threshold-detection scheme. The subject experienced no deficits in sensation or motor control while the array was implanted, nor up to nine months after removal. More recently, USEAs were implanted in median and ulnar nerves of two human amputees for 30 days and achieved promising results (Davis et al., 2016). Recordings of volitional motor signals from the USEAs allowed the subjects to control a virtual robotic hand, performing 15 different movements including proportional control of individual fingers. In one of the subjects, stimulation *via* various combinations of electrodes produced more than 80 different sensations in the phantom limb. SNR and stimulation thresholds did not significantly change throughout the implantation period. In another study, USEAs were implanted in the median and ulnar nerves of an amputee for 14 months (Page et al., 2018). They were used for stimulation of sensory percepts from a sensor-equipped prosthetic hand in combination with intramuscular recording electrodes for motor control. This study quantified an increase of prosthesis embodiment and a decrease in phantom limb pain arising from integration with the nervous system.

Christensen et al. (2016) performed a study in which USEAs were implanted in two human amputees for 30 days and subsequent histology of the nerve was performed. While electrophysiological tests had demonstrated success in both recording multiple units and stimulating sensory percepts, histology revealed that the electrode tips had only slightly penetrated into the outermost fascicles in the best cases, and in other cases had not penetrated the perineurium at all, as shown in Fig. 11. Still, in the penetrated cases, axons and myelin were found in close proximity to the electrode. Activated macrophages were present on the explanted device and at the implant site, though the administration of medication to the subjects likely affected the inflammatory response.

As the evidence from multiple studies suggests, the densely spaced silicon shanks have difficulty penetrating the tough perineurium. Attempting insertion by simply pressing the array into the nerve is likely result in a crush injury before penetration into the endoneurium. Therefore, implantation is assisted by a pneumatically powered tool that rapidly accelerates the array into the tissue (Branner and Normann, 2000). As illustrated by the examples above, this technique is not always effective. A study designed to assess the safety of pneumatic implantation of the hd-USEA in rat sciatic nerve found the amplitude of signals propagating across the implantation site before and after implantation dropped by 13–38% on average. Furthermore, signal propagation across the site ceased completely in 1 of 8 implantations (Mathews et al., 2014a).

After implantation, Utah arrays intended for chronic use are enclosed with the nerve inside of a silicone cuff or other wrap to hold it in place. This may be an additional source of nerve injury to consider, as discussed in Section 3.1.1. If the PNI is implanted near active muscles, EMG will be a significant problem for recording, and so a cuff/wrap may also serve a shielding role (Branner et al., 2004). Recent implantations in human amputees with favorable results report wrapping the nerve and array in a sheet of manufactured collagen or other decellularized biological material (Christensen et al., 2016; Davis et al., 2016; Page et al., 2018).

The literature on rigid penetrating arrays such as the Utah array seems to suggest use in sites that experience little motion, have minimal connective tissue, and have less fascicular division. The nerve roots match this description, and, indeed, several studies have shown rigid penetrating arrays to be highly effective when implanted there, though chronic stability is yet to be investigated (Aoyagi et al., 2003; Gaunt et al., 2009; Holinski et al., 2013; Stein et al., 2004; Weber et al., 2007).

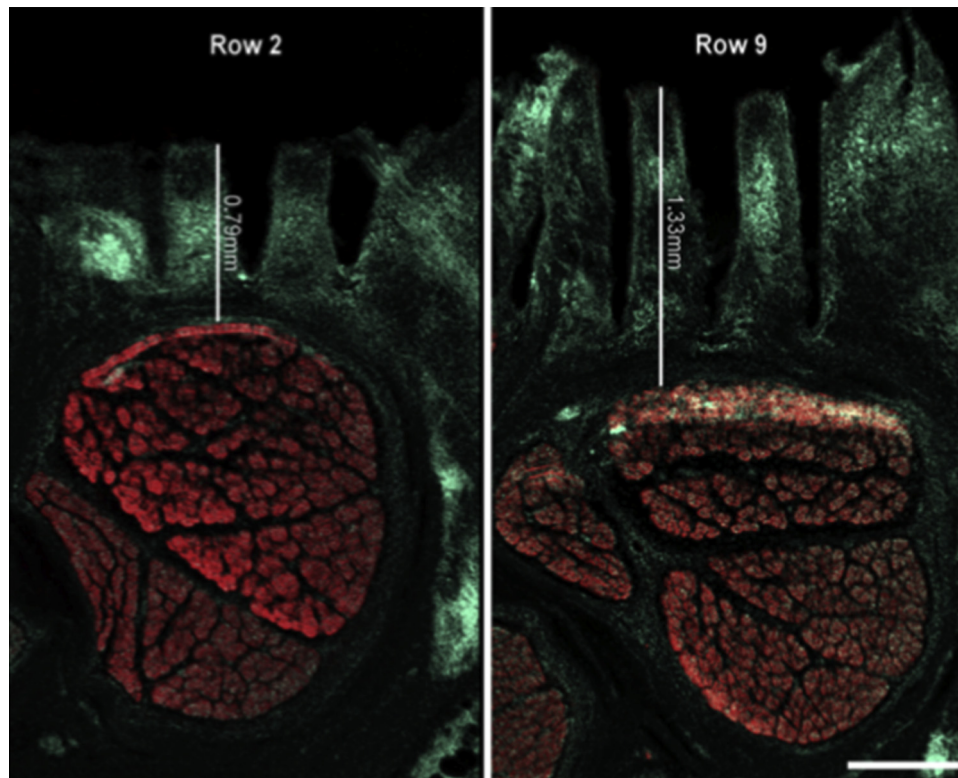


Fig. 11. Cross-sections of human nerve fascicles under the USEA implant at the locations of two rows of different-length shanks. It can be seen that neither row of shanks penetrated into the fascicle (red). Reprinted from (Christensen et al., 2016) with permission from Elsevier. Scale bar = 500  $\mu$ m.

### 3.4. Regenerative

Regenerative PNIs aim to take advantage of the long-known ability of peripheral nerves to regenerate and reconnect after transection (Guth, 1956). Instead of inserting electrodes into the nerve, the nerve fibers can integrate with electrodes in the PNI. If successful, regenerative PNIs could potentially offer far greater resolution and stability than any other of the PNI types discussed thus far. However, the drawback of the approach is the requirement for nerve transection so that the interface may be inserted between the proximal and distal portions. Because of this, any applications that require the interfaced nerve to remain intact, such as bioelectronic medicine, are excluded. This approach may be best suited to applications where distal innervation is unnecessary or not crucial, as in neural prosthesis integration with amputated limbs.

A number of difficult challenges face the implementation of regenerative PNIs. Foremost is the formation of healthy, mature nerve fibers, sufficiently reconnected after transection through and not around the interface. According to Sunderland (1990), axons have no particular compulsion to reconnect with the original distal axon, or even to grow into the same fascicle; they readily grow into other fascicles, the interfascicular space, or even out of the nerve. Furthermore, the foreign body response to the implanted device may interfere by blocking the path with fibrotic tissue before axons can grow through it. This is especially the case for mammals, in which fibrosis is more extensive as compared with amphibians or fish (Stein et al., 1975). Another challenge is interconnection when a large number of electrode sites are desired. Several regenerative PNIs were developed to address these challenges.

#### 3.4.1. Sieve

Sieve electrodes (Fig. 12) consist of a planar structure with a dense pattern of holes through it, some or all of which are ringed by a metal electrode site. Each end of the transected nerve is positioned against the

sieve, usually supported by a section of tubing, so that the axons grow through the holes to reconnect the two ends. Mannard et al., in 1974, fabricated a sieve electrode by drilling through silver wires embedded in an epoxy wafer, and successfully recorded sensory and motor signals in amphibians from 12 to 25 weeks after implantation (Mannard et al., 1974). Most sieve designs over the next few decades were made from silicon to take advantage of microfabrication techniques (Akin et al., 1994; Bradley et al., 1997; Della Santina et al., 1997; Edell, 1986; Kovacs et al., 1992; Mensinger et al., 2000), and since the late 1990s, several polyimide-based designs have been introduced (Jeong et al., 2016; Park et al., 2018; Stieglitz et al., 2002, 1997). In 1997, Bradley et al. (1997) briefly summarized the short history of sieve electrodes up to that time, stating that many had been designed but not published except in abstract form because chronic recordings were rarely successful. In one successful example, Bradley et al. (1997) were able to record spontaneous and mechanically evoked signals in rat with a silicon sieve electrode from week 7 post-implant up to week 20. Ramachandran et al. (2006) demonstrated axon conduction through a polyimide sieve by proximal nerve stimulation and measurement of resulting EMG distal to the sieve, and also captured recordings of mechanically and electrically stimulated afferent signals, though not reliably.

A few design considerations for sieve electrodes include “porosity” or “transparency,” referring to the ratio of the summed hole areas to the total substrate area in the path of the nerve (Jeong et al., 2016; Stieglitz et al., 2002). Higher porosity generally achieves greater axon growth but has adverse implications for mechanical strength. Hole size is also a trade-off. Spearman et al. (2018) state that there tends to be a sharp tipping point between holes that are too small (discouraging axon growth and constricting those that do grow), and too large (allowing too many axons to grow through a single hole and thereby diminishing selectivity). The hole size recommended in the literature is 40–65  $\mu$ m (Lago et al., 2007a; Navarro et al., 2005). Some notable design enhancements include coating the sieve with bioactive proteins to

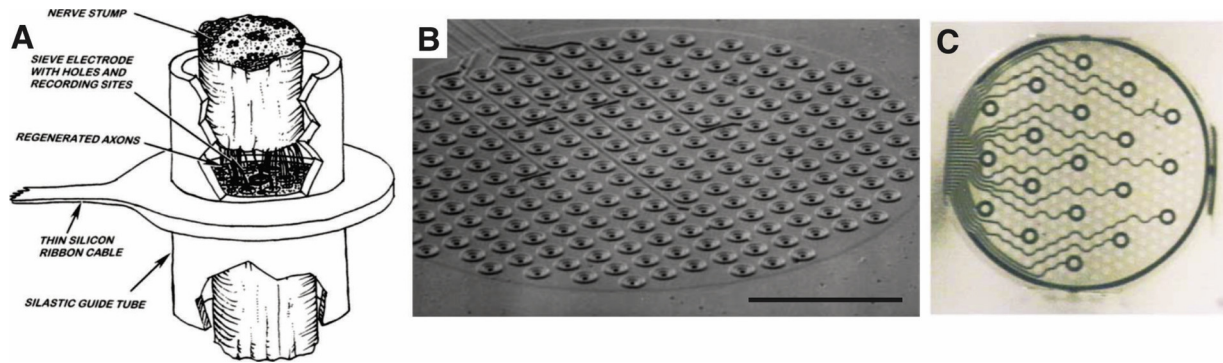


**Fig. 12.** Sieve electrodes. A) Diagram showing arrangement of transected nerve stumps, guide tube, and sieve. B) SEM of a silicon sieve. A) and B) reprinted from (Bradley et al., 1997) with permission from Elsevier. Scale bar = 100  $\mu\text{m}$ . C) Polyimide sieve. Holes are 40  $\mu\text{m}$  in diameter. Reprinted from (Stieglitz et al., 2002) with permission from Elsevier.

encourage growth (Mensingher et al., 2000), and a multi-layered design that helps address the trace-routing problem of many electrode sites on a planar structure (Jeong et al., 2016).

### 3.4.2. Microchannel

The microchannel electrode array, or tubular electrode array, developed alongside the sieve electrode. The design may be considered as a sieve that is extruded in the longitudinal direction, so that, instead of growing through holes in a plane, the axons grow through tubes in a volume. The microchannel electrode array has advantages akin to those of an extraneural cuff except applied to multiple smaller groups of fibers. These include confinement and amplification of the extracellular signals, and ability to incorporate multiple electrodes in a single lumen for noise rejection and selectivity techniques (FitzGerald et al., 2008). After early demonstrations of nerve regeneration through various plastic conduits and microscale gold cylinders in the late 1960s, a number of designs were explored to use electrodes inside of microchannels, though none of the early designs demonstrated successful regeneration and recording (Loeb et al., 1977; Marks, 1969; Spearman et al., 2018). In the last two decades, there has been a relative proliferation of regenerative microchannel PNIs.

One method to form conduits is casting of a silicone substrate around a bundle of microwires or filaments. The microwires are removed after casting, leaving behind an array of densely packed microchannels (Fig. 13a). A limitation is that electrodes are introduced after casting, obscuring part of the channel; microwires with diameters smaller than the conduit diameter can be placed in several of the channels (FitzGerald et al., 2012; Gore et al., 2015; Kim et al., 2015).

Alternatively, a bundle of conduits can be assembled from a planar structure. The rolled microchannel array is made by first

microfabricating a flat, flexible array of open-ended microchannels with integrated electrodes, comparable to a sheet of corrugated cardboard. This structure is then rolled up, creating a cylinder of multiple layers of microchannels (Fig. 13b). Virtues of this design include its amenability to standard microfabrication techniques, simple assembly into a 3D structure, and natural cylindrical form to match the cross section of the nerve. A variety of polymers were explored as the substrate for rolled microchannel arrays, including Parylene, polyimide, silicone, and SU-8 (FitzGerald et al., 2012; Lacour et al., 2008; Srinivasan et al., 2011; Suzuki et al., 2006).

Similarly, the stacked microchannel array is formed by stacking multiple flat arrays. This design was proposed by Loeb et al. in 1977 and the concept was recently revisited (Lancashire et al., 2016; Loeb et al., 1977; Musick et al., 2015). Advantages of the stacked array are better control of sealing separate layers of microchannels and greater amenability to dense electrical connections, though the overall shape is block-like and potentially incongruous with the nerve and the nerve groove.

Several regenerative microchannel PNIs achieved promising *in vivo* results. One study found axon growth into more than 95 % of a device's microchannels and recording of spontaneous and evoked single- and multiple-unit action potentials from anesthetized rats (Srinivasan et al., 2015). Other studies achieved similar recording success in ambulatory rats (Gore et al., 2015; Musick et al., 2015; Srinivasan et al., 2016).

As with sieve electrodes, open area ratio and channel size are key design considerations. In a study of *in vitro* neuron cultures, Lacour et al. (2008) found optimal growth of axons into microchannels when transparency was at least 50 %. FitzGerald et al. (2012) found greater axon growth *in vivo* with 62 % transparency as opposed to 21 %, though the two devices compared had other differences. Smaller microchannels

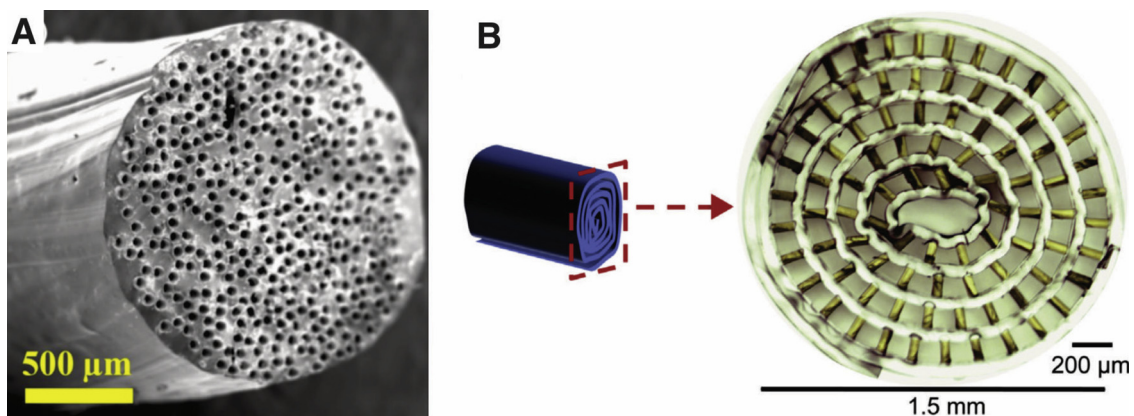


**Fig. 13.** Microchannel PNIs. A) Microchannel array formed by casting silicone around microwires. Reprinted from (Kim et al., 2015) with permission from Springer. B) Rolled microchannel array made of PDMS and SU-8. Reprinted from (Srinivasan et al., 2015) with permission from Elsevier.

may increase selectivity by isolating groups of fewer nerve fibers, however the channel must also accommodate vasculature and other supportive tissues if the regenerated fibers are to be healthy and robust. Several studies reported growth of “mini-fascicles” into channels whose cross sections were 75–200  $\mu\text{m}$  in diameter (FitzGerald et al., 2012; Gore et al., 2015; Srinivasan et al., 2015). These mini-fascicles included tens of nerve fibers, Schwann cells, a few blood vessels, and an outer sheath of connective tissue. While far from the ideal isolation of only a few fibers in each microchannel, this still represents a potentially higher electrode density than other PNI types and may be a productive compromise to achieve healthy integration. Inclusion of selectivity-enhancing techniques already used in cuffs could further improve the capabilities of interacting with each smaller group of regenerated nerve fibers.

The conduits need not be limited to a straight path; bifurcating or diverging microchannel arrays have also been explored. In this design, the microchannels bifurcate and grow smaller as they progress distally, with the purpose of having larger groups of regenerating fibers progressively divide until small numbers of fibers are isolated in each microchannel each with an electrode for increased selectivity (Stoyanova et al., 2013). *In vitro* and *in vivo* studies demonstrated feasibility of inducing the growth and separation of nerve fibers into such microchannels (Stoyanova et al., 2013; Wieringa et al., 2010a, 2010b). Further studies have shown that the bifurcating approach could possibly be used to induce separation of based on fiber type (e.g. sensory and motor) by preferential attraction to different neurotrophic factors (Lotfi et al., 2011).

### 3.4.3. Scaffold

A variety of synthetic supportive structures have been used to facilitate the repair of injured nerves. Several regenerative PNI designs position electrodes within these scaffolds to reduce distance to the regenerated nerve, as recently reviewed by Spearman et al. (2018). Distinct from the regenerative microchannel arrays described above, this approach incorporates techniques from the field of tissue engineering, using materials such as hydrogels and collagen to mimic properties of the nerve’s extracellular matrix. Various biomolecules and growth factors can also be incorporated to further enhance nerve regeneration.

A design called the regenerative multielectrode interface (REMI) places an array of microwires, similar in form to the Utah array, projecting transversely into a scaffold of collagen inside a section of polyurethane tubing, as shown in Fig. 14a (Garde et al., 2009; Seifert et al., 2012). REMI implantations of up to 120 days were able to record single units starting at 7 days post-implantation and remained stable throughout the study duration (Desai et al., 2014). Another design places individual SU-8 and gold probes longitudinally into a biodegradable agarose scaffold and achieved robust recordings for up to 51

weeks (Cho et al., 2008).

Several designs orient thin-film planar microfabricated electrode substrates parallel to the nerve axis (Clements et al., 2013, 2007; Delgado-Martínez et al., 2017; Judy et al., 2018; Kuliasha et al., 2018). Planar electrodes like these are maximally transparent in terms of cross-section, and potentially more scalable than others since they could be stacked to access a greater volume of the nerve (Spearman et al., 2018). The regenerative scaffold electrode (RSE) places a thin-film SU-8 electrode array onto a sheet of aligned nanofibers which serve as the scaffold (Clements et al., 2007). The RSE demonstrated recording of evoked potentials during an 8-week implantation (Clements et al., 2013). A similar design to the RSE is the double-aisle regenerative electrode, which instead uses a polyimide substrate with electrodes on both sides (Delgado-Martínez et al., 2017). This design explores the use of the electrode as a septum to divide the regenerating fibers into two fascicles. The tissue-engineered electronic nerve interface (TEENI), shown in Fig. 14b, consists of multiple thread-like arms suspended in a full-volume, carefully-designed, biodegradable composite hydrogel scaffold (Judy et al., 2018; Spearman et al., 2018). A 6-week implantation of the TEENI yielded single-unit recordings with good SNR (Kuliasha et al., 2018).

### 3.5. Optical

The present discussion of PNIs has focused solely on electrical means of stimulation and recording. However, recently-devised optogenetic methods have raised the possibility of interfacing with the nerve *via* light. While the majority of optogenetics research has focused on the brain, several groups have begun to adapt the methods for use in PNIs, as reviewed by Anderson and Weir (2019). Incorporation of light-sensitive ion channels into the axonal membrane can enable optical activation or inhibition of action potentials. Likewise, incorporation of voltage- or calcium-sensitive fluorescing proteins can enable optical read-out of neural activity. So, to implement an optical PNI, the necessary components are these light-transducing proteins, a method for introducing the proteins into the targeted nerve fibers, a light source, and a microscope.

A variety of optogenetic proteins were developed to provide spectral variety and specificity and optimize their temporal response (Anderson and Weir, 2019; Yizhar et al., 2011). Incorporation of these proteins into target cells is accomplished by deployment of the genetic material (transgenes) for transcription and translation by the cell. Use of transgenic animal models is common for optogenetic research purposes and yields the most stable long-term expression of the transgenes, though practical implementation of optical PNIs will require delivery by other means, namely viral or non-viral vectors (Anderson and Weir, 2019; Yizhar et al., 2011).

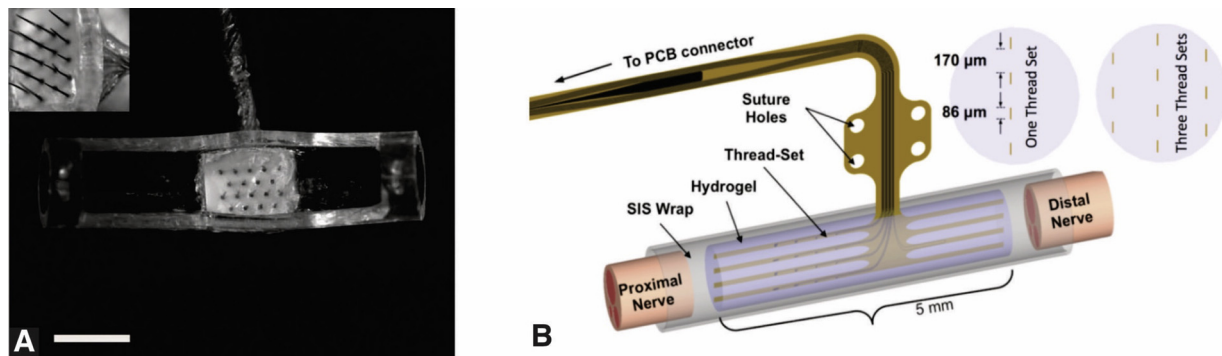


**Fig. 14.** Regenerative scaffold-type PNIs. A) Regenerative multielectrode interface (REMI) consisting of a microwire array projecting into a scaffold tube to be filled with collagen. Scale bar = 2 mm. Reprinted from (Garde et al., 2009). B) Tissue-engineered electronic nerve interface (TEENI) and cross section diagrams showing the potential for scaling by adding additional arrays. C is a reprint of Fig. 2 in: Kuliasha et al., “Robust and Scalable Tissue-Engineered Electronic Nerve Interfaces (TEENI),” 2018 Hilton Head Workshop on Sensors and Actuators, reprinted with the permission of the author and the Transducer Research Foundation.

While studies in anesthetized animals have successfully demonstrated and refined optical PNI concepts (Fontaine et al., 2017; Kapur et al., 2014; Liske et al., 2013; Sharp and Fromherz, 2011), hardware implementation of the light source and microscope in awake, freely-moving animals requires further development. For optical stimulation, extraneural silicone cuffs incorporating LEDs (Llewellyn et al., 2010; Park et al., 2015a,b; Song et al., 2018) and fiber optic connections (Michoud et al., 2018; Towne et al., 2013) were demonstrated. Optical read-out of peripheral nerve activity with an implanted device has not yet been demonstrated. A multi-modal approach may provide a stopgap until miniaturized optical PNI read-out methods are developed, such as the cuff presented by Song et al. (2018) which includes an LED for optical stimulation and platinum electrodes to record the response.

Other issues remaining to be addressed in optical PNI development include signal attenuation and distortion by the nerve tissue (Fontaine et al., 2018; Futia et al., 2018), management of heat generation during optical stimulation (Park et al., 2015a,b; Yizhar et al., 2011), and immune response to vector delivery (Anderson and Weir, 2019). Though much development remains, optical PNIs could eventually offer single-fiber resolution with low invasiveness to the nerve by combining spatial localization, optogenetic proteins that operate in distinct bandwidths, and targeted delivery of those proteins to particular sets of fibers

### 3.6. Hybrid approaches and other enhancements

Several devices combine design concepts and as such do not fit neatly into the above categories. A polyimide-based helical PNI was developed having probe shanks periodically projecting into the nerve along its length (Kim et al., 2017a,b; Park et al., 2018). The intraneural shanks potentially provide a thorough sampling of fibers throughout the nerve's cross section while the extraneural helical arrangement avoids both circumneural constriction and concentrated displacement of the nerve tissue.

A design that combines elements of extraneural cuffs and regenerative PNIs is the lyse-and-attract cuff electrode (LACE) shown in Fig. 15 (Cobo et al., 2019). The LACE is a Parylene-based extraneural cuff with integrated microfluidic channels inside which electrodes are embedded. Like a regenerative PNI, the LACE aims to induce growth of nerve fibers among its electrodes. However, it aims to do this from outside the nerve by inducing collateral sprouting of axons rather than transection and regeneration. Collagenase is delivered through the microfluidic channels to focally lyse an opening in the collagen-rich connective tissues, followed by a gradient of growth factors to induce

sprouting of the axons and growth into the microfluidic channels where the electrodes are located. Acute *in vivo* experiments with the LACE have demonstrated successful lysing of the epineurium, though chronic experiments are yet to be performed to demonstrate axonal sprouting into the channels (Larson et al., 2018).

Another proposed regenerative design without nerve transection is a direct adaptation of Kennedy's neurotrophic cone cortical probe, which aims to encourage axonal growth into a polyimide cone where several wires are housed (Jung et al., 2019, 2018a,b; Kennedy, 1989). After 19 weeks of implantation in rat, naturally-evoked potentials were captured by the electrode, and histology revealed axonal generation and minimal scar tissue inside the cone (Jung et al., 2019).

Other design enhancements which do not necessarily belong to a particular PNI category include integration of pH sensing as means of feedback towards closed-loop vagus nerve stimulation (Cork et al., 2018) and glucose sensing as a means of *in situ* inflammation monitoring around the PNI (Lee et al., 2016b).

Drug delivery is a PNI enhancement that can be used for several purposes and takes on several forms. Multiple studies have incorporated catheters into cuffs in order to modulate nerve activity with pharmacological agents (Hoffer and Kallesøe, 2001; Pohlmeier et al., 2009) and several designs use microfabrication techniques to directly integrate microfluidic channels (Cobo et al., 2019; Schuettler et al., 2011). PNI studies have also explored the use of drug-eluting coatings (Heo et al., 2016; Mensinger et al., 2000; Park et al., 2015a,b).

Aside from modulatory and regenerative goals, a common aim of drug delivery is mitigation of the host response. An early demonstration of dexamethasone elution from pacemaker leads showed a thinner fibrotic capsule, fewer activated immune cells, lower stimulation threshold, and lower interface impedance as compared with controls (Radovsky and Van Vleet, 1989). Following these results, dexamethasone coatings and various vehicles for controlled dexamethasone release from neural probes were investigated, including polypyrrole, hydrogels, and carbon nanotubes (Abidian and Martin, 2009; Luo et al., 2011; Wadhwa et al., 2006; Zhong and Bellamkonda, 2007). Park et al. (2015a,b) patterned dexamethasone-loaded coatings onto a polyimide cuff. Heo et al. (2016) developed a polyimide cuff with surface microwells and a hydrogel coating loaded with cyclosporine A, another anti-inflammatory agent. Five-week *in vivo* assessment of the microwell design showed increased ENG amplitude, decreased fibrotic thickness, and increased myelination as compared with controls (Kim et al., 2017a, b). Improved host response to PNIs has also been achieved with systemic delivery of dexamethasone (de la Oliva

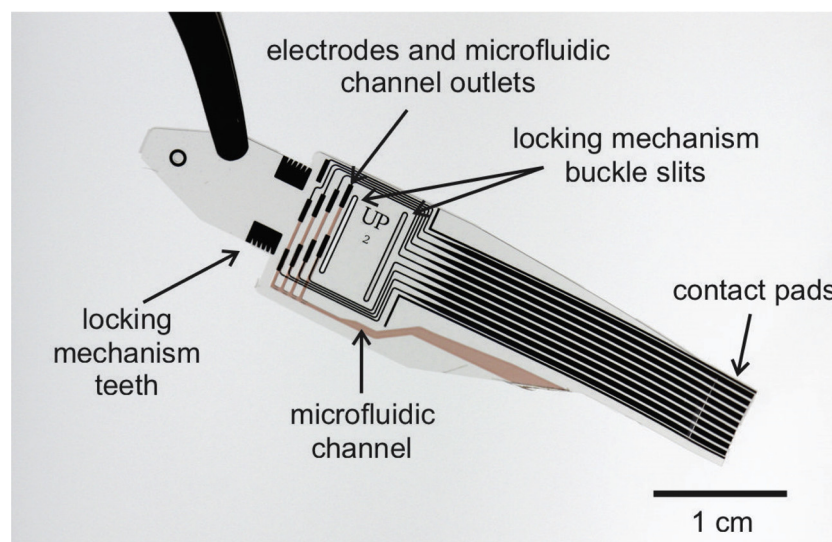


**Fig. 15.** The lyse-and-attract cuff electrode (LACE) has integrated microfluidic channels with embedded electrodes, combining extraneural and regenerative approaches to grow axons near the electrodes without nerve transection.

et al., 2019, 2018b) and anti-TNF- $\alpha$  (Vince et al., 2005).

#### 4. Characterization of peripheral nerve interfaces

Fundamental principles guiding PNI design and a survey of approaches and strategies used in PNI design were presented. Here we complement the prior discussion by highlighting concepts, guidelines, and best practices that emerged from literature and can be employed in evaluation of a PNI design both *in vitro* and *in vivo*. Many of these techniques also extend to evaluating certain aspects of other neural interface types.

##### 4.1. *In vitro* characterization

After successful PNI fabrication, a variety of *in vitro* tests evaluate a device's performance-related characteristics, either informing refinement of the design and fabrication methods or proving readiness for *in vivo* studies. The main categories of *in vitro* evaluations are electrochemical characterization, longevity testing, simulated implantations, and other tests particular to the unique features of a device.

##### 4.1.1. Electrochemical characterization

Electrochemical characterization is performed to evaluate the ability of an electrode site to deliver sufficient charge for stimulation and record signals with sufficiently low noise and estimate safe operating parameters. Common tests performed include cyclic voltammetry (CV), electrochemical impedance spectroscopy (EIS), and pulse testing. The metrics usually reported from these tests are cathodal charge storage capacity (CSC<sub>c</sub>), impedance, and reversible charge injection limit.

**4.1.1.1. Cyclic voltammetry.** CV characterizes the modes and quantities of charge transfer that occur on the surface of an electrode. A potentiostat sweeps the potential of an electrode (in solution) through a triangle wave profile between two potentials while it measures the current between the electrode (set as the working electrode, WE) and a large counter electrode (CE, typically platinum for inertness) (Elgrishi et al., 2018). A standard, specially-packaged Ag/AgCl electrode typically serves as the reference electrode (RE), though hydrogen electrodes and saturated calomel electrodes have also been used (Robblee and Rose, 1990). The applied potential drives charge transfer at the WE by mechanisms such as double layer charging and oxidation/reduction (redox) reactions, and the resulting current  $i$  is proportional to the rate at which these mechanisms occur (Cogan, 2008).

**4.1.1.1.1. Voltammogram interpretation.** The resulting voltammogram shows current plotted against potential over the entire

sweep (Fig. 16). At any point on the voltammogram, the equivalent capacitance is given by  $C = i/(dE/dt)$  where  $dE/dt$  is the scan rate (V/s) (Robblee and Rose, 1990). The negative and positive peaks are associated with reduction-oxidation reactions on the surface of the electrode, such as oxide formation and reduction and hydrogen adsorption/desorption on platinum, as illustrated in Fig. 16. At the relatively flat region (for platinum, approximately  $-0.2$  V versus Ag/AgCl in PBS),  $C$  is the capacitance of the double layer. The CV of a purely capacitive electrode will be smoother, lacking the peaks associated with redox reactions. The cathodal charge storage capacity is calculated as the negative area enclosed within the CV "loop" and is often divided by GSA to focus on the electrode material's surface quality. CSC<sub>c</sub> is roughly interpreted as the amount of charge available for a stimulation pulse. However, in practice, the equilibrium potential of the electrode from which a stimulation pulse starts limits the usable stored charge to a fraction of the total CSC<sub>c</sub> (Cogan, 2008). Strategies exist to increase use of the available CSC<sub>c</sub>, such as modified waveforms and positively biasing the electrode prior to pulse delivery (Cogan, 2008; Robblee and Rose, 1990).

**4.1.1.1.2. Water window.** The potential range swept during CV is designed to remain just inside the "water window," beyond which H<sub>2</sub> (at negative potentials) and O<sub>2</sub> (at positive potentials) gas evolve—this gas evolution is an irreversible process since the newly formed gas molecules diffuse away from the electrode surface (Hudak et al., 2010; Robblee and Rose, 1990). Because this diffusion prevents the immediate saturation and nucleation of gas bubbles, visual detection of microscopic bubble formation is not a reliable technique to estimate safe operating potentials (Robblee and Rose, 1990). Instead, excursions beyond the water window during CV may show as sharp increases in current at the extremes of the voltammogram (Hudak et al., 2010; Robblee and Rose, 1990). The water window of platinum and iridium in 1× phosphate-buffered saline (PBS, pH ~ 7.2) is taken to be approximately  $-0.6$  to  $0.8$  V versus Ag/AgCl, and in sulfuric acid (0.05 M H<sub>2</sub>SO<sub>4</sub>, pH ~ 1) it is approximately  $-0.2$  to  $1.2$  V (Cogan, 2008; Hudak et al., 2010).

**4.1.1.1.3. Factors influencing CV.** Factors influencing the CV include scan rate, solution composition and pH, temperature, and GSA of the electrode; any report of CV results should also state these parameters. A typical scan rate is 100 mV/s. Faster scan rates generally yield higher currents and may better reflect the frequencies involved in stimulation waveforms, though lower scan rates are often used to determine an estimate of CSC<sub>c</sub> (Cogan, 2008; Elgrishi et al., 2018; Robblee and Rose, 1990). Two standard solutions used for CV are sulfuric acid (typically 0.05 to 0.15 M) and PBS. Within their respective water windows, the two solutions will yield similar voltammograms. However, PBS is a closer approximation of the *in vivo* fluid environment and, outside the

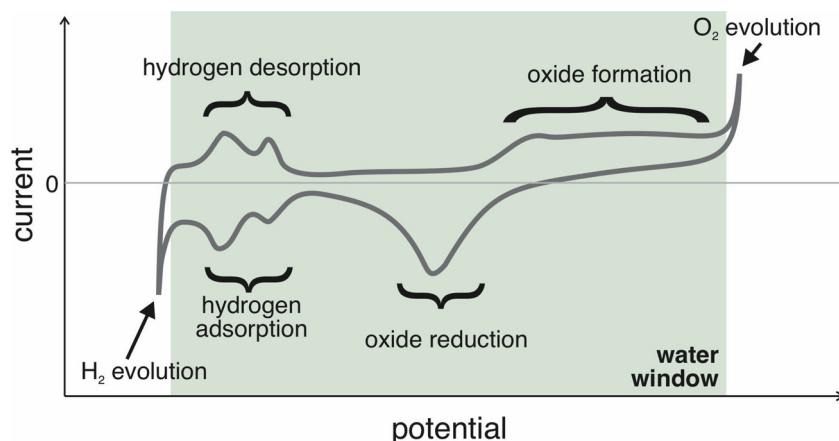


**Fig. 16.** Illustration of a typical cyclic voltammogram of a platinum electrode in PBS. Electrochemical processes corresponding to particular features are labelled. Sharp increases in current magnitude just outside the water window correspond to gas evolution.

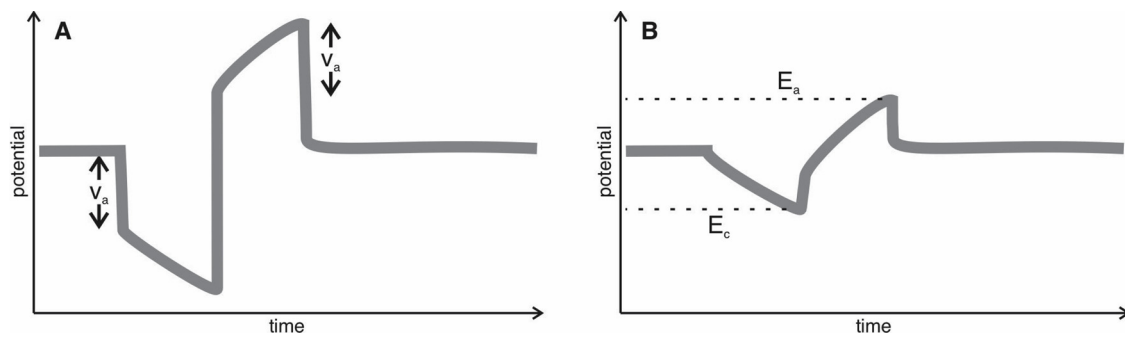


**Fig. 17.** Illustration showing removal of the access voltage ( $iR$  error) from pulse testing. A) Voltage measured during delivery of a biphasic current pulse includes offsets from the access voltage  $V_a$ . B) Same data with  $V_a$  removed, giving an accurate measure of the maximum cathodic and anodic potentials ( $E_c$  and  $E_a$ ). Most commercial electrochemical instruments offer automatic correction of this error.

water window, shows additional electrochemical activity involving chloride and phosphate which may be relevant to some electrodes and stimulation protocols (Hudak et al., 2010). Solution conductivity and redox reaction rates increase with temperature, so it is ideal to perform CV (and other electrochemical characterizations) at body temperature rather than room temperature (Cogan, 2008).

$O_2$  dissolved in solution is not inert and can interfere with the CV, so standard practice is to prepare the solution by purging with nitrogen gas, for example by bubbling pure nitrogen directly into the solution through a submerged section of polyetheretherketone (PEEK) or polytetrafluoroethylene (PTFE) tubing before and during the CV. However, when simulating the *in vivo* electrochemical environment, it should be considered that dissolved oxygen will be present. Hudak et al. (2010) compared CVs performed in PBS with nitrogen and oxygen purging, the latter of which yielded a cathodic current due to oxygen reduction that dominates at potentials below about 0.25 V versus Ag/AgCl, lowering the entire left half of the CV into the negative current range. It is suggested that the high amount of oxygen reduction in this range may not easily be reversed and may be a mechanism of stimulation-induced tissue damage; further investigation is warranted. Another possible source of distortion in CV is inaccurate potential measurement due to “ohmic drop,” also called  $iR$  error, which arises from the solution resistance between the WE and RE. To minimize this effect without changing the solution conductivity, the WE and RE should be positioned close together (Elgrishi et al., 2018). Many commercial electrochemical instruments offer automatic compensation of this error (*iR Compensation: Potentiostat Fundamentals / Basics of EIS*, 2019).

**4.1.1.1.4. Electrode cleaning.** Besides characterization, CV is also used to electrochemically clean electrodes and is a recommended step before other electrochemical characterizations (Rose and Robblee, 1990). During fabrication, by-products of machining processes or other contaminants from handling may deposit on the electrodes, decreasing the effective surface area. Cleaning is usually performed in sulfuric acid. As the cycles progress, cleaning of the surface is evidenced by increased currents. Depending on the initial electrode cleanliness, 30–50 cycles is usually sufficient to reach stabilized currents.

**4.1.1.2. Electrochemical impedance spectroscopy.** In electrochemical impedance spectroscopy (EIS), the impedance and phase of an electrode in PBS is measured in response to a small ( $\sim 10$  mV) sinusoidal signal across a range of frequencies (typically 1 to  $10^5$  Hz) (Cogan, 2008). The impedance at 1 kHz is typically reported to serve as an approximate predictor of an electrode’s recording merits, with 1 kHz presumably chosen to represent the frequency range of neural activity. Low impedance is generally desirable, however this is traded off with factors such as electrode size and placement. Consequently, a wide range of 1 kHz impedances is found in literature, ranging from single k $\Omega$  to tens of M $\Omega$ . The 1 kHz impedance is limited in its usefulness as it may not even indicate broken electrode leads, especially when the

intact electrodes have relatively high impedance (Straka et al., 2018; Takmakov et al., 2015). Another confounding factor in interpretation of EIS is that the reported impedance is contributed by the entire conductive path including the traces and insulation; compromised insulation may be difficult to isolate among other factors. Since most PNIs involve some polymer construction and polymers are not hermetic, EIS contributions arising from the polymer must also be considered. The impedance and phase data gained from EIS are perhaps most powerful when used to derive equivalent circuit models, yielding insight into electrode surface characteristics and insulation quality (Franks et al., 2005; Ortigoza-Diaz et al., 2018; Straka et al., 2018).

**4.1.1.3. Pulse testing.** The goal of pulse testing is to directly estimate the range of parameters for stimulation that can be delivered without excursion of the electrode potential beyond the water window. Current pulses are delivered to the WE, submerged in PBS with a RE and large return electrode, while the resulting potential transients are measured and compared to the water window. The ohmic drop (sometimes called “access voltage” to include other sources of offset) between the WE and RE can add a significant offset to the measured potential during cathodic and anodic pulses. Since this test relies on accurate measurement of the electrode potential, simply placing the WE and RE close together will not suffice as with CV. If the electrochemical instrument being used does not offer automatic  $iR$  compensation, the offset should be manually subtracted from each phase as demonstrated by Rose and Robblee (1990) and illustrated in Fig. 17. As noted by Cogan (2008), the value of this offset may be made clearer by inserting a brief interphase period during which  $i = 0$ ; the nearly instantaneous change in potential at the start of this period is the offset to be subtracted.

Another possible indicator of unsuitable stimulation parameters to be found during pulse testing is drift of the electrode’s equilibrium potential. For example, a long interphase period ( $> 1$  ms,  $i = 0$ ) will allow the potential to settle to an equilibrium. If the potential after cathodic pulses of the same charge per phase settles to different equilibria, irreversible charge transfer is likely occurring (Cogan, 2008).

As previously stated, solution conductivity and reaction rates increase with temperature, so pulse testing at room rather than body temperature may underestimate the range of suitable stimulation parameters. This may be especially true for porous electrodes which rely temperature-sensitive transport mechanisms occurring within their pore structure (Cogan, 2008).

#### 4.1.2. Longevity testing

The warm, saline, chemically active *in vivo* environment is inhospitable toward devices and over time can induce multiple failure modes including electrode damage and insulation breakdown. However, current benchtop models to simulate this environment are limited. Even so, there is utility in conducting exposure studies to determine

improvements to device construction and performance that will maximize success of future animal studies.

**4.1.2.1. Simulating the *in vivo* environment.** A basic simulated *in vivo* environment is a PBS bath set at 37 °C. In accordance with the Arrhenius equation, the chemical reactions involved in device aging can be exponentially accelerated by increasing temperature (Takmakov et al., 2015). To approximate the equivalent rate of aging imparted by elevated temperature, the “ten degree rule” states that every increase of 10 °C above the reference temperature doubles the rate of aging reactions in polymers (Hukins et al., 2008). Mathematically expressed, the ten degree rule’s accelerated aging factor  $f_{aa}$  is given by

$$f_{aa} = 2^{(T-T_{ref})/10}$$

where  $T_{ref}$  is body temperature. 57–87 °C is a common temperature range for accelerated aging as it provides a significant increase in testing throughput ( $f_{aa} = 4–32$ ) while being relatively safe for handling and avoiding initiation of other chemical processes that may invalidate the approximation, such as boiling. Selection of temperature should take into account the suggested operating temperature range for the materials and whether thermally induced changes to the materials can result that are not representative of expected *in vivo* failure modes.

Takmakov et al. proposed an enhancement to the simulation of *in vivo* device aging by including reactive oxygen species (ROS) in the solution—namely, hydrogen peroxide (Street et al., 2018; Takmakov et al., 2015). ROS are released by activated immune cells and are likely one of the agents responsible for *in vivo* device failure, so raising the performance standard by evaluating devices against harsh simulated environments including ROS should yield improved chronic performance.

**4.1.2.2. Evaluation techniques.** Several techniques are used to evaluate device performance and function during longevity testing. The first is EIS. Impedance tends to decrease over time for many devices when soaked. This decrease is thought to be attributed to insulation compromise that effectively increases the area of the electrode, but EIS alone does not provide enough information to differentiate among delamination, cracks, or moisture absorption through the bulk of the material, nor does it give information about the location of insulation defects (Takmakov, 2017). Matching the Bode plot of an electrode to that of an equivalent circuit model may lend some insight (Ortigoza-Diaz et al., 2018; Straka et al., 2018). As previously noted, monitoring impedance only at 1 kHz is insufficient to capture significant changes in electrode condition (Straka et al., 2018; Takmakov et al., 2015). Takmakov et al. (2015) found impedance at frequencies < 10 Hz to be most sensitive to aging processes.

Comparison of slow and fast CVs can also provide insight into electrode failure over time. In an example given by Cogan (2008), a scan rate of 50,000 mV/s provides information only on the exposed electrode site and should change minimally over time if the electrode surface is stable, or show decreased currents in the case of deterioration. On the other hand, a scan rate of 50 mV/s will access areas of the conductor where the insulation has been compromised by delamination or solution ingress, showing increased current magnitudes as the insulation deteriorates.

While EIS and CV may capture decreased impedance suggestive of compromised insulation, these data do not necessarily indicate a functional failure—an electrode with imperfect insulation may still be able to sufficiently stimulate and record. The functional deficit of concern with compromised insulation is loss of electrical isolation among electrodes, or cross-talk. Cross-talk degrades stimulation and recording selectivity by spreading the signals from one electrical channel to others, and so any attempts in the PNI design to increase selectivity will be negated. EIS performed between two electrodes may quantify changes in their mutual isolation, however the solution path

between the exposed electrode sites will likely obscure the smaller changes of interest which arise from insulation defects. To avoid this problem, test structures with insulated electrodes may be included, or interdigitated electrodes insulated by the same material can be used. These alternatives do not accurately represent the devices to be implanted, however, and may not reproduce the same failure modes. As of yet, no standard technique has emerged to monitor the development of cross-talk among electrodes in complete, unmodified devices.

Interpretation of data from the above techniques is helped immensely by visual inspection of the device *via* microscopy. Simple optical inspection can be performed repeatedly throughout the trial and may reveal the progression of structural damage. However, some feature sizes and damage indications may require the higher resolution of scanning electron microscopy (SEM) which, for many device types, is destructive and thus can only be performed at the end of the testing period.

#### 4.1.3. Simulated implantation

Since durability during handling and simplicity in surgical implantation are key determinants of PNI success (Section 2.6), a recommended benchtop study is to simulate the installation process. While a section of compliant tubing may provide the simplest geometrically-similar nerve phantom, fabrication of phantoms that mechanically approximate peripheral nerve is non-trivial due to inhomogeneous tissue composition and anisotropic mechanical properties. For example, agarose gel, which is often used as a phantom for other neural tissues, can be made to have similar transverse compressibility but lacks similar longitudinal tensile strength. A nerve phantom used by Cobo et al. (2019) to simulate dye absorption on the nerve surface consisted of paper tissue wrapped around a silicone core. In the field of anesthesia, a creative variety of nerve-in-tissue phantoms are used for training of local anesthetic delivery including gelatin, tofu, pork loin, and processed meats (Pollard, 2008; Rathbun et al., 2018; Sparks et al., 2014; Wells and Goldstein, 2010). 3D printing of hydrogels and composite structures may also offer a new method to fabricate more accurate nerve-like models. Until more refined nerve phantoms are developed, the most accurate implantation simulations are performed on cadaver nerve.

#### 4.1.4. Other *in vitro* tests

In addition to the generalized *in vitro* tests described above, the PNI designer should carefully consider what other tests should be performed to validate idiosyncratic features of a device. Examples from literature include neuron cultures to study regenerative approaches (Wieringa et al., 2010b), flow and pressure characterizations for microfluidic channels (Cobo et al., 2019), deformation tests for delicate structures (Ordonez et al., 2014), and force tests for insertion and anchoring mechanisms (Cutrone et al., 2015). Packaging components such as cables and connectors should also be subjected to a battery of bench top tests, as exemplified by Pena et al. (2017). It is noted that none of the *in vitro* tests mentioned can adequately simulate potential host response issues or disruption of devices by behaving animals.

## 4.2. *In vivo* characterization

Borrowing the FDA’s framework, the goals of *in vivo* characterization are to discern a PNI’s merits in terms of safety and efficacy. More specifically, this includes the PNI’s effects on nerve health and function, and its ability to initiate and measure nerve activity. Presented here is an introductory set of considerations and best practices which emerge from literature regarding *in vivo* characterization. Successful animal studies will depend on decisions made early in the development process, such as animal model selection. The reader is advised to consult examples in literature for more detailed guidance regarding methods of animal studies. Additionally, works by Loeb and Gans (1986) and Hoffer (1990) are recommended for foundational techniques and

practical tips.

#### 4.2.1. General considerations for *in vivo* studies

Some general considerations for *in vivo* studies include animal model selection, packaging, and device sterilization.

**4.2.1.1. Animal model selection.** Several factors should be considered when deciding whether to adopt one animal model or select another. Rat sciatic nerve has become the default model for PNI studies, offering a well-characterized, inexpensive, trainable mammalian model with established, consistent strains, a workable size-scale, and compliant behavior (Varejão et al., 2001). Concerning size and morphology, cat and rabbit models offer a larger size scale compared with rats, allowing implantation of multiple PNIs or interface with more distal, differentiated branches. Prior to the 1990s, cat was the model of choice for PN studies as its size accommodated the bulkier technologies of the time and the model was supported by a substantial body of research (Hoffer, 1990). Pig median nerve has been used to better approximate the large diameter and high fascicle count of human median nerve (Kundu et al., 2014). On the other hand, smaller animals (e.g. mice and song birds) may offer other desirable traits which must be weighed against the challenges that accompany smaller nerves and bodies, including microsurgical techniques and strict packaging weight limitations.

For long term experiments, it is important to select an animal model that will not grow substantially throughout the implantation period, as this will require length accommodation from the cabling and possibly other dimensions of the device. For this reason, it is advisable to implant in fully- or near-fully grown animals. Both male and female rats exhibit asymptotic growth trajectories, though female rats may be preferred over males since they remain smaller and their size stabilizes more quickly (Reichling and German, 2000). A controlled diet may slow the rate of growth, but final size will remain the same (Reichling and German, 2000).

Another factor in animal and nerve selection is the set of techniques that will be used to evaluate nerve health and device performance. Some useful characterization techniques found in literature (Sections 4.2.2 and 4.2.3) depend on particular behaviors such as fine motor tasks, walking patterns, or birdsongs (Lissandrello et al., 2017; Varejão et al., 2001; Wurth et al., 2017). Others depend on particular limb sizes and nerve targets in order to use specially-built measurement apparatuses (Grill and Mortimer, 1996b; Riso et al., 2000). PNIs intended for particular bioelectronic medicine applications must select from a subset of animals that offer an appropriate disease model.

Regenerative PNI studies are especially sensitive to animal model selection. Early regenerative studies experienced difficulties in mammals due to connective tissue proliferation while more success was achieved in amphibians (Stein et al., 1975). However, mammal models are preferable, assuming a goal of eventual use in humans. Tos et al. (2009) gave an account of multiple animal models used in nerve regeneration studies. While Lewis, Sprague Dawley, and Wistar rat strains are all used in PNI studies, regenerative PNI studies almost exclusively use Lewis rats, reportedly because they exhibit the least-problematic behavioral response to the limb numbness which follows nerve transection.

In summary, several animal models exist and selection can be guided by examples in literature that share similar goals. The animal model will dictate device dimensions and packaging design and should be decided upon at the beginning as designs may not always be interchangeable across models.

**4.2.1.2. Packaging for *in vivo* studies.** It is common for long-term *in vivo* studies to terminate not because of interface failure, but instead because of a packaging failure such as lead breakage (Bradley et al., 1997; Desai et al., 2014; Grill and Mortimer, 2000; Hoffer, 1990; Kuliasha et al., 2018; Stein et al., 1978). Therefore, careful

consideration of packaging is critical to gaining useful *in vivo* results, especially in chronic studies, and deserves significant attention from the PNI designer (Mortimer et al., 1995). Since PNI outcomes are so sensitive to packaging, successful packaging designs and experiences should be reported in detail to advance the field.

**4.2.1.2.1. Device-level connection.** In early PNI designs consisting of wires stitched into the wall of a silicone cuff, the lead wire and electrode were a single continuous conductor. In most other PNI designs, the electrodes and leads are separate conductors which must be electrically and mechanically connected. Since most contemporary and next-generation devices are microfabricated, “breaking out” microscale electrodes to interface with macroscale components is non-trivial. Most thin-film polymer devices include a short ribbon cable which carries the leads away and scales up the conductive traces to facilitate connection to macroscale leads.

Traditional ultrasonic and thermal wirebonding techniques used in the semiconductor industry are a well-established option for PNIs which have a rigid substrate, such as the Utah array. A similar method of connection is resistance welding, which involves application of pressure and a high current pulse to heat up the contact point between a wire and the electrode (Loeb and Gans, 1986; Ordonez et al., 2014; Rozman et al., 2018). However, the thin metals and flexible substrates of thin-film polymer devices may be prone to failure during these processes (Ortigoza-Diaz et al., 2018).

The “MicroFlex” technique introduced by Meyer et al. is an adaptation of wirebonding for flexible devices. A ball bond acts as a rivet through a hole in the thin-film conductor, connecting it electrically and mechanically to a rigid substrate (Meyer et al., 2001; Schuettler et al., 2008). This substrate may be an integrated circuit or an intermediate connector between the device and larger lead wires, such as the ceramic interconnect plate with screen-printed conductive tracks described by Yoshida et al. (Boretius et al., 2012; Yoshida et al., 2006).

Another tactic for device-level connection is to design the PNI for compatibility with off-the-shelf electrical connectors. In particular, the back end of thin-film polymer PNIs can easily be designed to mimic standard flat flexible cables (FFCs), and thus can be inserted into FFC connectors such as zero insertion force (ZIF) connectors (Gutierrez et al., 2011; Ortigoza-Diaz et al., 2018). Currently-available ZIFs are best mounted on printed circuit boards (PCBs) which can be used to facilitate connection to lead wires.

For all connection methods, the connection sites must be thoroughly potted with biocompatible epoxy and/or silicone to insulate the exposed conductors from fluids and tissues. Potting also lends crucial mechanical support to the connection and provides a smooth surface to minimize tissue irritation, though bulky potting should be avoided.

Based on the literature on packaging of neural interfaces, a few best practices are suggested. First, the materials used at the connection site should be biocompatible, which excludes many standard non-medical materials, such as solder and conductive epoxy. Second, junctions between dissimilar metals should be avoided. If such a junction comes into contact with saline, it will produce a battery effect, leading to a low-but-steady DC current and thus metal corrosion and possible tissue damage (Loeb and Gans, 1986). Finally, mechanical discontinuities should be avoided, as these present preferential bending sites. For this purpose, a tapered layer of silicone may be used to support a gradual transition between stiff and flexible regions. If including non-biocompatible materials or bi-metallic junctions, as would be the case with a PCB-mounted ZIF connector, these delicate connections must be thoroughly potted and insulated to prevent contact with body fluid. Potting may be sufficient for studies of limited duration but are a likely site of failure in long term studies. Overall, we note that the limited methods and materials available to the PNI designer make chronically reliable packaging a challenge and there is a need to develop more options for device-level connections.

**4.2.1.2.2. Cabling.** Electrode leads conduct signals from the PNI to a percutaneous connector and their design and placement is crucial to

PNI success (Naples et al., 1990). Multi-stranded lead wires, as opposed to solid core, exhibit best flexibility and dependability. A long-time standard wire for this purpose has been the stainless steel, multi-stranded, 40 AWG Cooner Wire AS 631. From the 1970s to the present, the most successful multi-conductor cable formation has been helically wound (individually insulated) wires embedded in silicone, thanks to its accommodation of bending, twisting, stretching, and, to a lesser degree, crushing (Boretius et al., 2012; Brindley, 1977; Donaldson, 1983). A modular connector for this type of cable is described by Donaldson (1985).

Mechanical force transmitted from the cable to the PNI and therefore the nerve has been suspected as a primary cause of nerve damage by PNI (Grill and Mortimer, 2000; Mortimer et al., 1995). Besides maximizing cable flexibility, careful cable placement can also help minimize this force transmission. The cable should be routed to leave the PNI longitudinally, though it also should not contact the nerve (Hoffer and Kallesøe, 2001; Naples et al., 1990). Moreover, increased strain relief has been achieved by routing the cable to leave the PNI's distal end and then form a 180° loop for routing in the proximal direction, anchored with a suture to the muscle (Grill and Mortimer, 2000; Larsen et al., 1998; Romero et al., 2001). Commercial VNS systems similarly advise installation of several strain-relief anchor points and formation of a strain-relief loop in the cable (VNS Therapy System Epilepsy Physician's Manual (US), 2018). Letechipia et al. devised a "spring-sleeve" cable connector which includes a strain relief mechanism and was used successfully in human studies (Letechipia et al., 1991; Tan et al., 2015).

**4.2.1.2.3. Percutaneous connection.** While some modular implantable wireless systems for electrophysiology are becoming available (Micro-Leads Research Products, 2019; Triangle BioSystems International, 2019; Pederson et al., 2019), percutaneous connection currently remains the most straightforward approach for most animal studies. In a rat model, percutaneous connector mounts or pedestals may be placed on the head or the back. While head-mounted connectors may limit tampering and damage by the animal, back-mounted connectors avoid repetitive cable bending at the neck, and the shorter cable is less susceptible to "antenna" noise. In general, a percutaneous connector should be located at a point where skin movement is minimal (*i.e.* the midline), require as small a skin opening as possible, not have any sharp or irritating edges, and be easy to clean. Commercial pedestals are available which are generally designed for screw- or dental cement-mounting onto solid bone—typically the skull, though the pelvis may also be suitable (Barrese et al., 2013; Seifert et al., 2012). Recently, high-resolution 3D printing services offer a convenient means to produce custom plastic and/or metal connector mounts (Straka et al., 2018; Vasudevan et al., 2016; Wurth et al., 2017). For mounting to the lumbar fascia instead of bone, a sheet of surgical mesh cloth may be attached to the bottom of the pedestal which is placed under the skin and encourages tissue ingrowth for stabilization (Straka et al., 2018). A back-mounted pedestal, or at least its top, is best made of metal to protect the connector from gnawing by the animal (Straka et al., 2018; Yaghouby et al., 2018). It is good practice to apply a coating of silicone to any surface of the pedestal that will contact soft tissues (Straka et al., 2018; Yaghouby et al., 2018). If a pedestal is not suited to the site, as with percutaneous connections located on a limb, Tan et al. (2015) reported use of individually-passed open-matrix helical leads which minimize the opening size and allow skin to better anchor the connection, thereby avoiding piston-like motion of the lead and decreasing the risk of infection.

The same considerations also apply to the connection between the cable and the external connector. If possible, the electrical junction between the two should be positioned outside the skin so that compromised potting poses less of a risk (Loeb and Gans, 1986). The customizability of 3D-printed pedestals makes it possible to mount any off-the-shelf external connectors for connection to electrophysiology equipment. In general, connectors which require significant force to

connect and disconnect from an external cable should be avoided, as this increases the risk of injuring the animal or breaking the mount. Loeb and Gans (1986) recommend that the mechanical and electrical roles of an external connector should be carried by separate elements in order to avoid wear and motion artifacts. Furthermore, the mechanical anchoring should be easily overcome in order to avoid damage or injury in the process of connection/disconnection, or in the case that the animal applies tension (Loeb and Gans, 1986). One possible solution is to use magnetic mating between the connector mount and the cable, easily achieved by placing magnets into the face of the connector mount and the mating face of the external cable (Yaghouby et al., 2018).

**4.2.1.2.4. Fluidic packaging.** Though there are fewer examples in literature, connections for fluidic access to a PNI presumably follow many of the same guidelines as electrical packaging. In contrast to the out-of-plane connections often used to connect to chip-type microfluidic devices, Cobo et al. (2019) made an in-plane connection to the Parylene microfluidic channel of an extraneural cuff by inserting a length of catheter and sealing it with a flexible, biocompatible cyanoacrylate glue (Loctite 4902). At the other end of the catheter, a number of different methods exist to drive infusion, including implantable active or osmotic pumps, subcutaneous injection ports (Pohlmeyer et al., 2009), or standard percutaneous ports for connection to an external pump. For rats, a backpack-like harness is conventionally used to support connection between a percutaneous catheter and an external catheter/tether system for continuous infusion. Harnesses may require supervision and regular human intervention to fix problems such as skin irritation and entanglement of limbs or teeth in the straps (Bellinger, 2015). An alternative to the infusion harness is a back-mounted pedestal-like infusion button, which omits the problematic straps and may be protected and kept clean with a magnetic metal cap (Instech Laboratories Inc., 2019).

An additional consideration for fluidic devices is maintaining patency. For this purpose, Hoffer and Kallesøe (2001) recommend periodic saline flushes to prevent connective tissue ingrowth from clogging the outlet.

**4.2.1.3. Device sterilization.** *In vivo* studies typically require thorough sterilization of the components to be implanted. Selection of an appropriate sterilization technique depends on multiple factors. Autoclaving is a widely available method which has been used to sterilize silicone and platinum foil devices, however the high temperature and moisture of autoclaving may damage other PNIs. Lower-temperature, dry methods include ethylene oxide and hydrogen peroxide plasma processes, with hydrogen peroxide plasma becoming the preferred choice for environmental and safety reasons. Electromagnetic radiation methods are often not ideal for PNIs as they tend to degrade many polymers (Ortigoza-Diaz et al., 2018). Whichever method is chosen, characterization should be performed before and after sterilization to confirm that the integrity of the device (and packaging components) remains intact.

#### 4.2.2. Characterizing PNI safety

A primary aim of *in vivo* studies is to characterize a PNI's effects on nerve health and function. The methods for accomplishing this can be grouped into functional tests, electrophysiological tests, and histology. In all of these characterizations, experimental controls should be carefully conceived and executed in order to elucidate the cause of any damage to the nerve. For further reading, an exceptionally thorough and authoritative reference on the topic of nerve injuries is provided by Sunderland (1978).

**4.2.2.1. Functional tests.** Of the methods used to evaluate PNI safety, functional tests are the most indirect, aiming to infer information about nerve health by observing the end results of nerve activity, *i.e.* sensory responses and motor tasks.

The general form of sensory tests is to apply a stimulus to the distal

part of the limb, and either quantify the degree of response or vary the stimulus intensity to determine the threshold at which a certain response is achieved. For example, the traditional von Frey test consists of poking the foot with a series of monofilaments of increasing stiffness and noting the stiffness which provokes a response (Chaplan et al., 1994; Nedic et al., 2013). A similar “foot flick” test uses electrical shock as the stimulus (Sta et al., 2014). Lago et al. (2007b) describe a pinprick test in which the foot is pricked at five different points, each response is scored on a simple 0–2 scale (absent, decreased, or normal), and scores are summed. Algesiometry tests follow a similar process but aim to separate pain fiber activation from mechanical stimulation, for example by irradiating the foot with heat and measuring the time to response (Lago et al., 2007b).

The primary functional motor test for the rat model is walking track analysis, in which video of the rat’s gait viewed from below is analysed for parameters such as foot spreading and toe spacing (Varejão et al., 2001; Vasudevan et al., 2017). These parameters are fed into a calculation which yields a value called the sciatic function index (SFI). Manifestation of nerve health in finer motor control tasks may be observed by kinematic tests. For example, Wurth et al. (2017) reported filming the rat’s leg motion (marked with infrared markers) as it ran over a ladder of unevenly-spaced rungs. The percentage of missed steps was taken as an indicator of motor control.

Overall, existing functional tests offer more qualitative value than quantitative as they are susceptible to a number of behavioral variables which cannot be tightly controlled. They also tend to quantify responses into broad ranges (i.e. absent, diminished, or normal function) and thus have low sensitivity. Furthermore, while each variety of functional test seems to emphasize one modality of nerve fiber over others, the output is truly a measure of entire-circuit function. For example, a diminished response to a pain stimulus does not necessarily correlate to damaged pain fibers; rather, it may be the motor fibers which are damaged and cannot conduct reflexive signals to the limb. Similarly, diminished motor control may be an indication of damaged motor neurons, or it may actually be a consequence of absent sensory feedback.

**4.2.2.2. Electrophysiological tests.** Electrophysiological tests possibly offer a more direct and quantitative measure of nerve health. The essence of nerve damage is degeneration and demyelination of nerve fibers, and these changes in the nerve’s fiber population can potentially be detected in electrophysiological measurements (Somann et al., 2018). The general form of these tests is to proximally/distally evoke action potentials in the nerve trunk and distally/proximally record the signals which are conducted across the implant site. Alternatively, a signal evoked at a third site may be recorded both proximally and distally to the implant site, providing a more direct comparison. A compound action potential (CAP) resulting from evocation is a relatively large signal which is the summation of the extracellular signals of all recruited fibers. Peak amplitude of the CAP depends in part on the synchronized arrival of individual APs at the recording electrode. Thus, variation among fibers’ conduction velocities gives rise to desynchronization which increases with distance from the stimulation site, accompanied by temporal spreading of the CAP and decrease of its peak amplitude. Alternatively, the integrated rectified value of a recorded CAP provides a more reliable reflection of the quantity of nerve fibers which are carrying a signal. Thus, a decrease in the CAP area as it crosses the implant may indicate fiber degeneration. Demyelination of fibers without complete degeneration manifests as a decrease in conduction velocity, which may be directly measured by multiple recording sites or observed as an increased latency in a portion of signals contributing to the CAP.

A limitation of using electrophysiological tests to evaluate nerve health is difficulty in achieving reproducible recording and stimulation on either side of the PNI. Acute insertion of needle probes is highly sensitive to changes in placement between tests. Surface EMG may be a more reproducibly recordable distal signal but yields limited

information (Krarup and Loeb, 1988). For a longitudinal study, the most effective option may be implantation of simple, well-characterized extraneural cuffs proximal and distal to the PNI under test, if space allows. Krarup et al. provided a rigorous example of this approach in a series of studies observing the conduction of cat nerve through nerve injury and recovery using multiple implanted cuffs and patch electrodes (Krarup et al., 1989, 1988; Krarup and Loeb, 1988). Experimental methods and controls should be firmly established to minimize any confounding nerve damage from the implanted electrodes other than the PNI under test.

**4.2.2.3. Histology.** The most direct and precise method of measuring a PNI’s effects on nerve health is visual observation of the nerve’s microanatomy. Histological methods for peripheral nerve vary widely, and once again the reader is advised to follow specific examples in literature which possess similar histological goals, and to consult further resources on the topic (Cold Spring Harbor Protocols, 2019; Ghnenis et al., 2018; Highley and Sullivan, 2018; Raimondo et al., 2009; Yuste, 2011). In general, excised nerve is prepared through a multi-step process of fixation, dehydration, embedding, sectioning, and staining. An osmium tetroxide pre-stain prior to embedding is recommended in most cases (Raimondo et al., 2009). Embedding is most often performed in paraffin, resin, or optimal cutting temperature medium (Highley and Sullivan, 2018; Raimondo et al., 2009). Transverse sections should be taken at three positions: proximal to, distal to, and at the location of the implant (Grill and Mortimer, 2000; Larsen et al., 1998; Naples et al., 1990). A longitudinal section at the implant site may also be valuable (Grill and Mortimer, 2000; Vasudevan et al., 2017). Silver-based preparations have been largely replaced by a number of simpler and more reliable stains, the most common of which are hematoxylin and eosin (H&E), Masson’s trichrome, and toluidine or methylene blue, though H&E does not stain myelin (Highley and Sullivan, 2018; Raimondo et al., 2009). Immunohistochemical labelling has become increasingly favored for its ability to differentially visualize specific cellular features and biomarkers, providing more detailed information about the nerve’s structural condition and immune response to an implant (Christensen et al., 2014; Highley and Sullivan, 2018; Raimondo et al., 2009; Wurth et al., 2017). In addition to post-sacrificial labelling, Somann et al. (2018) demonstrated administration of fluorogold tracer several days prior to sacrifice, revealing axonal transport as an indicator of fiber integrity across the implant site.

Variety is also found regarding microscopy techniques. In addition to light microscopy, transmission electron microscopy has also long been used to provide the highest resolution and is most effective to visualize small, unmyelinated fibers (Raimondo et al., 2009; Thomas, 1963). Confocal microscopy, in combination with immunofluorescent labelling, offers three-dimensional imaging and differentiation of structures and cells. Multiphoton microscopy (MPM) also offers imaging at depth up to several hundred microns. MPM additionally enables imaging by second harmonic generation (SHG) which acts as a non-photobleaching, label-free contrast (Vijayaraghavan et al., 2014). In SHG, emission from molecules of non-centrosymmetric structure is exactly half the excitation wavelength. Collagen has such a molecular structure and thus the collagen-rich connective tissue of peripheral nerve is well-suited for SHG imaging (Vijayaraghavan et al., 2014). Jung et al. (2014) applied tissue-clearing techniques to enhance imaging depth of whole-mount nerve after transection and regeneration.

As an alternative to the necessarily destructive techniques of nerve excision and sectioning, Vasudevan et al. (2019) presented a method for real-time *in vivo* imaging of nerve using optical coherence tomography (OCT) and a mechanically-stabilizing fixture. This method provides another mode of nerve health characterization by using OCT angiography to measure changes in microvasculature and blood flow.

After cross-sectional images of the nerve are acquired, morphometric (also called stereologic) analysis should be performed. The fiber

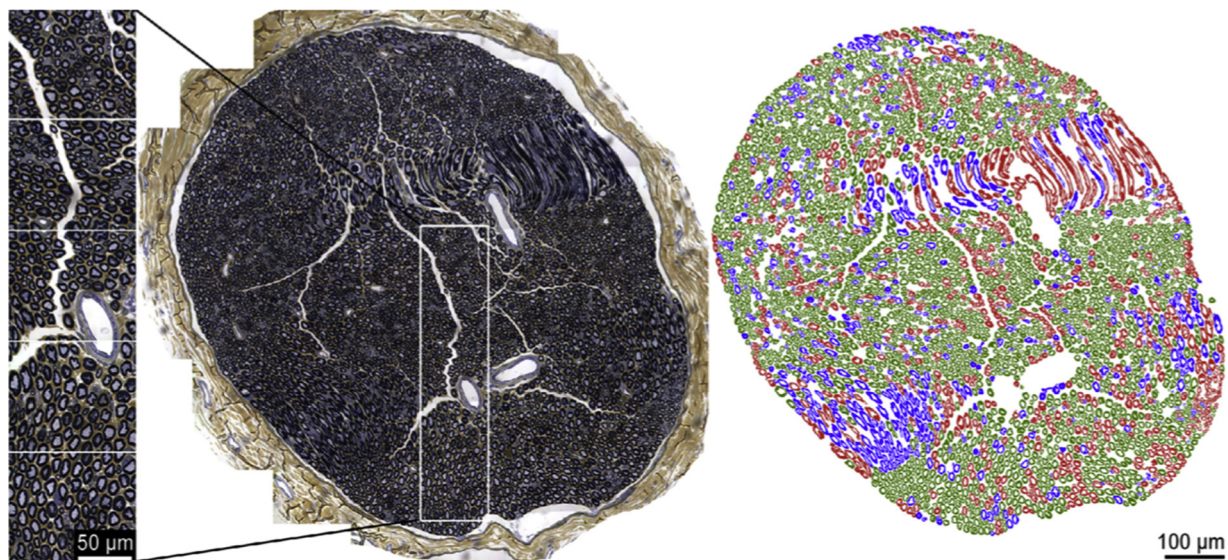


**Fig. 18.** In this example of software-aided morphometry, tiled images were stitched together to form an image of the whole nerve, followed by isolation of individual fibers and sorting into rejected (red), suspect (blue), or accepted (green) categories based on parameters that indicate distortion from sectioning or imaging. The suspect category is manually sorted by the researcher and the other categories are confirmed before morphometric analysis is performed. Reprinted from (Christensen and Tresco, 2018) with permission from Elsevier.

population is quantified in terms of number, density, size distribution, and myelination. A commonly reported measurement is the g-ratio which is the axon diameter divided by total fiber diameter which includes the myelin sheath (Raimondo et al., 2009). Previously, morphometry was a tedious, manual process prone to error and bias. Algorithms for sampling and counting were developed to standardize the process and remove bias, and readily-available software tools for image analysis have since improved efficiency (Christensen and Tresco, 2018; Jung et al., 2014; Larsen, 1998; Raimondo et al., 2009; Silva et al., 2007; Wurth et al., 2017). Shown in Fig. 18, Christensen and Tresco (2018) demonstrated an image processing method to help the researcher isolate and sort fibers prior to morphometric measurements.

#### 4.2.3. Characterizing PNI efficacy

For most PNIs, evaluation of efficacy includes stimulation and/or recording performance, plus long-term stability.

**4.2.3.1. Stimulation performance.** A common gauge of stimulation performance *in vivo* is the recruitment curve, which is an s-shaped plot of output signal as a function of the stimulation charge (or other stimulus parameter such as amplitude, duration, or frequency). The measured output may be neural CAP area, EMG amplitude, limb motion, muscle force, or joint torque, however these should not be taken to be equivalent or reliably correlated (Loeb and Gans, 1986). EMG for stimulation characterization can be recorded by multiple patch or wire electrodes implanted on/in the main muscles innervated by a nerve (Kundu et al., 2014; Loeb and Gans, 1986; Wurth et al., 2017). Limb motion can be recorded by film or multi-camera motion-capture systems for subsequent analysis and quantification (González-González et al., 2018; Wurth et al., 2017). Muscle force has been measured by attaching the tendons to load cells or by implanting tendon force transducers, though success with these methods was limited to acute or sub-chronic studies (Grill and Mortimer, 1996b; Hoffer, 1990; Loeb and Gans, 1986; Veraart et al., 1993). Grill and Mortimer (1996b) introduced an apparatus for non-invasive three-dimensional isometric joint torque measurements of the cat foot consisting of an aluminium boot coupled to a 3D force transducer. They found that the peak of the torque measurement correlated well with its time integral and thus served as a sufficient representation of fiber activation. Stieglitz et al. (2003) developed a similar apparatus for rat.

A shallow slope in the recruitment curve is generally desirable as it corresponds to more finely graded control of fiber recruitment. The recruitment curve also provides an indication of stimulus efficiency in terms of threshold and the amount of stimulus needed to achieve significant activation. Another desirable characteristic is to have one recruitment curve left-shifted from all other curves which arise from a particular stimulation condition (e.g. a given electrode or combination of electrodes). This indicates an ability to selectively achieve that output.

Quantification of selectivity varies based on the mode of output measurement. A common calculation in cases which involve multiple simultaneous measurements (e.g. EMGs from multiple patch electrodes) is the selectivity index (SI). Defined by Veraart et al. (1993), SI is the normalized output of the muscle of interest divided by the sum of the normalized outputs of all measured muscles for a given set of stimulus conditions. For example, for forces  $F$  measured from  $N$  muscles, the SI of activating muscle  $j$  is given by

$$SI(\text{stimulusconditions}) = \frac{F_j}{\sum_{i=1}^N F_i}$$

SI yields a range of values from 0 to 1. To summarize a device's ability to selectively activate multiple targets, Badia et al. (2011a) introduced a *device selectivity index* which is a product of the highest SIs achieved by each measured muscle. However, as Kundu et al. (2014) pointed out, this definition is biased towards smaller muscle counts and strongly penalizes a device for one low SI though its others may be high; instead, a simple mean of the SIs was proposed.

Leventhal and Durand (2003) offered another quantification of selectivity based on 3D joint torque measurements. Two electrodes of the PNI were independently stimulated, yielding different torque vectors. Then they were stimulated simultaneously. If the simultaneous stimulation yielded a torque vector that did not match the sum of the two independent vectors, it was presumed that there was some overlap in the fiber populations activated by each electrode. This measure of selectivity  $S$  is summarized by comparison of the experimental (simultaneous) and theoretical (summed) vectors, and calculated by

$$S = \frac{(\tau_s - \tau_h) \cdot \tau_1}{|\tau_1|^2}$$

where  $\tau_s$  is the simultaneous torque vector, and  $\tau_h$  and  $\tau_1$  are the are the

higher- and lower-magnitude independent vectors, respectively.

Non-motor applications of PN stimulation may have a wide variety of other physiological biomarkers to serve as the performance indicator. For example, with vagus nerve stimulation the physiological outputs of interest may be changes in heart rate, blood pressure, or concentration of blood analytes (Plachta et al., 2014; Somann et al., 2018). In cases like these, selectivity is presumed to manifest as the absence of unwanted side effects, though such studies will benefit from standardization and a more thorough accounting of all the potentially affected targets (Birmingham et al., 2014).

**4.2.3.2. Recording performance.** Fewer examples in literature demonstrate rigorous *in vivo* characterization of PNI recording performance. The signals recorded may be electrically evoked, naturally evoked, or spontaneous. Recording of large, electrically evoked CAPs may serve as a rudimentary demonstration of a PNI's basic recording functionality but provide little value as a performance indicator since such a signal would not naturally arise during clinical use. More meaningful signals can be evoked by natural mechanisms, such as mechanical stimulation *via* brushing or pinching of the foot. Spontaneous nerve activity can also be recorded, but without correlative observations provides little information. Wodlinger and Durand (2010) elicited "pseudo-spontaneous" nerve activity by stimulating with sine waves at 5 or 10 kHz which resulted in a random firing pattern.

The end goal of PNI recordings is to meaningfully distinguish signals (or functional ensembles of signals) from one another and correlate them to specific origins or functions, such as volitional motor control signals or proprioceptive muscle afferents. Riso et al. (2000) used an apparatus for precise rotation of the ankle of a rabbit which allowed detailed study of muscle afferent signals recorded *via* cuff. Many of the same output measurements described for stimulation performance can potentially serve as correlative signals to help interpret recorded signals, as can a variety of naturally evoked stimuli. To characterize a PNI's ability to localize signals within the nerve trunk, separate distal branches of the nerve may be stimulated so that the afferent CAPs are confined to a known fascicle (Aristovich et al., 2018; Wodlinger and Durand, 2010; Zariffa et al., 2011).

Signal-to-noise ratio (SNR) is frequently mentioned in PNI literature but not often clearly defined. In many cases, SNR is reported simply as the ratio of peak-to-peak amplitudes of a spike and the steady background noise. However, it should be noted that this definition may not be consistent with adjacent disciplines which use power rather than amplitude (Schultz, 2007). Furthermore, what is interpreted as noise may in some cases be ongoing spontaneous activity, and so the ratio might be better described as evoked-to-spontaneous.

Since PNI experimental setups can be prone to multiple interference signals such as EMG, motion artifacts, and stimulus artifacts, the neural nature of recorded signals should be verified by subsequent application of local anesthetic to the nerve, such as lidocaine or bupivacaine, which block action potential propagation and should suppress the previously recorded signal (Elyahoodayan et al., 2019; Lissandrello et al., 2017; Riso et al., 2000). Temporary placement of parafilm or plastic wrap under or around the nerve can also help reject EMG interference in acute setups, and also limits dehydration of the nerve during extended surgical exposures (Vasudevan et al., 2017, 2016).

**4.2.3.3. Stability.** In both stimulation and recording characterizations, a crucial dimension of PNI performance is long-term stability. Clinical usefulness of a PNI will depend on predictable operation throughout the implant duration. Host response, tissue rearrangement, and device deterioration may cause changes in a PNI's input-output properties and signal capturing. Throughout a long-term study, the researcher should monitor for changes in such benchmarks as electrode impedance, stimulation threshold, and stimulated or recorded targets. After a long-term trial, close examination of the explanted device and

histology should be performed to illuminate causes of change or to reveal detrimental changes which were not previously detected.

## 5. Conclusion

This review has covered guiding principles for PNI design, PNI types and strategies for enhancing performance, and methods of PNI characterization. These topics may serve as a starting point for a new entrant to the field who wishes to design a PNI. They may also serve as a starting point for further discussion in the PNI community and a call to conduct further comparative studies of different approaches so that the strengths of each approach might be more definitively elucidated. While an attempt has been made to provide an initial collection of best practices in PNI design and development, there is a strong need for PNI designers to further consider and converge on the most effective paths to further the field toward highly functional, long-lasting PNIs.

## Declaration of Competing Interest

None.

## Acknowledgements

This work was sponsored in part by the Defense Advanced Research Projects Agency (DARPA) BTO under the auspices of Drs. Doug Weber and Eric Van Gieson through the DARPA Contracts Management Office Cooperative Agreement HR0011-15-2-0006. C.L. was partially supported by the University of Southern California Provost Fellowship.

## References

- Abidian, M.R., Martin, D.C., 2009. Multifunctional nanobiomaterials for neural interfaces. *Adv. Funct. Mater.* 19, 573–585. <https://doi.org/10.1002/adfm.200801473>.
- About us – Finetech Medical, n.d. URL <https://finetech-medical.co.uk/about-us/> (Accessed 4.26.19).
- Agnew, W.F., McCreery, D.B., 1990. Considerations for safety with chronically implanted nerve electrodes. *Epilepsia* 31, S27–S32. <https://doi.org/10.1111/j.1528-1157.1990.tb05845.x>.
- Agnew, W.F., McCreery, D.B., Bullara, L.A., Yuen, T.G.H., 1990. Effects of prolonged electrical stimulation of peripheral nerve. In: Agnew, W.F., McCreery, D.B. (Eds.), *Neural Prostheses: Fundamental Studies*, Prentice Hall Biophysics and Bioengineering Series. Prentice Hall, Englewood Cliffs, N.J., pp. 147–168.
- Agnew, W.F., McCreery, D.B., Yuen, T.G.H., Bullara, L.A., 1999. Evolution and resolution of stimulation-induced axonal injury in peripheral nerve. *Muscle Nerve* 22, 1393–1402. [https://doi.org/10.1002/\(SICI\)1097-4598\(199910\)22:10<1393::AID-MUS9>3.0.CO;2-E](https://doi.org/10.1002/(SICI)1097-4598(199910)22:10<1393::AID-MUS9>3.0.CO;2-E).
- Agnew, W.F., McCreery, D.B., Yuen, T.G.H., Bullara, L.A., 1989. Histologic and physiologic evaluation of electrically stimulated peripheral nerve: considerations for the selection of parameters. *Ann. Biomed. Eng.* 17, 39–60. <https://doi.org/10.1007/BF02364272>.
- Akin, T., Najafi, K., Smoke, R.H., Bradley, R.M., 1994. A micromachined silicon sieve electrode for nerve regeneration applications. *IEEE Trans. Biomed. Eng.* 41, 305–313. <https://doi.org/10.1109/10.284958>.
- Alexander, S., Rowan, D., 1968. Electrical control of urinary incontinence by radio implant. A report of 14 patients. *Br. J. Surg.* 55, 358–364. <https://doi.org/10.1002/bjs.1800550508>.
- Al-Shueli, A.I.K., Clarke, C.T., Donaldson, N., Taylor, J., 2014. Improved signal processing methods for velocity selective neural recording using multi-electrode cuffs. *IEEE Trans. Biomed. Circuits Syst.* 8, 401–410. <https://doi.org/10.1109/TBCAS.2013.2277561>.
- Anderson, H.E., Weir, R.F.F., 2019. On the development of optical peripheral nerve interfaces. *Neural Regen. Res.* 14, 425. <https://doi.org/10.4103/1673-5374.245461>.
- Andreasen, L.N.S., Struijk, J.J., 2002. Signal strength versus cuff length in nerve cuff electrode recordings. *IEEE Trans. Biomed. Eng.* 49, 1045–1050. <https://doi.org/10.1109/TBME.2002.800785>.
- Aoyagi, Y., Stein, R.B., Branner, A., Pearson, K.G., Normann, R.A., 2003. Capabilities of a penetrating microelectrode array for recording single units in dorsal root ganglia of the cat. *J. Neurosci. Methods* 128, 9–20. [https://doi.org/10.1016/S0165-0270\(03\)00143-2](https://doi.org/10.1016/S0165-0270(03)00143-2).
- Aristovich, K., Donegá, M., Blochet, C., Avery, J., Hannan, S., Chew, D.J., Holder, D., 2018. Imaging fast neural traffic at fascicular level with electrical impedance tomography: proof of principle in rat sciatic nerve. *J. Neural Eng.* 15, 056025. <https://doi.org/10.1088/1741-2552/aad78e>.
- Avery, R.E., Wepsic, J.S., 1973. *Implantable Electrodes for the Stimulation of the SCIATIC Nerve*. US3738368.
- Badia, J., Boretius, T., Andreu, D., Azevedo-Coste, C., Stieglitz, T., Navarro, X., 2011a.

- Comparative analysis of transverse intrafascicular multichannel, longitudinal intrafascicular and multipolar cuff electrodes for the selective stimulation of nerve fascicles. *J. Neural Eng.* 8, 036023. <https://doi.org/10.1088/1741-2560/8/3/036023>.
- Badia, J., Boretius, T., Pascual-Font, A., Udina, E., Stieglitz, T., Navarro, X., 2011b. Biocompatibility of chronically implanted transverse intrafascicular multichannel electrode (TIME) in the rat sciatic nerve. *IEEE Trans. Biomed. Eng.* 58, 2324–2332. <https://doi.org/10.1109/TBME.2011.2153850>.
- Badia, J., Raspopovic, S., Carpaneto, J., Micera, S., Navarro, X., 2016. Spatial and functional selectivity of peripheral nerve signal recording with the transversal intrafascicular multichannel electrode (TIME). *IEEE Trans. Neural Syst. Rehabil. Eng.* 24, 20–27. <https://doi.org/10.1109/TNSRE.2015.2440768>.
- Baker, R.G., 1993. Electrode Assembly for Nerve Stimulation. US5215089.
- Bakula, T., Mortimer, J.T., 2000. Spiral Nerve Cuff Electrode Implantation Tool. US6093197.
- Ballini, M., Bae, J., Marrocco, N., Verplancke, R., Schaubroeck, D., Cuyppers, D., Cauwe, M., O'Callaghan, J., Fahmy, A., Maghari, N., Bashirullah, R., Van Hoof, C., Van Helleputte, N., de Beeck, M.O., Braeken, D., Mitra, S., 2017. Intraneural active probe for bidirectional peripheral nerve interface. In: 2017 Symposium on VLSI Circuits. Presented at the 2017 Symposium on VLSI Circuits. IEEE, Kyoto, Japan. pp. C50–C51. <https://doi.org/10.23919/VLSIC.2017.8008544>.
- Banni, S., Carta, G., Murrù, E., Cordeddu, L., Giordano, E., Marrosu, F., Puligheddu, M., Floris, G., Asuni, G.P., Cappai, A.L., Deriu, S., Follasa, P., 2012. Vagus nerve stimulation reduces body weight and fat mass in rats. *PLoS One* 7, e44813. <https://doi.org/10.1371/journal.pone.0044813>.
- Barrese, J.C., Rao, N., Paroo, K., Triebwasser, C., Vargas-Irwin, C., Franquemont, L., Donoghue, J.P., 2013. Failure mode analysis of silicon-based intracortical micro-electrode arrays in non-human primates. *J. Neural Eng.* 10, 066014. <https://doi.org/10.1088/1741-2560/10/6/066014>.
- Bellinger, D., 2015. Harness Versus Button Device With Automated Blood Sampler.
- Bhadra, N., Kilgore, K.L., 2018. Fundamentals of kilohertz frequency alternating current nerve conduction block of the peripheral nervous system. *Neuromodulation*. Elsevier, pp. 111–120. <https://doi.org/10.1016/B978-0-12-805353-9.00010-3>.
- Birmingham, K., Gradinaru, V., Anikeeva, P., Grill, W.M., Pikov, V., McLaughlin, B., Pasricha, P., Weber, D., Ludwig, K., Famm, K., 2014. Bioelectronic medicines: a research roadmap. *Nat. Rev. Drug Discov.* 13, 399–400. <https://doi.org/10.1038/nrd4351>.
- Boretius, T., Badia, J., Pascual-Font, A., Schuettler, M., Navarro, X., Yoshida, K., Stieglitz, T., 2010. A transverse intrafascicular multichannel electrode (TIME) to interface with the peripheral nerve. *Biosens. Bioelectron.* 26, 62–69. <https://doi.org/10.1016/j.bios.2010.05.010>.
- Boretius, T., Yoshida, K., Badia, J., Hareby, K., Kundu, A., Navarro, X., Jensen, W., Stieglitz, T., 2012. A transverse intrafascicular multichannel electrode (TIME) to treat phantom limb pain: towards human clinical trials. In: 2012 4th IEEE RAS & EMBS International Conference on Biomedical Robotics and Biomechanics (BioRob). Presented at the 2012 4th IEEE RAS & EMBS International Conference on Biomedical Robotics and Biomechanics (BioRob 2012). IEEE, Rome, Italy. pp. 282–287. <https://doi.org/10.1109/BioRob.2012.6290787>.
- Bossi, S., Mencias, A., Koch, K.P., Hoffmann, K.-P., Yoshida, K., Dario, P., Micera, S., 2007. Shape memory alloy microactuation of tF-LIFEs: preliminary results. *IEEE Trans. Biomed. Eng.* 54, 1115–1120. <https://doi.org/10.1109/TBME.2007.895186>.
- Bradley, R.M., Cao, X., Akin, T., Najafi, K., 1997. Long term chronic recordings from peripheral sensory fibers using a sieve electrode array. *J. Neurosci. Methods* 73, 177–186. [https://doi.org/10.1016/S0165-0270\(97\)02225-5](https://doi.org/10.1016/S0165-0270(97)02225-5).
- Branner, A., Normann, R.A., 2000. A multielectrode array for intrafascicular recording and stimulation in sciatic nerve of cats. *Brain Res. Bull.* 51, 293–306. [https://doi.org/10.1016/S0304-7320\(99\)00231-2](https://doi.org/10.1016/S0304-7320(99)00231-2).
- Branner, A., Stein, R.B., Fernandez, E., Aoyagi, Y., Normann, R.A., 2004. Long-term stimulation and recording with a penetrating microelectrode array in cat sciatic nerve. *IEEE Trans. Biomed. Eng.* 51, 146–157. <https://doi.org/10.1109/TBME.2003.820321>.
- Branner, A., Stein, R.B., Normann, R.A., 2001. Selective stimulation of cat sciatic nerve using an array of varying-length microelectrodes. *J. Neurophysiol.* 85, 1585–1594. <https://doi.org/10.1152/jn.2001.85.4.1585>.
- Brelén, M.E., Duret, F., Gérard, B., Delbeke, J., Veraart, C., 2005. Creating a meaningful visual perception in blind volunteers by optic nerve stimulation. *J. Neural Eng.* 2, S22–S28. <https://doi.org/10.1088/1741-2560/2/1/004>.
- Brindley, G.S., 1977. An implant to empty the bladder or close the urethra. *J. Neurol. Neurosurg. Psychiatry* 40, 358–369. <https://doi.org/10.1136/jnnp.40.4.358>.
- Brindley, G.S., 1972. Electrode-arrays for making long-lasting electrical connexion to spinal roots. *J. Physiol.* 222, 135P–136P.
- Brindley, G.S., Polkey, C.E., Rushton, D.N., 1982. Sacral anterior root stimulators for bladder control in paraplegia. *Spinal Cord* 20, 365–381. <https://doi.org/10.1038/sc.1982.65>.
- Brindley, G.S., Polkey, C.E., Rushton, D.N., 1979. Electrical splinting of the knee in paraplegia. *Spinal Cord* 16, 428–435. <https://doi.org/10.1038/sc.1978.78>.
- Brindley, G.S., Polkey, C.E., Rushton, D.N., Cardozo, L., 1986. Sacral anterior root stimulators for bladder control in paraplegia: the first 50 cases. *J. Neurol. Neurosurg. Psychiatry* 49, 1104–1114. <https://doi.org/10.1136/jnnp.49.10.1104>.
- Bullara, L.A., 1990. Bidirectional Helical Electrode for Nerve Stimulation. US4920979.
- Bullara, L.A., 1986. Implantable Electrode Array. US4573481.
- Caparso, A.V., Durand, D.M., Mansour, J.M., 2009. A nerve cuff electrode for controlled reshaping of nerve geometry. *J. Biomater. Appl.* 24, 247–273. <https://doi.org/10.1177/0885328208097426>.
- Caravaca, A.S., Tsaava, T., Goldman, L., Silverman, H., Riggett, G., Chavan, S.S., Bouton, C., Tracey, K.J., Desimone, R., Boyden, E.S., Sohal, H.S., Olofsson, P.S., 2017. A novel flexible cuff-like microelectrode for dual purpose, acute and chronic electrical interfacing with the mouse cervical vagus nerve. *J. Neural Eng.* 14, 066005. <https://doi.org/10.1088/1741-2552/aa7a42>.
- Chaplan, S.R., Bach, F.W., Pogrel, J.W., Chung, J.M., Yaksh, T.L., 1994. Quantitative assessment of tactile allodynia in the rat paw. *J. Neurosci. Methods* 53, 55–63. [https://doi.org/10.1016/0165-0270\(94\)90144-9](https://doi.org/10.1016/0165-0270(94)90144-9).
- Charkhkar, H., Shell, C.E., Marasco, P.D., Pinault, G.J., Tyler, D.J., Triolo, R.J., 2018. High-density peripheral nerve cuffs restore natural sensation to individuals with lower-limb amputations. *J. Neural Eng.* 15, 056002. <https://doi.org/10.1088/1741-2552/aac964>.
- Cho, S.-H., Lu, H.M., Caulier, L., Romero-Ortega, M.I., Lee, J.-B., Hughes, G.A., 2008. Biocompatible SU-8-based microprobes for recording neural spike signals from regenerated peripheral nerve fibers. *IEEE Sens. J.* 8, 1830–1836. <https://doi.org/10.1109/JSEN.2008.2006261>.
- Christensen, M.B., Pearce, S.M., Ledbetter, N.M., Warren, D.J., Clark, G.A., Tresco, P.A., 2014. The foreign body response to the Utah Slant Electrode Array in the cat sciatic nerve. *Acta Biomater.* 10, 4650–4660. <https://doi.org/10.1016/j.actbio.2014.07.010>.
- Christensen, M.B., Tresco, P.A., 2018. The foreign body response and morphometric changes associated with mesh-style peripheral nerve cuffs. *Acta Biomater.* 67, 79–86. <https://doi.org/10.1016/j.actbio.2017.11.059>.
- Christensen, M.B., Wark, H.A.C., Hutchinson, D.T., 2016. A histological analysis of human median and ulnar nerves following implantation of Utah slanted electrode arrays. *Biomaterials* 77, 235–242. <https://doi.org/10.1016/j.biomaterials.2015.11.012>.
- Christie, B.P., Freeberg, M., Memberg, W.D., Pinault, G.J.C., Huyen, H.A., Tyler, D.J., Triolo, R.J., 2017. Long-term stability of stimulating spiral nerve cuff electrodes on human peripheral nerves. *J. NeuroEng. Rehabil.* 14. <https://doi.org/10.1186/s12984-017-0285-3>.
- Chu, J.-U., Song, K.-I., Han, S., Lee, S.H., Kim, J., Kang, J.Y., Hwang, D., Suh, J.-K.F., Choi, K., Youn, I., 2012. Improvement of signal-to-interference ratio and signal-to-noise ratio in nerve cuff electrode systems. *Physiol. Meas.* 33, 943–967. <https://doi.org/10.1088/0967-3334/33/6/943>.
- Ciancio, A.L., Cordella, F., Hoffmann, K.-P., Schneider, A., Guglielmelli, E., Zollo, L., 2017. Current achievements and future directions of hand prostheses controlled via peripheral nervous system. In: Bertoloso, M., Di Stefano, N. (Eds.), *The Hand*. Springer International Publishing, Cham, pp. 75–95. [https://doi.org/10.1007/978-3-319-66881-9\\_5](https://doi.org/10.1007/978-3-319-66881-9_5).
- Clements, I.P., Kim, Y., Andreasen, D., Bellamkonda, R.V., 2007. A regenerative electrode scaffold for peripheral nerve interfacing. In: 2007 3rd International IEEE/EMBS Conference on Neural Engineering. Presented at the 2007 3rd International IEEE/EMBS Conference on Neural Engineering. IEEE, Kohala Coast, HI, USA. pp. 390–393. <https://doi.org/10.1109/CNE.2007.369691>.
- Clements, I.P., Mukhatyar, V.J., Srinivasan, A., Bentley, J.T., Andreasen, D.S., Bellamkonda, R.V., 2013. Regenerative scaffold electrodes for peripheral nerve interfacing. *IEEE Trans. Neural Syst. Rehabil. Eng.* 21, 554–566. <https://doi.org/10.1109/TNSRE.2012.2217352>.
- Cobo, A.M., Larson, C.E., Scholten, K., Miranda, J.A., Elyahoodayan, S., Song, D., Pikov, V., Meng, E., 2019. Parylene-based cuff electrode with integrated microfluidics for peripheral nerve recording, stimulation, and drug delivery. *J. Microelectromech. Syst.* 28, 36–49. <https://doi.org/10.1109/JMEMS.2018.2881908>.
- Cogan, S.F., 2008. Neural stimulation and recording electrodes. *Annu. Rev. Biomed. Eng.* 10, 275–309. <https://doi.org/10.1146/annurev.bioeng.10.061807.160518>.
- Cogan, S.F., Hara, S., Ludwig, K.A., 2018. The safe delivery of electrical currents and neuromodulation. *Neuromodulation*. Elsevier, pp. 83–94. <https://doi.org/10.1016/B978-0-12-805353-9.00007-3>.
- Cogan, S.F., Ludwig, K.A., Welle, C.G., Takmakov, P., 2016. Tissue damage thresholds during therapeutic electrical stimulation. *J. Neural Eng.* 13, 021001. <https://doi.org/10.1088/1741-2560/13/2/021001>.
- Cold Spring Harbor Protocols [WWW Document], n.d. URL <http://cshprotocols.cshlp.org/> (Accessed 4.21.19).
- Coleman, D.L., King, R.N., Andrade, J.D., 1974. The foreign body reaction: a chronic inflammatory response. *J. Biomed. Mater. Res.* 8, 199–211. <https://doi.org/10.1002/jbm.820080503>.
- Cork, S.C., Eftekhar, A., Mirza, K.B., Zuliani, C., Nikolic, K., Gardiner, J.V., Bloom, S.R., Toumazou, C., 2018. Extracellular pH monitoring for use in closed-loop vagus nerve stimulation. *J. Neural Eng.* 15, 016001. <https://doi.org/10.1088/1741-2552/aa8239>.
- Crampon, M.-A., Sawan, M., Brailovski, V., Trochu, F., 1999. New easy to install nerve cuff electrode using shape memory alloy armature. *Artif. Organs* 23, 392–395. <https://doi.org/10.1046/j.1525-1594.1999.06357.x>.
- Cuoco, F.A., Durand, D.M., 2000. Measurement of external pressures generated by nerve cuff electrodes. *IEEE Trans. Rehabil. Eng.* 8, 35–41. <https://doi.org/10.1109/86.830947>.
- Cutrone, A., Bossi, S., Micera, S., 2013. Development of a self-opening neural interface. *Am. J. Respir. Med.* 7, 020938. <https://doi.org/10.1115/1.4024379>.
- Cutrone, A., Sergi, P.N., Bossi, S., Micera, S., 2011. Modelization of a self-opening peripheral neural interface: a feasibility study. *Med. Eng. Phys.* 33, 1254–1261. <https://doi.org/10.1016/j.medengphy.2011.06.001>.
- Cutrone, A., Valle, J.D., Santos, D., Badia, J., Filipposchi, C., Micera, S., Navarro, X., Bossi, S., 2015. A three-dimensional self-opening intraneural peripheral interface (SELINe). *J. Neural Eng.* 12, 016016. <https://doi.org/10.1088/1741-2560/12/1/016016>.
- Davis, T.S., Wark, H.A.C., Hutchinson, D.T., Warren, D.J., O'Neill, K., Scheinblum, T., Clark, G.A., Normann, R.A., Greger, B., 2016. Restoring motor control and sensory feedback in people with upper extremity amputations using arrays of 96 microelectrodes implanted in the median and ulnar nerves. *J. Neural Eng.* 13, 036001. <https://doi.org/10.1088/1741-2560/13/3/036001>.

- de la Oliva, N., del Valle, J., Delgado-Martinez, I., Mueller, M., Stieglitz, T., Navarro, X., 2019. Long-term functionality of transverse intraneural electrodes is improved by dexamethasone treatment. *IEEE Trans. Neural Syst. Rehabil. Eng.* <https://doi.org/10.1109/TNSRE.2019.2897256>. 1–1.
- de la Oliva, N., Mueller, M., Stieglitz, T., Navarro, X., del Valle, J., 2018a. On the use of Parylene C polymer as substrate for peripheral nerve electrodes. *Sci. Rep.* 8. <https://doi.org/10.1038/s41598-018-24502-z>.
- de la Oliva, N., Navarro, X., del Valle, J., 2018b. Dexamethasone reduces the foreign body reaction to intraneural electrode implants in the peripheral nerve of the rat. *Anat. Rec.* 301, 1722–1733. <https://doi.org/10.1002/ar.23920>.
- de la Oliva, N., Navarro, X., Valle, J., 2018c. Time course study of long-term biocompatibility and foreign body reaction to intraneural polyimide-based implants. *J. Biomed. Mater. Res. A* 106, 746–757. <https://doi.org/10.1002/jbm.a.36274>.
- Deberge, L., Delleci, C., Joseph, P.A., Cassoudesalle, H., Glize, B., 2018. Longitudinal long-term evaluation of patients with a Brindley's neurostimulator and followed in Bordeaux university hospital: return on 30 years of use. *Ann. Phys. Rehabil. Med.* 61, e380. <https://doi.org/10.1016/j.rehab.2018.05.884>.
- del Valle, J., de la Oliva, N., Muller, M., Stieglitz, T., Navarro, X., 2015. Biocompatibility evaluation of parylene C and polyimide as substrates for peripheral nerve interfaces. In: 2015 7th International IEEE/EMBS Conference on Neural Engineering (NER). Presented at the 2015 7th International IEEE/EMBS Conference on Neural Engineering (NER). IEEE, Montpellier, France. pp. 442–445. <https://doi.org/10.1109/NER.2015.7146654>.
- del Valle, J., Navarro, X., 2013. Interfaces with the peripheral nerve for the control of neuroprostheses. *International Review of Neurobiology*. Elsevier, pp. 63–83. <https://doi.org/10.1016/B978-0-12-420045-6.00002-X>.
- Delgado-Martínez, I., Righi, M., Santos, D., Cutrone, A., Bossi, S., D'Amico, S., Del Valle, J., Micera, S., Navarro, X., 2017. Fascicular nerve stimulation and recording using a novel double-axle regenerative electrode. *J. Neural Eng.* 14, 046003. <https://doi.org/10.1088/1741-2552/aa6bac>.
- Della Santina, C.C., Kovacs, G.T.A., Lewis, E.R., 1997. Multi-unit recording from regenerative bullfrog eighth nerve using implantable silicon-substrate microelectrodes. *J. Neurosci. Methods* 72, 71–86. [https://doi.org/10.1016/S0165-0270\(96\)00159-8](https://doi.org/10.1016/S0165-0270(96)00159-8).
- Desai, V.H., Anand, S., Tran, M., Kanneganti, A., Vasudevan, S., Seifert, J.L., Cheng, J., Keefer, E.W., Romero-Ortega, M.I., 2014. Chronic sensory-motor activity in behaving animals using regenerative multi-electrode interfaces. 2014 36th Annual International Conference of the IEEE Engineering in Medicine and Biology Society. Presented at the 2014 36th Annual International Conference of the IEEE Engineering in Medicine and Biology Society 1973–1976. <https://doi.org/10.1109/EMBC.2014.6944000>.
- Dhillon, G.S., Krüger, T.B., Sandhu, J.S., Horch, K.W., 2005. Effects of short-term training on sensory and motor function in severed nerves of long-term human amputees. *J. Neurophysiol.* 93, 2625–2633. <https://doi.org/10.1152/jn.00937.2004>.
- Djilas, M., Yoshida, K., Kurstjens, M., Azevedo-Coste, C., 2007. Improving the signal-to-noise ratio in recordings with thin-film longitudinal intra-fascicular electrodes using shielding cuffs. In: 2007 3rd International IEEE/EMBS Conference on Neural Engineering. Presented at the 2007 3rd International IEEE/EMBS Conference on Neural Engineering. IEEE, Kohala Coast, HI, USA. pp. 167–170. <https://doi.org/10.1109/CNE.2007.369638>.
- Donaldson, N., Donaldson, P.E.K., 1986. When are actively balanced biphasic ('Lilly') stimulating pulses necessary in a neurological prosthesis? I Historical background; Pt resting potential; Q studies. *Med. Biol. Eng. Comput.* 24, 41–49. <https://doi.org/10.1007/BF02441604>.
- Donaldson, N., Rieger, R., Schuettler, M., Taylor, J., 2008. Noise and selectivity of velocity-selective multi-electrode nerve cuffs. *Med. Biol. Eng. Comput.* 46, 1005–1018. <https://doi.org/10.1007/s11517-008-0365-4>.
- Donaldson, P.E.K., 1985. The craggs connector; a termination for cooper cable. *Med. Biol. Eng. Comput.* 23, 195–196. <https://doi.org/10.1007/BF02456759>.
- Donaldson, P.E.K., 1983. The Cooper cable: an implantable multiconductor cable for neurological prostheses. *Med. Biol. Eng. Comput.* 21, 371–374. <https://doi.org/10.1007/BF02478508>.
- Eastwood, P.R., Barnes, M., Walsh, J.H., Maddison, K.J., Hee, G., Schwartz, A.R., Smith, P.L., Malhotra, A., McEvoy, R.D., Wheatley, J.R., O'Donoghue, F.J., Rochford, P.D., Churchward, T., Campbell, M.C., Palme, C.E., Robinson, S., Goding, G.S., Eckert, D.J., Jordan, A.S., Catcheside, P.G., Tyler, L., Antic, N.A., Worsnop, C.J., Kezirian, E.J., Hillman, D.R., 2011. Treating obstructive sleep apnea with hypoglossal nerve stimulation. *Sleep* 34, 1479–1486. <https://doi.org/10.5665/sleep.1380>.
- Edell, D.J., 1986. A peripheral nerve information transducer for amputees: long-term multichannel recordings from rabbit peripheral nerves. *IEEE Trans. Biomed. Eng.* BME-33, 203–214. <https://doi.org/10.1109/TBME.1986.325892>.
- Elgrishi, N., Rountree, K.J., McCarthy, B.D., Rountree, E.S., Eisenhart, T.T., Dempsey, J.L., 2018. A practical beginner's guide to cyclic voltammetry. *J. Chem. Educ.* 95, 197–206. <https://doi.org/10.1021/acs.jchemed.7b00361>.
- Elyahoodayan, S., Larson, C., Cobo, A., Meng, E., Song, D., 2019. Acute *in vivo* testing of a polymer cuff electrode with integrated microfluidic channels for stimulation, recording, and drug delivery on rat sciatic nerve. *J. Neurosci. Methods*.
- Fattahi, P., Yang, G., Kim, G., Abidian, M.R., 2014. A review of organic and inorganic biomaterials for neural interfaces. *Adv. Mater.* 26, 1846–1885. <https://doi.org/10.1002/adma.201304496>.
- FDA Approves Inspire Upper Airway Stimulation Therapy for Obstructive Sleep Apnea, 2014. Press Releases Inspire Med. Syst. [WWW Document] URL <https://www.inspiresleep.com/wp-content/uploads/2015/10/FDA-Approves-Inspire-Upper-Airway-Stimulation-UAS-Therapy-for-Obstructive-Sleep-Apnea.pdf> (Accessed 2.1.19).
- Finetech-Brindley Sacral Anterior Root Stimulator (CPC2): Notes for Surgeons and Physicians.
- Fisher, L.E., Tyler, D.J., Anderson, J.S., Triolo, R.J., 2009. Chronic stability and selectivity of four-contact spiral nerve-cuff electrodes in stimulating the human femoral nerve. *J. Neural Eng.* 6, 046010. <https://doi.org/10.1088/1741-2560/6/4/046010>.
- FitzGerald, J.J., Lacour, S.P., McMahon, S.B., Fawcett, J.W., 2008. Microchannels as axonal amplifiers. *IEEE Trans. Biomed. Eng.* 55, 1136–1146. <https://doi.org/10.1109/TBME.2007.909533>.
- FitzGerald, J.J., Lago, N., Benmerah, S., Serra, J., Watling, C.P., Cameron, R.E., Tarte, E., Lacour, S.P., McMahon, S.B., Fawcett, J.W., 2012. A regenerative microchannel neural interface for recording from and stimulating peripheral axons in vivo. *J. Neural Eng.* 9, 016010. <https://doi.org/10.1088/1741-2560/9/1/016010>.
- Foldes, E.L., Ackermann, D.M., Bhadra, Niloy, Kilgore, K.L., Bhadra, Narendra, 2011. Design, fabrication and evaluation of a conforming circumferential peripheral nerve cuff electrode for acute experimental use. *J. Neurosci. Methods* 196, 31–37. <https://doi.org/10.1016/j.jneumeth.2010.12.020>.
- Fontaine, A.K., Gibson, E.A., Caldwell, J.H., Weir, R.F., 2017. Optical read-out of neural activity in mammalian peripheral axons: calcium signaling at nodes of ranvier. *Sci. Rep.* 7, 4744. <https://doi.org/10.1038/s41598-017-03541-y>.
- Fontaine, A.K., Kirchner, M.S., Caldwell, J.H., Weir, R.F., Gibson, E.A., 2018. deep-tissue two-photon imaging in brain and peripheral nerve with a compact high-pulse energy ytterbium fiber laser. In: Optical Interactions with Tissue and Cells XXIX. Presented at the Optical Interactions with Tissue and Cells XXIX. International Society for Optics and Photonics. pp. 1049217. <https://doi.org/10.1117/12.2309490>.
- Franks, W., Schenker, I., Schmutz, P., Hierlemann, A., 2005. Impedance characterization and modeling of electrodes for biomedical applications. *IEEE Trans. Biomed. Eng.* 52, 1295–1302. <https://doi.org/10.1109/TBME.2005.847523>.
- Freeberg, M.J., Stone, M.A., Triolo, R.J., Tyler, D.J., 2017. The design of and chronic tissue response to a composite nerve electrode with patterned stiffness. *J. Neural Eng.* 14, 036022. <https://doi.org/10.1088/1741-2552/aa6632>.
- Futia, G.L., Fontaine, A., McCullough, C., Caldwell, J., Restrepo, D., Weir, R., Gibson, E.A., Ozbay, B.N., George, N.M., 2018. Measurement of wavefront aberrations in cortex and peripheral nerve using a two-photon excitation guidestar. In: Bifano, T.G., Gigan, S., Kubly, J. (Eds.), Adaptive Optics and Wavefront Control for Biological Systems IV. Presented at the Adaptive Optics and Wavefront Control for Biological Systems IV. SPIE, San Francisco, United States, pp. 58. <https://doi.org/10.1117/12.2309492>.
- Ganzer, P., Sharma, G., 2019. Opportunities and challenges for developing closed-loop bioelectronic medicines. *Neural Regen. Res.* 14, 46. <https://doi.org/10.4103/1673-5374.243697>.
- Garde, K., Keefer, E., Botterman, B., Galvan, P., Romero-Ortega, M.I., 2009. Early interfaced neural activity from chronic amputated nerves. *Front. Neuroeng.* 2. <https://doi.org/10.3389/neuro.16.005.2009>.
- Garrido, L., Pfeleiderer, B., Papisov, M., Ackerman, J.L., 1993. In vivo degradation of silicones. *Magn. Reson. Med.* 29, 839–843. <https://doi.org/10.1002/mrm.1910290620>.
- Gasson, M., Hutt, B., Goodhew, I., Kyberd, P., Warwick, K., 2004. Invasive neural prosthesis for neural signal detection and nerve stimulation. *Int. J. Adapt. Control Signal Process.* <https://doi.org/10.1002/acs.854>.
- Gaunt, R.A., Hokanson, J.A., Weber, D.J., 2009. Microstimulation of primary afferent neurons in the L7 dorsal root ganglia using multielectrode arrays in anesthetized cats: thresholds and recruitment properties. *J. Neural Eng.* 6, 055009. <https://doi.org/10.1088/1741-2560/6/5/055009>.
- Geddes, L.A., Roeder, R., 2003. Criteria for the selection of materials for implanted electrodes. *Ann. Biomed. Eng.* 31, 879–890. <https://doi.org/10.1114/1.1581292>.
- Ghnenis, A.B., Czaikowski, R.E., Zhang, Z.J., Bushman, J.S., 2018. Toluidine blue staining of resin-embedded sections for evaluation of peripheral nerve morphology. *J. Vis. Exp.* 58031. <https://doi.org/10.3791/58031>.
- Giagka, V., Serdijn, W.A., 2018. Realizing flexible bioelectronic medicines for accessing the peripheral nerves – technology considerations. *Bioelectron. Med.* 4. <https://doi.org/10.1186/s42234-018-0010-y>.
- Glenn, W.W.L., Phelps, M.L., 1985. Diaphragm pacing by electrical stimulation of the phrenic nerve. *Neurosurgery* 17, 974–984. <https://doi.org/10.1227/00006123-198512000-00021>.
- González-González, M.A., Kanneganti, A., Joshi-Imre, A., Hernandez-Reynoso, A.G., Bendale, G., Modi, R., Ecker, M., Khurram, A., Cogan, S.F., Voit, W.E., Romero-Ortega, M.I., 2018. Thin film multi-electrode softening cuffs for selective neuromodulation. *Sci. Rep.* 8. <https://doi.org/10.1038/s41598-018-34566-6>.
- Goodall, E.V., Lefurge, T.M., Horch, K.W., 1991. Information contained in sensory nerve recordings made with intrafascicular electrodes. *IEEE Trans. Biomed. Eng.* 38, 846–850. <https://doi.org/10.1109/10.83604>.
- Gore, R.K., Choi, Y., Bellamkonda, R., English, A., 2015. Functional recordings from awake, behaving rodents through a microchannel based regenerative neural interface. *J. Neural Eng.* 12, 016017. <https://doi.org/10.1088/1741-2560/12/1/016017>.
- Gorman, P.H., Mortimer, J.T., 1983. The effect of stimulus parameters on the recruitment characteristics of direct nerve stimulation. *IEEE Trans. Biomed. Eng.* BME-30, 407–414. <https://doi.org/10.1109/TBME.1983.325041>.
- Green, R., Abidian, M.R., 2015. Conducting polymers for neural prosthetic and neural interface applications. *Adv. Mater.* 27, 7620–7637. <https://doi.org/10.1002/adma.201501810>.
- Grill, W.M., 2018. Waveforms for neural stimulation. *Neuromodulation*. Elsevier, pp. 95–102. <https://doi.org/10.1016/B978-0-12-805353-9.00008-5>.
- Grill, W.M., 1995. Spatially Selective Activation of Peripheral Nerve for Neuroprosthetic Applications. Case Western Reserve University.
- Grill, W.M., Mortimer, J.T., 2000. Neural and connective tissue response to long-term implantation of multiple contact nerve cuff electrodes. *J. Biomed. Mater. Res.* 50, 215–226. [https://doi.org/10.1002/\(SICI\)1097-4636\(200005\)50:2<215::AID-JBM17>3.0.CO;2-A](https://doi.org/10.1002/(SICI)1097-4636(200005)50:2<215::AID-JBM17>3.0.CO;2-A).
- Grill, W.M., Mortimer, J.T., 1998. Stability of the input-output properties of chronically

- implanted multiple contact nerve cuff stimulating electrodes. *IEEE Trans. Rehabil. Eng.* 6, 364–373. <https://doi.org/10.1109/86.736150>.
- Grill, W.M., Mortimer, J.T., 1997. Inversion of the current-distance relationship by transient depolarization. *IEEE Trans. Biomed. Eng.* 44, 1–9. <https://doi.org/10.1109/10.553708>.
- Grill, W.M., Mortimer, J.T., 1996a. The effect of stimulus pulse duration on selectivity of neural stimulation. *IEEE Trans. Biomed. Eng.* 43, 161–166. <https://doi.org/10.1109/10.481985>.
- Grill, W.M., Mortimer, J.T., 1996b. Non-invasive measurement of the input-output properties of peripheral nerve stimulating electrodes. *J. Neurosci. Methods* 65, 43–50. [https://doi.org/10.1016/0165-0270\(95\)00143-3](https://doi.org/10.1016/0165-0270(95)00143-3).
- Grill, W.M., Norman, S.E., Bellamkonda, R.V., 2009. Implanted neural interfaces: bio-challenges and engineered solutions. *Annu. Rev. Biomed. Eng.* 11, 1–24. <https://doi.org/10.1146/annurev-bioeng-061008-124927>.
- Grill, W.M., Veraart, C., Mortimer, J.T., 1991. Selective activation of peripheral nerve fascicles: use of field steering currents. In: 1991, IEEE, Orlando, FL, USA. Proceedings of the Annual International Conference of the IEEE Engineering in Medicine and Biology Society Volume 13: 1991. Presented at the Annual International Conference of the IEEE Engineering in Medicine and Biology Society 13. pp. 904–905. <https://doi.org/10.1109/EMBS.1991.684254>.
- Guiraud, D., Andreu, D., Bonnet, S., Carrault, G., Couderc, P., Hagege, A., Henry, C., Hernandez, A., Karam, N., Le Rolle, V., Mabo, P., Maciejasz, P., Malbert, C.-H., Marjion, E., Maubert, S., Picq, C., Rossel, O., Bonnet, J.-L., 2016. Vagus nerve stimulation: state of the art of stimulation and recording strategies to address autonomic function neuromodulation. *J. Neural Eng.* 13, 041002. <https://doi.org/10.1088/1741-2560/13/4/041002>.
- Günter, C., Delbeke, J., Ortiz-Catalan, M., 2019. Safety of long-term electrical peripheral nerve stimulation: review of the state of the art. *J. NeuroEng. Rehabil.* 16. <https://doi.org/10.1186/s12984-018-0474-8>.
- Guth, L., 1956. Regeneration in the mammalian peripheral nervous system. *Physiol. Rev.* 36, 441–478. <https://doi.org/10.1152/physrev.1956.36.4.441>.
- Gutiérrez, C.A., Lee, C., Kim, B., Meng, E., 2011. Epoxy-less packaging methods for electrical contact to parylene-based flat flexible cables. In: Presented at the 16th International Solid-State Sensors, Actuators and Microsystems Conference (TRANSDUCERS). IEEE. pp. 2299–2302.
- Hara, S.A., Kim, B.J., Kuo, J.T.W., Lee, C.D., Meng, E., Pikov, V., 2016. Long-term stability of intracortical recordings using perforated and arrayed Parylene sheath electrodes. *J. Neural Eng.* 13, 066020. <https://doi.org/10.1088/1741-2560/13/6/066020>.
- Hassler, C., Boretius, T., Stieglitz, T., 2011. Polymers for neural implants. *J. Polym. Sci. Part B: Polym. Phys.* 49, 18–33. <https://doi.org/10.1002/polb.22169>.
- Heiduschka, P., Thanos, S., 1998. Implantable bioelectronic interfaces for lost nerve functions. *Prog. Neurobiol.* 55, 433–461. [https://doi.org/10.1016/S0301-0082\(98\)00013-6](https://doi.org/10.1016/S0301-0082(98)00013-6).
- Heo, D.N., Song, S.-J., Kim, H.-J., Lee, Y.J., Ko, W.-K., Lee, S.J., Lee, D., Park, S.J., Zhang, L.G., Kang, J.Y., Do, S.H., Lee, S.H., Kwon, I.K., 2016. Multifunctional hydrogel coatings on the surface of neural cuff electrode for improving electrode-nerve tissue interfaces. *Acta Biomater.* 39, 25–33. <https://doi.org/10.1016/j.actbio.2016.05.009>.
- Hess, A.E., Dunning, J., Tyler, D., Zorman, C.A., 2007. Development of a microfabricated flat interface nerve electrode based on liquid crystal polymer and polynorborene multilayered structures. In: 2007 3rd International IEEE/EMBS Conference on Neural Engineering. Presented at the 2007 3rd International IEEE/EMBS Conference on Neural Engineering. IEEE, Kohala Coast, HI. pp. 32–35. <https://doi.org/10.1109/CNE.2007.369604>.
- Highley, J.R., Sullivan, N., 2018. 18 - Neuropathology and muscle biopsy techniques. In: Suvarna, S.K., Layton, C., Bancroft, J.D. (Eds.), *Bancroft's Theory and Practice of Histological Techniques*. Elsevier, Amsterdam, pp. 306–336.
- Hoffer, J.A., 1990. Techniques to study spinal-cord, peripheral nerve, and muscle activity in freely moving animals. In: Boulton, A.A., Baker, G.B., Vanderwolf, C.H. (Eds.), *Neurophysiological Techniques, Neuromethods*. Humana Press, Clifton, N.J.
- Hoffer, J.A., Chen, Y., Strange, K.D., Christensen, P.R., 1998. Nerve Cuff Having One or More Isolated Chambers. US5824027A. .
- Hoffer, J.A., Kalløse, K., 2001. How to use nerve cuffs to stimulate, record or modulate neural activity. In: Moxon, K.A., Chapin, J.K. (Eds.), *Neural Prostheses for Restoration of Sensory and Motor Function*. CRC Press, pp. 139–175.
- Hoffer, J.A., Loeb, G.E., 1980. Implantable electrical and mechanical interfaces with nerve and muscle. *Ann. Biomed. Eng.* 8, 351–360. <https://doi.org/10.1007/BF02363438>.
- Hoffer, J.A., Loeb, G.E., Pratt, C.A., 1981. Single unit conduction velocities from averaged nerve cuff electrode records in freely moving cats. *J. Neurosci. Methods* 4, 211–225. [https://doi.org/10.1016/0165-0270\(81\)90033-9](https://doi.org/10.1016/0165-0270(81)90033-9).
- Holinski, B.J., Everaert, D.G., Mushahwar, V.K., Stein, R.B., 2013. Real-time control of walking using recordings from dorsal root ganglia. *J. Neural Eng.* 10, 056008. <https://doi.org/10.1088/1741-2560/10/5/056008>.
- Howell, B., Grill, W.M., 2015. Design of electrodes for stimulation and recording. *Implantable Neuroprostheses for Restoring Function*. Elsevier, pp. 59–93. <https://doi.org/10.1016/B978-1-78242-101-6.00004-5>.
- Hudak, E.M., Mortimer, J.T., Martin, H.B., 2010. Platinum for neural stimulation: voltammetric considerations. *J. Neural Eng.* 7, 026005. <https://doi.org/10.1088/1741-2560/7/2/026005>.
- Hukins, D.W.L., Mahomed, A., Kukureka, S.N., 2008. Accelerated aging for testing polymeric biomaterials and medical devices. *Med. Eng. Phys.* 30, 1270–1274. <https://doi.org/10.1016/j.medengphy.2008.06.001>. Special issue to commemorate the 30th anniversary of Medical Engineering & Physics.
- Hursh, J.B., 1939. Conduction velocity and diameter of nerve fibers. *Am. J. Physiol.-Leg. Content* 127, 131–139. <https://doi.org/10.1152/ajplegacy.1939.127.1.131>.
- Instech Laboratories Inc., n.d. Instech Laboratories [WWW Document]. URL <https://www.instechlabs.com/products/buttons-tethers/vascular-access> (Accessed 3.26.19).
- R Compensation: Potentiostat Fundamentals / Basics of EIS [WWW Document], n.d. Gamry Instrum. URL <https://www.gamry.com/application-notes/instrumentation/understanding-ir-compensation/> (Accessed 4.24.19).
- Israel, J.S., Dingle, A.M., Sanchez, R.J., Kapur, S.K., Brodnick, S., Richner, T.J., Ness, J.P., Novello, J., Williams, J.C., Poore, S.O., 2018. Neuroma Implantation Into Long Bones: Clinical Foundation for a Novel Osseointegrated Peripheral Nerve Interface 4.
- Jeong, J., Jung, W., Kim, O., Chu, J.-U., Youn, I., Kim, K., Sang Rok, O., Park, J.W., Kim, J., 2016. 64-channel double-layered sieve electrode with increased porosity for improved axon regeneration and high spatial resolution. In: 2016 6th IEEE International Conference on Biomedical Robotics and Biomechanics (BioRob). Presented at the 2016 6th IEEE International Conference on Biomedical Robotics and Biomechanics (BioRob). IEEE, Singapore, Singapore. pp. 1148–1153. <https://doi.org/10.1109/BIOROB.2016.7523786>.
- Ju, M.-S., Lin, C.-C.K., Fan, J.-L., Chen, R.-J., 2006. Transverse elasticity and blood perfusion of sciatic nerves under in situ circular compression. *J. Biomech.* 39, 97–102. <https://doi.org/10.1016/j.jbiomech.2004.10.026>.
- Judson, J.P., 1968. Radio-frequency electrophrenic respiration: long-term application to a patient with primary hypoventilation. *JAMA* 203, 1033. <https://doi.org/10.1001/jama.1968.03140120031007>.
- Judy, J., Schmidt, C.E., Otto, K., Rinaldi, C., KULIASHA, C.A., 2018. Tissue-engineered Electronic Peripheral Nerve Interface.
- Jung, R., Abbas, J.J., Kuntaegowdanahalli, S., Thota, A.K., 2018a. Bionic intrafascicular interfaces for recording and stimulating peripheral nerve fibers. *Bioelectron. Med.* 1, 55–69. <https://doi.org/10.2217/bem-2017-0009>.
- Jung, W., Jung, S., Kim, O., Park, H., Choi, W., Son, D., Chung, S., Kim, J., 2019. Wire electrodes embedded in artificial conduit for long-term monitoring of the peripheral nerve signal. *Micromachines* 10, 184. <https://doi.org/10.3390/mi10030184>.
- Jung, W., Jung, S., Kim, O., Park, H., Choi, W., Son, D., Kim, J., 2018b. Neural electrode with artificial conduit for chronic signal recording. Presented at the Society for Biomaterials 2018 Annual Meeting & Exposition.
- Jung, Y., Ng, J.H., Keating, C.P., Senthil-Kumar, P., Zhao, J., Randolph, M.A., Winograd, J.M., Evans, C.L., 2014. Comprehensive evaluation of peripheral nerve regeneration in the acute healing phase using tissue clearing and optical microscopy in a rodent model. *PLoS One* 9, e94054. <https://doi.org/10.1371/journal.pone.0094054>.
- Kalløse, K., Hoffer, J., Strange, K., Valenzuela, I., 1996. Implantable Cuff Having Improved Closure. US5487756. .
- Kandel, E.R. (Ed.), 2013. *Principles of Neural Science*, 5th ed. McGraw-Hill, New York.
- Kang, X., Liu, J.-Q., Tian, H., Yang, B., Nuli, Y., Yang, C., 2015. Self-closed parylene cuff electrode for peripheral nerve recording. *J. Microelectromech. Syst.* 24, 319–332. <https://doi.org/10.1109/JMEMS.2014.2381634>.
- Kapur, S.K., Richner, T., Brodnick, S., Williams, J.C., Poore, S.O., 2014. Abstract 62: development of an optogenetic sensory peripheral nerve interface. *Plast. Reconstr. Surg.* 133, 10–99. <https://doi.org/10.1097/01.prs.0000445095.84222.cc>.
- Kennedy, P.R., 1989. The cone electrode: a long-term electrode that records from neurites grown onto its recording surface. *J. Neurosci. Methods* 29, 181–193. [https://doi.org/10.1016/0165-0270\(89\)90142-8](https://doi.org/10.1016/0165-0270(89)90142-8).
- Kim, B., Reyes, A., Garza, B., Choi, Y., 2015. A microchannel neural interface with embedded microwires targeting the peripheral nervous system. *Microsyst. Technol.* 21, 1551–1557. <https://doi.org/10.1007/s00542-014-2340-3>.
- Kim, H.-J., Heo, D.N., Lee, Y.J., Lee, S.J., Kang, J.Y., Lee, S.H., Kwon, I.K., Do, S.H., 2017a. Biological assessments of multifunctional hydrogel-decorated implantable neural cuff electrode for clinical neurology application. *Sci. Rep.* 7, 15245. <https://doi.org/10.1038/s41598-017-15551-x>.
- Kim, O., Choi, W., Jung, W., Jung, S., Park, H., Park, J.W., Kim, J., 2017b. Novel neural interface electrode array for the peripheral nerve. In: 2017 International Conference on Rehabilitation Robotics (ICORR). Presented at the 2017 International Conference on Rehabilitation Robotics (ICORR). IEEE, London. pp. 1067–1072. <https://doi.org/10.1109/ICORR.2017.8009391>.
- Kim, Y., Romero-Ortega, M.I., 2012. Material considerations for peripheral nerve interfacing. *MRS Bull.* 37, 573–580. <https://doi.org/10.1557/mrs.2012.99>.
- Koole, P., Holsheimer, J., Struijk, J.J., Verloop, A.J., 1997. Recruitment characteristics of nerve fascicles stimulated by a multigroove electrode. *IEEE Trans. Rehabil. Eng.* 5, 40–50. <https://doi.org/10.1109/86.559348>.
- Koopman, F.A., Chavan, S.S., Miljko, S., Grazio, S., Sokolovic, S., Schuurman, P.R., Mehta, A.D., Levine, Y.A., Faltys, M., Zitnik, R., Tracey, K.J., Tak, P.P., 2016. Vagus nerve stimulation inhibits cytokine production and attenuates disease severity in rheumatoid arthritis. *Proc. Natl. Acad. Sci.* 113, 8284–8289. <https://doi.org/10.1073/pnas.1605635113>.
- Kovacs, G.T.A., Stormont, C.W., Rosen, J.M., 1992. Regeneration microelectrode array for peripheral nerve recording and stimulation. *IEEE Trans. Biomed. Eng.* 39, 893–902. <https://doi.org/10.1109/10.256422>.
- Krapur, C., Loeb, G.E., 1988. Conduction studies in peripheral cat nerve using implanted electrodes: I. Methods and findings in controls. *Muscle Nerve* 11, 922–932. <https://doi.org/10.1002/mus.880110905>.
- Krapur, C., Loeb, G.E., Pezeshkpour, G.H., 1989. Conduction studies in peripheral cat nerve using implanted electrodes: III. The effects of prolonged constriction on the distal nerve segment. *Muscle Nerve* 12, 915–928. <https://doi.org/10.1002/mus.880121108>.
- Krapur, C., Loeb, G.E., Pezeshkpour, G.H., 1988. Conduction studies in peripheral cat nerve using implanted electrodes: II. The effects of prolonged constriction on regeneration of crushed nerve fibers. *Muscle Nerve* 11, 933–944. <https://doi.org/10.1002/mus.880110906>.
- Kuliasha, C.A., Spearman, B.S., Atkinson, E.W., Rustogi, P., Furniturewalla, A.S., Nunamaker, E.A., Otto, K.J., Schmidt, C.E., Judy, J.W., 2018. Robust and scalable

- tissue-engineered electronic nerve interfaces (Teeni). In: Presented at the Solid-State Sensors, Actuators and Microsystems Workshop. Hilton Head. pp. 4. <https://doi.org/10.31438/trf.hh2018.13>.
- Kundu, A., Harreby, K.R., Yoshida, K., Boretius, T., Stieglitz, T., Jensen, W., 2014. Stimulation selectivity of the “Thin-film longitudinal intrafascicular electrode” (tlLIFE) and the “Transverse intrafascicular multi-channel electrode” (TIME) in the large nerve animal model. *IEEE Trans. Neural Syst. Rehabil. Eng.* 22, 400–410. <https://doi.org/10.1109/TNSRE.2013.2267936>.
- Lacour, S.P., Atta, R., FitzGerald, J.J., Blamire, M., Tarte, E., Fawcett, J., 2008. Polyimide micro-channel arrays for peripheral nerve regenerative implants. *Sens. Actuators Phys.* 147, 456–463. <https://doi.org/10.1016/j.sna.2008.05.031>.
- Lago, N., Udina, E., Ramachandran, A., Navarro, X., 2007a. Neurobiological assessment of regenerative electrodes for bidirectional interfacing injured peripheral nerves. *IEEE Trans. Biomed. Eng.* 54, 1129–1137. <https://doi.org/10.1109/TBME.2007.891168>.
- Lago, N., Yoshida, K., Koch, K.P., Navarro, X., 2007b. Assessment of biocompatibility of chronically implanted polyimide and platinum intrafascicular electrodes. *IEEE Trans. Biomed. Eng.* 54, 281–290. <https://doi.org/10.1109/TBME.2006.886617>.
- Lancashire, H., Jiang, D., Demosthenous, A., Donaldson, N., 2018. A MicroChannel neural interface ASIC. In: 2018 IEEE International Symposium on Circuits and Systems (ISCAS). Presented at the 2018 IEEE International Symposium on Circuits and Systems (ISCAS). IEEE, Florence. pp. 1–4. <https://doi.org/10.1109/ISCAS.2018.8351380>.
- Lancashire, H.T., Jiang, D., Demosthenous, A., Donaldson, N., 2019. An ASIC for recording and stimulation in stacked microchannel neural interfaces. *IEEE Trans. Biomed. Circuits Syst.* <https://doi.org/10.1109/TBCAS.2019.2891284>. 1–1.
- Lancashire, H.T., Vanhoestenbergh, A., Pendegrass, C.J., Ajam, Y.A., Magee, E., Donaldson, N., Blunn, G.W., 2016. Microchannel neural interface manufacture by stacking silicone and metal foil laminae. *J. Neural Eng.* 13, 034001. <https://doi.org/10.1088/1741-2560/13/3/034001>.
- Larsen, J.O., 1998. Stereology of nerve cross sections. *J. Neurosci. Methods* 85, 107–118. [https://doi.org/10.1016/S0165-0270\(98\)00129-0](https://doi.org/10.1016/S0165-0270(98)00129-0).
- Larsen, J.O., Thomsen, M., Haugland, M., Sinkjaer, T., 1998. Degeneration and regeneration in rabbit peripheral nerve with long-term nerve cuff electrode implant: a stereological study of myelinated and unmyelinated axons. *Acta Neuropathol. (Berl.)* 96, 365–378. <https://doi.org/10.1007/s004010050907>.
- Larson, C., Elyahoodayan, S., Cobo, A., Scholten, K., Song, D., Meng, E., 2018. Reliability and acute in vivo testing of the lyse-and-attract cuff electrode. In: *Neuroscience Meeting Planner*. Presented at the Society for Neuroscience. San Diego, CA. pp. 700.15.
- Larson, P.J., Towe, B.C., 2011. Miniature ultrasonically powered wireless nerve cuff stimulator. 2011 5th International IEEE/EMBS Conference on Neural Engineering. Presented at the 2011 5th International IEEE/EMBS Conference on Neural Engineering 265–268. <https://doi.org/10.1109/NER.2011.5910538>.
- Lawrence, S.M., Dhillon, G.S., Horch, K.W., 2003. Fabrication and characteristics of an implantable, polymer-based, intrafascicular electrode. *J. Neurosci. Methods* 131, 9–26. [https://doi.org/10.1016/S0165-0270\(03\)00231-0](https://doi.org/10.1016/S0165-0270(03)00231-0).
- Lawrence, S.M., Larsen, J.O., Horch, K.W., Riso, R., Sinkjaer, T., 2002. Long-term biocompatibility of implanted polymer-based intrafascicular electrodes: implanted Polymer-Based Intrafascicular Electrodes. *J. Biomed. Mater. Res.* 63, 501–506. <https://doi.org/10.1002/jbm.10303>.
- Lebedev, M.A., Nicolelis, M.A.L., 2006. Brain-machine interfaces: past, present and future. *Trends Neurosci.* 29, 536–546. <https://doi.org/10.1016/j.tins.2006.07.004>.
- Lecomte, A., Degache, A., Descamps, E., Dahan, L., Bergaud, C., 2017. In vitro and in vivo biostability assessment of chronically-implanted Parylene C neural sensors. *Sens. Actuators B Chem.* 251, 1001–1008. <https://doi.org/10.1016/j.snb.2017.05.057>.
- Lee, B., Koripalli, M.K., Jia, Y., Acosta, J., Sendi, M.S.E., Choi, Y., Ghovanloo, M., 2018a. An implantable peripheral nerve recording and stimulation system for experiments on freely moving animal subjects. *Sci. Rep.* 8. <https://doi.org/10.1038/s41598-018-24465-1>.
- Lee, S., Peh, W.Y.X., Ho, J.S., Thakor, N.V., Yen, S.-C., Lee, C., 2018b. Batteryless pelvic nerve direct modulation for bladder voiding using an active neural clip. In: *Proceedings of the 13th Annual IEEE International Conference on Nano/Micro Engineered and Molecular Systems*. Singapore. pp. 4.
- Lee, S., Sheshadri, S., Xiang, Z., Delgado-Martinez, I., Xue, N., Sun, T., Thakor, N.V., Yen, S.-C., Lee, C., 2017. Selective stimulation and neural recording on peripheral nerves using flexible split ring electrodes. *Sens. Actuators B Chem.* 242, 1165–1170. <https://doi.org/10.1016/j.snb.2016.09.127>.
- Lee, Y.J., Kim, H.-J., Do, S.H., Kang, J.Y., Lee, S.H., 2016a. Characterization of nerve-cuff electrode interface for biocompatible and chronic stimulating application. *Sens. Actuators B Chem.* 237, 924–934. <https://doi.org/10.1016/j.snb.2016.06.169>.
- Lee, Y.J., Park, S.J., Yun, K.-S., Kang, J.Y., Lee, S.H., 2016b. Enzymeless glucose sensor integrated with chronically implantable nerve cuff electrode for in-situ inflammation monitoring. *Sens. Actuators B Chem.* 222, 425–432. <https://doi.org/10.1016/j.snb.2015.08.091>.
- Lefurge, T., Goodall, E., Horch, K., Stensaas, L., Schoenberg, A., 1991. Chronically implanted intrafascicular recording electrodes. *Ann. Biomed. Eng.* 19, 197–207. <https://doi.org/10.1007/BF02368469>.
- Lertmanorat, Z., Durand, D.M., 2004. A novel electrode array for diameter-dependent control of axonal excitability: a simulation study. *IEEE Trans. Biomed. Eng.* 51, 1242–1250. <https://doi.org/10.1109/TBME.2004.827347>.
- Lertmanorat, Z., Gustafson, K.J., Durand, D.M., 2006. Electrode array for reversing the recruitment order of peripheral nerve stimulation: experimental studies. *Ann. Biomed. Eng.* 34, 152–160. <https://doi.org/10.1007/s10439-005-9012-5>.
- Lertmanorat, Z., Montague, F.W., Durand, D.M., 2009. A flat interface nerve electrode with integrated multiplexer. *IEEE Trans. Neural Syst. Rehabil. Eng.* 17, 176–182. <https://doi.org/10.1109/TNSRE.2008.2009307>.
- Letchipia, J.E., Peckham, P.H., Gazdik, M., Smith, B., 1991. In-line lead connector for use with implanted neuroprostheses. *IEEE Trans. Biomed. Eng.* 38, 707–709.
- Leventhal, D.K., Cohen, M., Durand, D.M., 2006. Chronic histological effects of the flat interface nerve electrode. *J. Neural Eng.* 3, 102–113. <https://doi.org/10.1088/1741-2560/3/2/004>.
- Leventhal, D.K., Durand, D.M., 2004. Chronic measurement of the stimulation selectivity of the flat interface nerve electrode. *IEEE Trans. Biomed. Eng.* 51, 1649–1658. <https://doi.org/10.1109/TBME.2004.827535>.
- Leventhal, D.K., Durand, D.M., 2003. Subfascicle stimulation selectivity with the flat interface nerve electrode. *Ann. Biomed. Eng.* 31, 643–652. <https://doi.org/10.1114/1.1569266>.
- Lichtenberg, B.K., De Luca, C.J., 1979. Distinguishability of functionally distinct evoked neuroelectric signals on the surface of a nerve. *IEEE Trans. Biomed. Eng.* BME-26, 228–237. <https://doi.org/10.1109/TBME.1979.326507>.
- Liske, H., Qian, X., Anikeeva, P., Deisseroth, K., Delp, S., 2013. Optical control of neuronal excitation and inhibition using a single opsin protein, ChR2. *Sci. Rep.* 3, 3110. <https://doi.org/10.1038/srep03110>.
- Lissandrello, C.A., Gillis, W.F., Shen, J., Pearre, B.W., Vitale, F., Pasquali, M., Holinski, B.J., Chew, D.J., White, A.E., Gardner, T.J., 2017. A micro-scale printable nanoclip for electrical stimulation and recording in small nerves. *J. Neural Eng.* 14, 036006. <https://doi.org/10.1088/1741-2552/aa5a5b>.
- Liu, Y., Liu, J., Chen, S., Lei, T., Kim, Y., Niu, S., Wang, H., Wang, X., Foudeh, A.M., Tok, J.B.-H., Bao, Z., 2019. Soft and elastic hydrogel-based microelectronics for localized low-voltage neuromodulation. *Nat. Biomed. Eng.* 3, 58–68. <https://doi.org/10.1038/s41551-018-0335-6>.
- Llewellyn, M.E., Thompson, K.R., Deisseroth, K., Delp, S.L., 2010. Orderly recruitment of motor units under optical control in vivo. *Nat. Med.* 16, 1161–1165. <https://doi.org/10.1038/nm.2228>.
- Loeb, G.E., Gans, C., 1986. *Electromyography for Experimentalists*. University of Chicago Press, Chicago.
- Loeb, G.E., Marks, W.B., Beatty, P.G., 1977. Analysis and microelectronic design of tubular electrode arrays intended for chronic, multiple single-unit recording from captured nerve fibres. *Med. Biol. Eng. Comput.* 15, 195–201. <https://doi.org/10.1007/BF02442964>.
- Loeb, G.E., Peck, R.A., 1996. Cuff electrodes for chronic stimulation and recording of peripheral nerve activity. *J. Neurosci. Methods* 64, 95–103. [https://doi.org/10.1016/0165-0270\(95\)00123-9](https://doi.org/10.1016/0165-0270(95)00123-9).
- Lotfi, P., Garde, K., Chouhan, A.K., Bengali, E., Romero-Ortega, M.I., 2011. Modality-specific axonal regeneration: toward selective regenerative neural interfaces. *Front. Neuroeng.* 4. <https://doi.org/10.3389/fneng.2011.00011>.
- Lu, C.W., Patil, P.G., Chestek, C.A., 2012. Current challenges to the clinical translation of brain machine interface technology. *International Review of Neurobiology*. Elsevier, pp. 137–160. <https://doi.org/10.1016/B978-0-12-404706-8.00008-5>.
- Chapter 3 - The nerve trunk. In: Lundborg, G. (Ed.), *Nerve Injury and Repair*, Second Edition. Churchill Livingstone, Philadelphia. <https://doi.org/10.1016/B978-0-443-06711-2.50006-8>. 27–cp2.
- Luo, X., Matraga, C., Tan, S., Alba, N., Cui, X.T., 2011. Carbon nanotube nanoreservoir for controlled release of anti-inflammatory dexamethasone. *Biomaterials* 32, 6316–6323. <https://doi.org/10.1016/j.biomaterials.2011.05.020>.
- Malagodi, M.S., Horch, K.W., Schoenberg, A.A., 1989. An intrafascicular electrode for recording of action potentials in peripheral nerves. *Ann. Biomed. Eng.* 17, 397–410. <https://doi.org/10.1007/BF02368058>.
- Mannard, A., Stein, R.B., Charles, D., 1974. Regeneration electrode units: implants for recording from single peripheral nerve fibers in freely moving animals. *Science* 183, 547–549. <https://doi.org/10.1126/science.183.4124.547>.
- Marks, A., 1969. *Bullfrog nerve regeneration into porous implants*. In: Presented at the *Anatomical Record*. Wiley-Liss Div John Wiley & Sons Inc, 605 Third Ave, New York, NY 10158-0012. pp. 226.
- Marks, W.B., Loeb, G.E., 1976. Action currents, internodal potentials, and extracellular records of myelinated mammalian nerve fibers derived from node potentials. *Biophys. J.* 16, 655–668. [https://doi.org/10.1016/S0006-3495\(76\)85719-0](https://doi.org/10.1016/S0006-3495(76)85719-0).
- Mathews, K.S., Wark, H.A.C., Normann, R.A., 2014a. Assessment of rat sciatic nerve function following acute implantation of high density Utah slanted electrode array (25 electrodes/mm<sup>2</sup>) based on neural recordings and evoked muscle activity: nerve Function with Multielectrode Array. *Muscle Nerve* 50, 417–424. <https://doi.org/10.1002/mus.24171>.
- Mathews, K.S., Wark, H.A.C., Warren, D.J., Christensen, M.B., Nolte, N.F., Cartwright, P.C., Normann, R.A., 2014b. Acute monitoring of genitourinary function using intrafascicular electrodes: selective pudendal nerve activity corresponding to bladder filling, bladder fullness, and genital stimulation. *Urology* 84, 722–729. <https://doi.org/10.1016/j.urology.2014.05.021>.
- McCreery, D., 2004. *Apparatus and Methods for Differential Stimulation of Nerve Fibers*. US2004011139A1.
- McCreery, D.B., Agnew, W.F., Yuen, T.G.H., Bullara, L., 1990. Charge density and charge per phase as cofactors in neural injury induced by electrical stimulation. *IEEE Trans. Biomed. Eng.* 37, 996–1001. <https://doi.org/10.1109/10.102812>.
- McCreery, D.B., Agnew, W.F., Yuen, T.G.H., Bullara, L.A., 1995. Relationship between stimulus amplitude, stimulus frequency and neural damage during electrical stimulation of sciatic nerve of cat. *Med. Biol. Eng. Comput.* 33, 426–429. <https://doi.org/10.1007/BF02510526>.
- McNaughton, T.G., Horch, K.W., 1996. Metallized polymer fibers as leadwires and intrafascicular microelectrodes. *J. Neurosci. Methods* 70, 103–107. [https://doi.org/10.1016/S0165-0270\(96\)00111-2](https://doi.org/10.1016/S0165-0270(96)00111-2).
- McNeal, D.R., Bowman, B.R., 1985. Selective activation of muscles using peripheral nerve electrodes. *Med. Biol. Eng. Comput.* 23, 249–253. <https://doi.org/10.1007/BF02446866>.

- Mendell, L.M., Henneman, E., 1971. Terminals of single Ia fibers: location, density, and distribution within a pool of 300 homonymous motoneurons. *J. Neurophysiol.* 34, 171–187. <https://doi.org/10.1152/jn.1971.34.1.171>.
- Mensingher, A.F., Anderson, D.J., Buchko, C.J., Johnson, M.A., Martin, D.C., Tresco, P.A., Silver, R.B., Highstein, S.M., 2000. Chronic recording of regenerating VIIIth nerve axons with a sieve electrode. *J. Neurophysiol.* 83, 611–615. <https://doi.org/10.1152/jn.2000.83.1.611>.
- Metcalfe, B., Chew, D., Clarke, C., Donaldson, N., Taylor, J., 2014. An enhancement to velocity selective discrimination of neural recordings: extraction of neuronal firing rates. In: 2014 36th Annual International Conference of the IEEE Engineering in Medicine and Biology Society. Presented at the 2014 36th Annual International Conference of the IEEE Engineering in Medicine and Biology Society (EMBC). IEEE, Chicago, IL, pp. 4111–4114. <https://doi.org/10.1109/EMBC.2014.6944528>.
- Metcalfe, B., Nielsen, T.N., Donaldson, N., de, N., Hunter, A.J., Taylor, J.T., 2018. First demonstration of velocity selective recording from the pig vagus using a nerve cuff shows respiration afferents. *Biomed. Eng. Lett.* 8, 127–136. <https://doi.org/10.1007/s13534-017-0054-z>.
- Meyer, J., Stieglitz, T., Scholz, O., Haberer, W., Beutel, H., 2001. High density interconnects and flexible hybrid assemblies for active biomedical implants. *IEEE Trans. Adv. Packag.* 24, 366–374. <https://doi.org/10.1109/6040.938305>.
- Micera, S., Carrozza, M.C., Beccai, L., Vecchi, F., Dario, P., 2006. Hybrid bionic systems for the replacement of hand function. *Proc. IEEE* 94, 1752–1762. <https://doi.org/10.1109/JPROC.2006.881294>.
- Micera, S., Citi, L., Rigosa, J., Carpaneto, J., Raspopovic, S., Di Pino, G., Rossini, L., Yoshida, K., Denaro, L., Dario, P., Rossini, P.M., 2010. Decoding information from neural signals recorded using intraneural electrodes: toward the development of a neurocontrolled hand prosthesis. *Proc. IEEE* 98, 407–417. <https://doi.org/10.1109/JPROC.2009.2038726>.
- Micera, S., Navarro, X., 2009. Chapter 2 bidirectional interfaces with the peripheral nervous system. *International Review of Neurobiology*. Elsevier, pp. 23–38. [https://doi.org/10.1016/S0074-7742\(09\)86002-9](https://doi.org/10.1016/S0074-7742(09)86002-9).
- Michoud, F., Sottas, L., Browne, L.E., Asboth, L., Latremoliere, A., Sakuma, M., Courtine, G., Woolf, C.J., Lacour, S.P., 2018. Optical cuff for optogenetic control of the peripheral nervous system. *J. Neural Eng.* 15, 015002. <https://doi.org/10.1088/1741-2552/aa9126>.
- Micro-Leads Research Products [WWW Document], n.d. Wirel. Nerve Cuff Electrodes U. S. Micro-Leads. URL <https://www.micro-leads.com/research> (Accessed 4.21.19).
- Millesi, H., Zöch, G., Reihner, R., 1995. Mechanical properties of peripheral nerves. *Clin. Orthop.* 76–83.
- Mortimer, J.T., 1990. Electrical excitation of nerve. In: Agnew, W.F., McCreery, D.B. (Eds.), *Neural Prostheses: Fundamental Studies*, Prentice Hall Biophysics and Bioengineering Series. Prentice Hall, Englewood Cliffs, N.J., pp. 67–84.
- Mortimer, J.T., Bhadra, N., 2018. Fundamentals of electrical stimulation. *Neuromodulation*. Elsevier, pp. 71–82. <https://doi.org/10.1016/B978-0-12-805353-9.00006-1>.
- Mortimer, J.T., Bhadra, N., 2004. Peripheral nerve and muscle stimulation, in: neuroprosthetics: theory and practice, series on bioengineering and biomedical engineering. World Sci. 638–682. [https://doi.org/10.1142/9789812561763\\_0020](https://doi.org/10.1142/9789812561763_0020).
- Mortimer, T., Agnew, W.F., Horch, K., Citron, P., Creasey, G., Kantor, C., 1995. Perspectives on new electrode technology for stimulating peripheral nerves with implantable motor prostheses. *IEEE Trans. Rehabil. Eng.* 3, 145–154. <https://doi.org/10.1109/86.392373>.
- Musick, K.M., Rigosa, J., Narasimhan, S., Wurth, S., Capogrosso, M., Chew, D.J., Fawcett, J.W., Micera, S., Lacour, S.P., 2015. Chronic multichannel neural recordings from soft regenerative microchannel electrodes during gait. *Sci. Rep.* 5. <https://doi.org/10.1038/srep14363>.
- Naples, G.G., Mortimer, J.T., Scheiner, A., Sweeney, J.D., 1988. A spiral nerve cuff electrode for peripheral nerve stimulation. *IEEE Trans. Biomed. Eng.* 35, 905–916. <https://doi.org/10.1109/10.8670>.
- Naples, G.G., Mortimer, J.T., Yuen, T.G.H., 1990. Overview of peripheral nerve electrode design and implantation. In: Agnew, W.F., McCreery, D.B. (Eds.), *Neural Prostheses: Fundamental Studies*, Prentice Hall Biophysics and Bioengineering Series. Prentice Hall, Englewood Cliffs, N.J., pp. 85–106.
- Naples, G.G., Sweeney, J.D., Mortimer, J.T., 1986. *Implantable Cuff, Method of Manufacture, and Method of Installation*. US4602624. .
- Navarro, X., Krueger, T.B., Lago, N., Micera, S., Stieglitz, T., Dario, P., 2005. A critical review of interfaces with the peripheral nervous system for the control of neuroprostheses and hybrid bionic systems. *J. Peripher. Nerv. Syst.* 10, 229–258. <https://doi.org/10.1111/j.1085-9489.2005.10303.x>.
- Navarro, X., Lago, N., Vivo, M., Yoshida, K., Koch, K.P., Poppendieck, W., Micera, S., 2007. Neurobiological evaluation of thin-film longitudinal intrafascicular electrodes as a peripheral nerve interface. In: 2007 IEEE 10th International Conference on Rehabilitation Robotics. Presented at the 2007 IEEE 10th International Conference on Rehabilitation Robotics. IEEE, Noordwijk, Netherlands, pp. 643–649. <https://doi.org/10.1109/ICORR.2007.4428492>.
- Nedic, A., Moon, J.D., Kung, T.A., Langhals, N.B., Cederna, P.S., Urbanchek, M.G., 2013. Von frey monofilament testing successfully discriminates between sensory function of mixed nerve and sensory nerve regenerative peripheral nerve interfaces. In: 2013 6th International IEEE/EMBS Conference on Neural Engineering (NER). Presented at the 2013 6th International IEEE/EMBS Conference on Neural Engineering (NER). IEEE, San Diego, CA, USA, pp. 255–258. <https://doi.org/10.1109/NER.2013.6695920>.
- Neural Cuff | Ardiem Medical, (2019) n.d. URL <http://www.ardiemmedical.com/neural-cuff/> (Accessed 4.25.19).
- Nielsen, T.N., Sevencu, C., Struijk, J.J., 2014. Comparison of mono-, Bi-, and tripolar configurations for stimulation and recording with an interfascicular interface. *IEEE Trans. Neural Syst. Rehabil. Eng.* 22, 88–95. <https://doi.org/10.1109/TNSRE.2013.2278479>.
- Nielsen, T.N., Sevencu, C., Struijk, J.J., 2012. Fascicle-selectivity of an intraneural stimulation electrode in the rabbit sciatic nerve. *IEEE Trans. Biomed. Eng.* 59, 192–197. <https://doi.org/10.1109/TBME.2011.2169671>.
- Nordhausen, C.T., Maynard, E.M., Normann, R.A., 1996. Single unit recording capabilities of a 100 microelectrode array. *Brain Res.* 12.
- Oddo, C.M., Raspopovic, S., Artoni, F., Mazzoni, A., Spigler, G., Petrini, F., Giambattistelli, F., Vecchio, F., Miraglia, F., Zollo, L., Di Pino, G., Camboni, D., Carrozza, M.C., Guglielmelli, E., Rossini, P.M., Faraguna, U., Micera, S., 2016. Intraneural stimulation elicits discrimination of textural features by artificial fingertip in intact and amputee humans. *eLife* 5. <https://doi.org/10.7554/eLife.09148>.
- Ong, X.C., Huang, W.-C., Kwon, I.S., Gopinath, C., Wu, H., Fisher, L.E., Gaunt, R.A., Bettinger, C.J., Fedder, G.K., 2018. Ultra-compliant peripheral nerve cuff electrode with hydrogel adhesion. In: 2018 IEEE Micro Electro Mechanical Systems (MEMS). Presented at the 2018 IEEE Micro Electro Mechanical Systems (MEMS). IEEE, Belfast, pp. 376–379. <https://doi.org/10.1109/MEMSYS.2018.8346566>.
- Ordonez, J.S., Pikov, V., Wiggins, H., Patten, C., Stieglitz, T., Rickert, J., Schuettler, M., 2014. Cuff electrodes for very small diameter nerves — Prototyping and first recordings in vivo. *IEEE* 6846–6849. <https://doi.org/10.1109/EMBC.2014.6945201>.
- Ortizgoza-Diaz, J., Scholten, K., Larson, C., Cobo, A., Hudson, T., Yoo, J., Baldwin, A., Weltman Hirschberg, A., Meng, E., 2018. Techniques and considerations in the microfabrication of polyene C microelectromechanical systems. *Micromachines* 9, 422. <https://doi.org/10.3390/mi9090422>.
- Ortiz-Catalan, M., Brånemark, R., Håkansson, B., Delbeke, J., 2012. On the viability of implantable electrodes for the natural control of artificial limbs: review and discussion. *Biomed. Eng. Online* 11, 33. <https://doi.org/10.1186/1475-925X-11-33>.
- Page, D.M., George, J.A., Kluger, D.T., Duncan, C., Wendelken, S., Davis, T., Hutchinson, D.T., Clark, G.A., 2018. Motor control and sensory feedback enhance prosthesis embodiment and reduce phantom pain after long-term hand amputation. *Front. Hum. Neurosci.* 12. <https://doi.org/10.3389/fnhum.2018.00352>.
- Park, H., Choi, W., Jung, W., Kim, O., Chu, J.-U., Son, D., Park, W., Kim, J., 2018. Towards the development of bidirectional peripheral nerve interface for long-term implantation. In: *Proceedings of the 2018 IEEE International Conference on Cyborg and Bionic Systems*. Presented at the International Conference on Cyborg and Bionic Systems. Shenzhen, China, pp. 4.
- Park, S.I., Brenner, D.S., Shin, G., Morgan, C.D., Copits, B.A., Chung, H.U., Pullen, M.Y., Noh, K.N., Davidson, S., Oh, S.J., Yoon, J., Jang, K.-I., Saminini, V.K., Norman, M., Grajales-Reyes, J.G., Vogt, S.K., Sundaram, S.S., Wilson, K.M., Ha, J.S., Xu, R., Pan, T., Kim, T., Huang, Y., Montana, M.C., Golden, J.P., Bruchas, M.R., Gereau IV, R.W., Rogers, J.A., 2015a. Soft, stretchable, fully implantable miniaturized optoelectronic systems for wireless optogenetics. *Nat. Biotechnol.* 33, 1280–1286. <https://doi.org/10.1038/nbt.3415>.
- Park, S.J., Lee, Y.J., Heo, D.N., Kwon, I.K., Yun, K.-S., Kang, J.Y., Lee, S.H., 2015b. Functional nerve cuff electrode with controllable anti-inflammatory drug loading and release by biodegradable nanofibers and hydrogel deposition. *Sens. Actuators B Chem.* 215, 133–141. <https://doi.org/10.1016/j.snb.2015.03.036>.
- Pasluosta, C., Kiele, P., Stieglitz, T., 2018. Paradigms for restoration of somatosensory feedback via stimulation of the peripheral nervous system. *Clin. Neurophysiol.* 129, 851–862. <https://doi.org/10.1016/j.clinph.2017.12.027>.
- Payne, S.C., Burns, O., Stebbing, M., Thomas, R., Silva, A., Sedo, A., Weissenborn, F., Hyakumura, T., Huynh, M., May, C.N., Williams, R.A., Furness, J.B., Fallon, J.B., Shepherd, R.K., 2019. Vagus nerve stimulation to treat inflammatory bowel disease: a chronic, preclinical safety study in sheep. *Bioelectron. Med.* <https://doi.org/10.2217/bem-2018-0011>.
- Pederson, D.J., Quinkert, C.J., Arafat, M.A., Somann, J.P., Williams, J.D., Bercich, R.A., Wang, Z., Albers, G.O., Jefferys, J.G.R., Irazoqui, P.P., 2019. The bionode: a closed-loop neuromodulation implant. *ACM Trans Embed Comput Syst* 18 (9), 1–9. <https://doi.org/10.1145/3301310>. 20.
- Pena, A.E., Kuntaogodanahalli, S.S., Abbas, J.J., Patrick, J., Horch, K.W., Jung, R., 2017. Mechanical fatigue resistance of an implantable branched lead system for a distributed set of longitudinal intrafascicular electrodes. *J. Neural Eng.* 14, 066014. <https://doi.org/10.1088/1741-2552/aa814d>.
- Pflaum, C., Riso, R.R., Wiesspeiner, G., 1997. Performance of alternative amplifier configurations for tripolar nerve cuff recorded ENG. In: *Proceedings of 18th Annual International Conference of the IEEE Engineering in Medicine and Biology Society*. Presented at the 18th Annual International Conference of the IEEE Engineering in Medicine and Biology Society. IEEE, Amsterdam, Netherlands, pp. 375–376. <https://doi.org/10.1109/IEMBS.1996.657000>.
- Picaza, J.A., Hunter, S.E., Cannon, B.W., 1977. Pain suppression by peripheral nerve stimulation. *Stereotact. Funct. Neurosurg.* 40, 223–234. <https://doi.org/10.1159/000102446>.
- Plachta, D.T.T., Gierthmuehlen, M., Cota, O., Espinosa, N., Boeser, F., Herrera, T.C., Stieglitz, T., Zentner, J., 2014. Blood pressure control with selective vagal nerve stimulation and minimal side effects. *J. Neural Eng.* 11, 036011. <https://doi.org/10.1088/1741-2560/11/3/036011>.
- Pohlmeier, E.A., Jordon, L.R., Kim, P., Miller, L.E., 2009. A fully implanted drug delivery system for peripheral nerve blocks in behaving animals. *J. Neurosci. Methods* 182, 165–171. <https://doi.org/10.1016/j.jneumeth.2009.06.006>.
- Polasek, K.H., Hoyen, H.A., Keith, M.W., Kirsch, R.F., Taylor, D.J., 2009. Stimulation stability and selectivity of chronically implanted multicontact nerve cuff electrodes in the human upper extremity. *IEEE Trans. Neural Syst. Rehabil. Eng.* 17, 428–437. <https://doi.org/10.1109/TNSRE.2009.2032603>.
- Pollard, B.A., 2008. New model for learning ultrasound-guided needle to target localization. *Reg. Anesth. Pain Med.* 33, 360–362. <https://doi.org/10.1016/j.rapm.2008.02.006>.
- Popovic, M.R., Popovic, D.B., Keller, T., 2002. Neuroprostheses for grasping. *Neural Res.*

- 24, 443–452. <https://doi.org/10.1179/016164102101200311>.
- Radovsky, A.S., Van Vleet, J.F., 1989. Effects of dexamethasone elution on tissue reaction around stimulating electrodes of endocardial pacing leads in dogs. *Am. Heart J.* 117, 1288–1298. [https://doi.org/10.1016/0002-8703\(89\)90408-0](https://doi.org/10.1016/0002-8703(89)90408-0).
- Rahal, M., Taylor, J., Donaldson, N., 2000a. The effect of nerve cuff geometry on interference reduction: a study by computer modeling. *IEEE Trans. Biomed. Eng.* 47, 136–138. <https://doi.org/10.1109/10.817629>.
- Rahal, M., Winter, J., Taylor, J., Donaldson, N., 2000b. An improved configuration for the reduction of EMG in electrode cuff recordings: a theoretical approach. *IEEE Trans. Biomed. Eng.* 47, 1281–1284. <https://doi.org/10.1109/10.867963>.
- Raimondo, S., Fornaro, M., Di Scipio, F., Ronchi, G., Giacobini-Robecchi, M.G., Geuna, S., 2009. Chapter 5 Methods and protocols in peripheral nerve regeneration experimental research: part ii—morphological techniques. *International Review of Neurobiology*. Academic Press, pp. 81–103. [https://doi.org/10.1016/S0074-7742\(09\)87005-0](https://doi.org/10.1016/S0074-7742(09)87005-0).
- Ramachandran, A., Schuettler, M., Lago, N., Doerge, T., Koch, K.P., Navarro, X., Hoffmann, K.-P., Stieglitz, T., 2006. Design, *in vitro* and *in vivo* assessment of a multi-channel sieve electrode with integrated multiplexer. *J. Neural Eng.* 3, 114–124. <https://doi.org/10.1088/1741-2560/3/2/005>.
- Rathbun, K.M., Brader, W.T., Norbury, J.W., 2018. A simple, realistic, inexpensive nerve phantom. *J. Ultrasound Med.* <https://doi.org/10.1002/jum.14905>.
- Rattay, F., 1986. Analysis of models for external stimulation of axons. *IEEE Trans. Biomed. Eng.* BME-33, 974–977. <https://doi.org/10.1109/TBME.1986.325670>.
- Reichling, T.D., German, R.Z., 2000. Bones, muscles and visceral organs of protein-malnourished rats (*Rattus norvegicus*) grow more slowly but for longer durations to reach normal final size. *J. Nutr.* 130, 2326–2332. <https://doi.org/10.1093/jn/130.9.2326>.
- Restaino, S.M., Abliz, E., Wachrathit, K., Krauthamer, V., Shah, S.B., 2014. Biomechanical and functional variation in rat sciatic nerve following cuff electrode implantation. *J. NeuroEng. Rehabil.* 11, 73. <https://doi.org/10.1186/1743-0003-11-73>.
- Rise, M., Klepinski, R.J., 1992. Tool for Implantable Neural Electrode. U55143067.
- Riso, R.R., Mosallaei, F.K., Jensen, W., Sinkjaer, T., 2000. Nerve cuff recordings of muscle afferent activity from tibial and peroneal nerves in rabbit during passive ankle motion. *IEEE Trans. Rehabil. Eng.* 8, 244–258. <https://doi.org/10.1109/86.847826>.
- Robblee, L.S., Rose, T.L., 1990. Electrochemical guidelines for selection of protocols and electrode materials for neural stimulation. In: Agnew, W.F., McCreery, D.B. (Eds.), *Neural Prostheses: Fundamental Studies*, Prentice Hall Biophysics and Bioengineering Series. Prentice Hall, Englewood Cliffs, N.J. pp. 25–66.
- Rodríguez, F.J., Ceballos, D., Schuettler, M., Valero, A., Valderrama, E., Stieglitz, T., Navarro, X., 2000. Polyimide cuff electrodes for peripheral nerve stimulation. *J. Neurosci. Methods* 98, 105–118. [https://doi.org/10.1016/S0165-0270\(00\)00192-8](https://doi.org/10.1016/S0165-0270(00)00192-8).
- Rognini, G., Petrini, F.M., Raspopovic, S., Valle, G., Granata, G., Strauss, I., Solcà, M., Bello-Ruiz, J., Herbelin, B., Mange, R., D'Anna, E., Di Iorio, R., Di Pino, G., Andreu, D., Guiraud, D., Stieglitz, T., Rossini, P.M., Serino, A., Micera, S., Blanke, O., 2018. Multisensory bionic limb to achieve prosthesis embodiment and reduce distorted phantom limb perceptions. *J. Neurol. Neurosurg. Psychiatry*. <https://doi.org/10.1136/jnnp-2018-318570>.
- Romero, E., Deneff, J.F., Delbeke, J., Robert, A., Veraart, C., 2001. Neural morphological effects of long-term implantation of the self-sizing spiral cuff nerve electrode. *Med. Biol. Eng. Comput.* 39, 90–100. <https://doi.org/10.1007/BF02345271>.
- Rose, T.L., Robblee, L.S., 1990. Electrical stimulation with Pt electrodes. VIII. Electrochemically safe charge injection limits with 0.2 ms pulses (neuronal application). *IEEE Trans. Biomed. Eng.* 37, 1118–1120. <https://doi.org/10.1109/10.61038>.
- Rossini, P.M., Micera, S., Benvenuto, A., Carpaneto, J., Cavallo, G., Citi, L., Cipriani, C., Denaro, D., Denaro, V., Di Pino, G., Ferreri, F., Guglielmelli, E., Hoffmann, K.-P., Raspopovic, S., Rigosa, J., Rossini, L., Tombini, M., Dario, P., 2010. Double nerve intraneural interface implant on a human amputee for robotic hand control. *Clin. Neurophysiol.* 121, 777–783. <https://doi.org/10.1016/j.clinph.2010.01.001>.
- Rozman, J., Pečlin, P., Ribarič, S., Godec, M., Burja, J., 2018. An improved method of crafting a multi-electrode spiral cuff for the selective stimulation of peripheral nerves. *Sci. Rep.* 8. <https://doi.org/10.1038/s41598-018-19318-w>.
- Rubehn, B., Stieglitz, T., 2010. *In vitro* evaluation of the long-term stability of polyimide as a material for neural implants. *Biomaterials* 31, 3449–3458. <https://doi.org/10.1016/j.biomaterials.2010.01.053>.
- Rush, A.J., George, M.S., Sackeim, H.A., Marangell, L.B., Husain, M.M., Giller, C., Nahas, Z., Haines, S., Simpson, R.K., Goodman, R., 2000. Vagus nerve stimulation (VNS) for treatment-resistant depressions: a multicenter study. *Biol. Psychiatry* 47, 276–286. [https://doi.org/10.1016/S0006-3223\(99\)00304-2](https://doi.org/10.1016/S0006-3223(99)00304-2).
- Russell, C., Roche, A.D., Chakrabarty, S., 2019. Peripheral nerve bionic interface: a review of electrodes. *Int. J. Intell. Robot. Appl.* <https://doi.org/10.1007/s41315-019-00086-3>.
- Rutten, W.L.C., 2002. Selective electrical interfaces with the nervous system. *Annu. Rev. Biomed. Eng.* 4, 407–452. <https://doi.org/10.1146/annurev.bioeng.4.020702.153427>.
- Rydevik, B., Lundborg, G., Bagge, U., 1981. Effects of graded compression on intraneural blood flow. *J. Hand Surg.* 6, 3–12. [https://doi.org/10.1016/S0363-5023\(81\)80003-2](https://doi.org/10.1016/S0363-5023(81)80003-2).
- Rydevik, B.L., Danielsen, N., Dahlin, L.B., Lundborg, G., 1990. Pathophysiology of peripheral nerve injury with special reference to electrode implantation. In: Agnew, W.F., McCreery, D.B. (Eds.), *Neural Prostheses: Fundamental Studies*, Prentice Hall Biophysics and Bioengineering Series. Prentice Hall, Englewood Cliffs, N.J. pp. 85–106.
- Saal, H.P., Bensmaia, S.J., 2015. Biomimetic approaches to bionic touch through a peripheral nerve interface. *Neuropsychologia* 79, 344–353. <https://doi.org/10.1016/j.neuropsychologia.2015.06.010>.
- Sabetian, P., Sadeghlo, B., Zhang, C.H., Yoo, P.B., 2017. Characterizing the reduction of stimulation artifact noise in a tripolar nerve cuff electrode by application of a conductive shield layer. *Med. Eng. Phys.* 40, 39–46. <https://doi.org/10.1016/j.medengphy.2016.11.010>.
- Sadeghlo, B., 2013. Design of a Peripheral Nerve Electrode for Improved Neural Recording of the Cervical Vagus Nerve. University of Toronto.
- Sahin, M., Durand, D.M., 1997. Selective recording with a multi-contact nerve cuff electrode. In: Proceedings of 18th Annual International Conference of the IEEE Engineering in Medicine and Biology Society. Presented at the 18th Annual International Conference of the IEEE Engineering in Medicine and Biology Society. IEEE, Amsterdam, Netherlands. pp. 369–370. <https://doi.org/10.1109/IEMBS.1996.656997>.
- Sarnoff, S.J., Hardenbergh, E., Whittenberger, J.L., 1948. Electrophrenic respiration. *Am. J. Physiol.* 155, 9.
- Sassen, M., Zimmermann, M., 1973. Differential blocking of myelinated nerve fibres by transient depolarization. *Pflügers Arch. Eur. J. Physiol.* 341, 179–195. <https://doi.org/10.1007/BF00592788>.
- Schiefer, M.A., Freeberg, M., Pinault, G.C.J., Anderson, J., Hoyen, H., Tyler, D.J., Triolo, R.J., 2013. Selective activation of the human tibial and common peroneal nerves with a flat interface nerve electrode. *J. Neural Eng.* 10, 056006. <https://doi.org/10.1088/1741-2560/10/5/056006>.
- Schiefer, M.A., Polasek, K.H., Triolo, R.J., Pinault, G.C.J., Tyler, D.J., 2010. Selective stimulation of the human femoral nerve with a flat interface nerve electrode. *J. Neural Eng.* 7, 026006. <https://doi.org/10.1088/1741-2560/7/2/026006>.
- Schiefer, M.A., Triolo, R.J., Tyler, D.J., 2008. A model of selective activation of the femoral nerve with a flat interface nerve electrode for a lower extremity neuroprosthesis. *IEEE Trans. Neural Syst. Rehabil. Eng.* 16, 195–204. <https://doi.org/10.1109/TNSRE.2008.918425>.
- Schiefer, M.A., Tyler, D.J., Triolo, R.J., 2012. Probabilistic modeling of selective stimulation of the human sciatic nerve with a flat interface nerve electrode. *J. Comput. Neurosci.* 33, 179–190. <https://doi.org/10.1007/s10827-011-0381-5>.
- Schmalbruch, H., 1986. Fiber composition of the rat sciatic nerve. *Anat. Rec.* 215, 71–81. <https://doi.org/10.1002/ar.1092150111>.
- Schmidt, R.A., Bruschini, H., Tanagho, E.A., 1978. Feasibility of inducing micturition through chronic stimulation of sacral roots. *Urology* 12, 471–477. [https://doi.org/10.1016/0090-4295\(78\)90309-6](https://doi.org/10.1016/0090-4295(78)90309-6).
- Scholten, K., Meng, E., 2015. Materials for microfabricated implantable devices: a review. *Lab Chip* 15, 4256–4272. <https://doi.org/10.1039/C5LC00809C>.
- Schuettler, M., Donaldson, N., Seetohul, V., Taylor, J., 2013. Fibre-selective recording from the peripheral nerves of frogs using a multi-electrode cuff. *J. Neural Eng.* 10, 036016. <https://doi.org/10.1088/1741-2560/10/3/036016>.
- Schuettler, M., Henle, C., Ordenez, J.S., Meier, W., Guenther, T., Stieglitz, T., 2008. Interconnection technologies for laser-patterned electrode arrays. In: 2008 30th Annual International Conference of the IEEE Engineering in Medicine and Biology Society. Presented at the 2008 30th Annual International Conference of the IEEE Engineering in Medicine and Biology Society. IEEE, Vancouver, BC. pp. 3212–3215. <https://doi.org/10.1109/IEMBS.2008.4649887>.
- Schuettler, M., Koch, K.P., Stieglitz, T., Scholz, O., Haberer, W., Keller, R., Meyer, J.-U., 2000. Multichannel neural cuff electrodes with integrated multiplexer circuit. In: 1st Annual International IEEE-EMBS Special Topic Conference on Microtechnologies in Medicine and Biology. Proceedings (Cat. No.00EX451). Presented at the 1st Annual International IEEE-EMBS Special Topic Conference on Microtechnologies in Medicine and Biology. Proceedings, IEEE, Lyon, France. pp. 624–629. <https://doi.org/10.1109/MMB.2000.893861>.
- Schuettler, M., Schroeder, S., Ordenez, J.S., Stieglitz, T., 2011. Laser-fabrication of peripheral nerve cuff electrodes with integrated microfluidic channels. In: 2011 5th International IEEE/EMBS Conference on Neural Engineering. Presented at the 5th International IEEE/EMBS Conference on Neural Engineering (NER 2011). IEEE, Cancun. pp. 245–248. <https://doi.org/10.1109/NER.2011.5910533>.
- Schultz, A.E., Kuiken, T.A., 2011. Neural interfaces for control of upper limb prostheses: the state of the art and future possibilities. *PMR* 3, 55–67. <https://doi.org/10.1016/j.pmrj.2010.06.016>.
- Schultz, S., 2007. Signal-to-noise ratio in neuroscience. *Scholarpedia* 2, 2046. <https://doi.org/10.4249/scholarpedia.2046>.
- Schwartz, A.R., Bennett, M.L., Smith, P.L., Backer, W.D., Hedner, J., Boudewyns, A., de Heyning, P.V., Ejinell, H., Hochban, W., Knaack, L., Podszus, T., Penzel, T., Peter, J.H., Goding, G.S., Erickson, D.J., Testerman, R., Ottenhoff, F., Eisele, D.W., 2001. Therapeutic electrical stimulation of the hypoglossal nerve in obstructive sleep apnea. *Arch. Otolaryngol. Head Neck Surg.* 127, 8.
- Seifert, J.L., Desai, V., Watson, R.C., Musa, T., Kim, Y., Keefer, E.W., Romero, M.L., 2012. Normal molecular repair mechanisms in regenerative peripheral nerve interfaces allow recording of early spike activity despite immature myelination. *IEEE Trans. Neural Syst. Rehabil. Eng.* 20, 220–227. <https://doi.org/10.1109/TNSRE.2011.2179811>.
- Seki, Y., Yamagiwa, S., Morikawa, Y., Sawahata, H., Numano, R., Ishida, M., Kawano, T., 2017. Hook and loop microfastener: flexible microelectrodes tied to a nerve. In: 2017 IEEE 30th International Conference on Micro Electro Mechanical Systems (MEMS). Presented at the 2017 IEEE 30th International Conference on Micro Electro Mechanical Systems (MEMS). IEEE, Las Vegas, NV, USA. pp. 117–120. <https://doi.org/10.1109/MEMSYS.2017.7863354>.
- SetPoint Medical [WWW Document], n.d. SetPoint Med. URL <https://setpointmedical.com/> (Accessed 4.21.19).
- Shannon, R.V., 1992. A model of safe levels for electrical stimulation. *IEEE Trans. Biomed. Eng.* 39, 424–426. <https://doi.org/10.1109/10.126616>.
- Sharma, A., Rieth, L., Tathireddy, P., Harrison, R., Oppermann, H., Klein, M., Töpfer, M., Jung, E., Normann, R., Clark, G., Solzbacher, F., 2011. Long term *in vitro* functional stability and recording longevity of fully integrated wireless neural interfaces based

- on the Utah Slant Electrode Array. *J. Neural Eng.* 8, 045004. <https://doi.org/10.1088/1741-2560/8/4/045004>.
- Sharp, A.A., Fromherz, S., 2011. Optogenetic regulation of leg movement in midstage chick embryos through peripheral nerve stimulation. *J. Neurophysiol.* 106, 2776–2782. <https://doi.org/10.1152/jn.00712.2011>.
- Silva, A.P.D., Jordão, C.E.R., Fazan, V.P.S., 2007. Peripheral nerve morphometry: comparison between manual and semi-automated methods in the analysis of a small nerve. *J. Neurosci. Methods* 159, 153–157. <https://doi.org/10.1016/j.jneumeth.2006.06.012>.
- Silveira, C., Brunton, E., Spendiff, S., Nazarpour, K., 2018. Influence of nerve cuff channel count and implantation site on the separability of afferent ENG. *J. Neural Eng.* 15, 046004. <https://doi.org/10.1088/1741-2552/aaabca0>.
- Sohal, H.S., Vassilevski, K., Jackson, A., Baker, S.N., O'Neill, A., 2016. Design and microfabrication considerations for reliable flexible intracortical implants. *Front. Mech. Eng. China* 2. <https://doi.org/10.3389/fmech.2016.00005>.
- Somann, J.P., Albors, G.O., Neihouser, K.V., Lu, K.-H., Liu, Z., Ward, M.P., Durkes, A., Robinson, J.P., Powley, T.L., Irazoqui, P.P., 2018. Chronic cuffing of cervical vagus nerve inhibits efferent fiber integrity in rat model. *J. Neural Eng.* 15, 036018. <https://doi.org/10.1088/1741-2552/aa039>.
- Song, K.-I., Park, S.E., Lee, S., Kim, H., Lee, S.H., Youn, I., 2018. Compact optical nerve cuff electrode for simultaneous neural activity monitoring and optogenetic stimulation of peripheral nerves. *Sci. Rep.* 8. <https://doi.org/10.1038/s41598-018-33695-2>.
- Sparks, S., Evans, D., Byars, D., 2014. A low cost, high fidelity nerve block model. *Crit. Ultrasound J.* 6, 12. <https://doi.org/10.1186/s13089-014-0012-2>.
- Spearman, B.S., Desai, V.H., Mobini, S., McDermott, M.D., Graham, J.B., Otto, K.J., Judy, J.W., Schmidt, C.E., 2018. Tissue-engineered peripheral nerve interfaces. *Adv. Funct. Mater.* 28, 1701713. <https://doi.org/10.1002/adfm.201701713>.
- Srinivasan, A., Guo, L., Bellamkonda, R.V., 2011. Regenerative microchannel electrode array for peripheral nerve interfacing. In: 2011 5th International IEEE/EMBS Conference on Neural Engineering. Presented at the 5th International IEEE/EMBS Conference on Neural Engineering (NER 2011). IEEE, Cancun. pp. 253–256. <https://doi.org/10.1109/NER.2011.5910535>.
- Srinivasan, A., Tahirramani, M., Bentley, J.T., Gore, R.K., Millard, D.C., Mukhatyar, V.J., Joseph, A., Haque, A.S., Stanley, G.B., English, A.W., Bellamkonda, R.V., 2015. Microchannel-based regenerative scaffold for chronic peripheral nerve interfacing in amputees. *Biomaterials* 41, 151–165. <https://doi.org/10.1016/j.biomaterials.2014.11.035>.
- Srinivasan, A., Tipton, J., Tahirramani, M., Kharbouch, A., Gaupp, E., Song, C., Venkataraman, P., Falcone, J., Lacour, S.P., Stanley, G.B., English, A.W., Bellamkonda, R.V., 2016. A regenerative microchannel device for recording multiple single-unit action potentials in awake, ambulatory animals. *Eur. J. Neurosci.* 43, 474–485. <https://doi.org/10.1111/ejn.13080>.
- Sta, M., Cappaert, N.L.M., Ramekers, D., Baas, F., Wadman, W.J., 2014. The functional and morphological characteristics of sciatic nerve degeneration and regeneration after crush injury in rats. *J. Neurosci. Methods* 222, 189–198. <https://doi.org/10.1016/j.jneumeth.2013.11.012>.
- Standards and Guidelines for Neurological Devices, 2018. US Food Drug Adm. [WWW Document] URL <https://www.fda.gov/MedicalDevices/ProductsandMedicalProcedures/NeurologicalDevices/ucm528789.htm> (Accessed 2.2.19).
- Stein, R.B., Charles, D., Davis, L., Jhamandas, J., Mannard, A., Nichols, T.R., 1975. Principles underlying new methods for chronic neural recording. *Can. J. Neurol. Sci. J. Can. Sci. Neurol.* 2, 235–244. <https://doi.org/10.1017/S0317167100020333>.
- Stein, R.B., Charles, D., Gordon, T., Hoffer, J.-A., Jhamandas, J., 1978. Impedance properties of metal electrodes for chronic recording from mammalian nerves. *IEEE Trans. Biomed. Eng.* BME-25, 532–537. <https://doi.org/10.1109/TBME.1978.326287>.
- Stein, R.B., Nichols, T.R., Jhamandas, J., Davis, L., Charles, D., 1977. Stable long-term recordings from cat peripheral nerves. *Brain Res.* 128, 21–38. [https://doi.org/10.1016/0006-8993\(77\)90233-5](https://doi.org/10.1016/0006-8993(77)90233-5).
- Stein, R.B., Ögütörel, M.N., 1978. The radial decline of nerve impulses in a restricted cylindrical extracellular space. *Biol. Cybern.* 28, 159–165. <https://doi.org/10.1007/BF00337137>.
- Stein, R.B., Weber, D.J., Aoyagi, Y., Prochazka, A., Wagenaar, J.B.M., Shoham, S., Normann, R.A., 2004. Coding of position by simultaneously recorded sensory neurons in the cat dorsal root ganglion: coding of dorsal root ganglion neurons. *J. Physiol.* 560, 883–896. <https://doi.org/10.1113/jphysiol.2004.068668>.
- Stieglitz, T., Beutel, H., Meyer, J.-U., 1997. A flexible, light-weight multichannel sieve electrode with integrated cables for interfacing regenerating peripheral nerves. *Sens. Actuators Phys.* 60, 240–243. [https://doi.org/10.1016/S0924-4247\(97\)01494-5](https://doi.org/10.1016/S0924-4247(97)01494-5).
- Stieglitz, T., Ruf, H.H., Gross, M., Schuettler, M., Meyer, J.-U., 2002. A biohybrid system to interface peripheral nerves after traumatic lesions: design of a high channel sieve electrode. *Biosens. Bioelectron.* 17, 685–696. [https://doi.org/10.1016/S0956-5663\(02\)00019-2](https://doi.org/10.1016/S0956-5663(02)00019-2).
- Stieglitz, T., Schuettler, M., Koch, K.P., 2005. Implantable biomedical microsystems for neural prostheses. *IEEE Eng. Med. Biol. Mag.* 24, 58–65. <https://doi.org/10.1109/EMEMB.2005.1511501>.
- Stieglitz, T., Schuettler, M., Rubehn, B., Boretius, T., Badia, J., Navarro, X., 2011. Evaluation of polyimide as substrate material for electrodes to interface the peripheral nervous system. In: 2011 5th International IEEE/EMBS Conference on Neural Engineering. Presented at the 5th International IEEE/EMBS Conference on Neural Engineering (NER 2011). IEEE, Cancun. pp. 529–533. <https://doi.org/10.1109/NER.2011.5910602>.
- Stieglitz, T., Schuettler, M., Schneider, A., Valderrama, E., Navarro, X., 2003. Noninvasive measurement of torque development in the rat foot: measurement setup and results from stimulation of the sciatic nerve with polyimide-based cuff electrodes. *IEEE Trans. Neural Syst. Rehabil. Eng.* 11, 427–437. <https://doi.org/10.1109/TNSRE.2003.819793>.
- Stolinski, C., 1995. Structure and composition of the outer connective tissue sheaths of peripheral nerve. *J. Anat.* 186 (Pt. 1), 123–130.
- Stoyanova, I.L., van Wezel, R.J.A., Rutten, W.L.C., 2013. In vivo testing of a 3D bifurcating microchannel scaffold inducing separation of regenerating axon bundles in peripheral nerves. *J. Neural Eng.* 10, 066018. <https://doi.org/10.1088/1741-2560/10/6/066018>.
- Straka, M., Shafer, B., Vasudevan, S., Welle, C., Rieth, L., 2018. Characterizing longitudinal changes in the impedance spectra of in-vivo peripheral nerve electrodes. *Micromachines* 9, 587. <https://doi.org/10.3390/mi9110587>.
- Street, M.G., Welle, C.G., Takmakov, P.A., 2018. Automated reactive accelerated aging for rapid *in vitro* evaluation of neural implant performance. *Rev. Sci. Instrum.* 89, 094301. <https://doi.org/10.1063/1.5024686>.
- Stroneck, J.D., Reichert, W.M., 2008. Overview of wound healing in different tissue types. In: Reichert, W.M. (Ed.), *Indwelling Neural Implants: Strategies for Contending with the in Vivo Environment*, Frontiers in Neuroengineering. CRC Press, Boca Raton.
- Struijk, J.J., Haugland, M.K., Thomsen, M., 1997. Fascicle selective recording with a nerve cuff electrode. In: Proceedings of 18th Annual International Conference of the IEEE Engineering in Medicine and Biology Society. Presented at the 18th Annual International Conference of the IEEE Engineering in Medicine and Biology Society. IEEE, Amsterdam, Netherlands. pp. 361–362. <https://doi.org/10.1109/IEMBS.1996.656993>.
- Struijk, J.J., Thomsen, M., 1995. Tripolar nerve cuff recording: stimulus artifact, EMG and the recorded nerve signal. In: Proceedings of 17th International Conference of the Engineering in Medicine and Biology Society. Presented at the 17th International Conference of the Engineering in Medicine and Biology Society. IEEE, Montreal, Que., Canada. pp. 1105–1106. <https://doi.org/10.1109/IEMBS.1995.579534>.
- Sun, F.T., Morrell, M.J., 2014. Closed-loop neurostimulation: the clinical experience. *Neurotherapeutics* 11, 553–563. <https://doi.org/10.1007/s13311-014-0280-3>.
- Sunderland, S., 1978. *Nerves and Nerve Injuries*, 2nd ed. Churchill Livingstone; distributed by Longman, Edinburgh; New York: New York.
- Sunderland, S., 1965. The connective tissues of peripheral nerves. *Brain* 88, 841–854. <https://doi.org/10.1093/brain/88.4.841>.
- Sunderland, S.S., 1990. The anatomy and physiology of nerve injury. *Muscle Nerve* 13, 771–784. <https://doi.org/10.1002/mus.880130903>.
- Suzuki, T., Kotake, N., Mabuchi, K., Takeuchi, S., 2006. Flexible regeneration-type nerve electrode with integrated microfluidic channels. In: 2006 International Conference on Microtechnologies in Medicine and Biology. Presented at the 2006 International Conference on Microtechnologies in Medicine and Biology. IEEE, Okinawa. pp. 303–305. <https://doi.org/10.1109/MMB.2006.251557>.
- Sweeney, J.D., Ksienski, D.A., Mortimer, J.T., 1990. A nerve cuff technique for selective excitation of peripheral nerve trunk regions. *IEEE Trans. Biomed. Eng.* 37, 706–715. <https://doi.org/10.1109/10.55681>.
- Takmakov, P., Ruda, K., Scott Phillips, K., Isayeva, I.S., Krauthamer, V., Welle, C.G., 2015. Rapid evaluation of the durability of cortical neural implants using accelerated aging with reactive oxygen species. *J. Neural Eng.* 12, 026003. <https://doi.org/10.1088/1741-2560/12/2/026003>.
- Takmakov, P.A., 2017. Electrochemistry of a robust neural interface. *Electrochem. Soc. Interface* 26, 49–51. <https://doi.org/10.1149/2.F05173if>.
- Tan, D.W., Schiefer, M.A., Keith, M.W., Anderson, J.R., Tyler, D.J., 2015. Stability and selectivity of a chronic, multi-contact cuff electrode for sensory stimulation in human amputees. *J. Neural Eng.* 12, 026002. <https://doi.org/10.1088/1741-2560/12/2/026002>.
- Tarler, H., Grill, W.M., Mortimer, J.T., 1995. Comparison between monopolar and tripolar configurations in chronically implanted nerve cuff electrodes. In: Proceedings of 17th International Conference of the Engineering in Medicine and Biology Society. Presented at the 17th International Conference of the Engineering in Medicine and Biology Society. IEEE, Montreal, Que., Canada. pp. 1093–1094. <https://doi.org/10.1109/IEMBS.1995.579515>.
- Tarler, M.D., Mortimer, J.T., 2004. Selective and independent activation of four motor fascicles using a four contact nerve-cuff electrode. *IEEE Trans. Neural Syst. Rehabil. Eng.* 12, 251–257. <https://doi.org/10.1109/TNSRE.2004.828415>.
- Tarler, M.D., Mortimer, J.T., 2003. Comparison of joint torque evoked with monopolar and tripolar-cuff electrodes. *IEEE Trans. Neural Syst. Rehabil. Eng.* 11, 227–235. <https://doi.org/10.1109/TNSRE.2003.818687>.
- Taylor, J., Donaldson, N., Winter, J., 2004. Multiple-electrode nerve cuffs for low-velocity and velocity-selective neural recording. *Med. Biol. Eng. Comput.* 42, 634–643. <https://doi.org/10.1007/BF02347545>.
- Taylor, J., Metcalfe, B., Clarke, C., Chew, D., Nielsen, T., Donaldson, N., 2015. A summary of current and new methods in velocity selective recording (VSR) of electro-neurogram (ENG). In: 2015 IEEE Computer Society Annual Symposium on VLSI. Presented at the 2015 IEEE Computer Society Annual Symposium on VLSI (ISVLSI). IEEE, Montpellier, France. pp. 221–226. <https://doi.org/10.1109/ISVLSI.2015.34>.
- Thomas, P.K., 1963. The connective tissue of peripheral nerve: an electron microscope study. *J. Anat.* 97, 35–44.
- Thota, A.K., Kuntaegowdanahalli, S., Starosciak, A.K., Abbas, J.J., Orbay, J., Horch, K.W., Jung, R., 2015. A system and method to interface with multiple groups of axons in several fascicles of peripheral nerves. *J. Neurosci. Methods* 244, 78–84. <https://doi.org/10.1016/j.jneumeth.2014.07.020>.
- Tian, P., Yi, W., Chen, C., Hu, J., Qi, J., Zhang, B., Cheng, M.M.-C., 2018. Flexible 3D carbon nanotubes cuff electrodes as a peripheral nerve interface. *Biomed. Microdevices* 20. <https://doi.org/10.1007/s10544-018-0268-6>.
- Tos, P., Ronchi, G., Papalia, I., Sallen, V., Legagneux, J., Geuna, S., Giacobini-Robecchi, M.G., 2009. Chapter 4 Methods and protocols in peripheral nerve regeneration experimental research: part I—experimental models. *International Review of*

- Neurobiology. Elsevier, pp. 47–79. [https://doi.org/10.1016/S0074-7742\(09\)87004-9](https://doi.org/10.1016/S0074-7742(09)87004-9).
- Towne, C., Montgomery, K.L., Iyer, S.M., Deisseroth, K., Delp, S.L., 2013. Optogenetic control of targeted peripheral axons in freely moving animals. *PLoS One* 8, e72691. <https://doi.org/10.1371/journal.pone.0072691>.
- Triangle BioSystems International (2019) [WWW Document], n.d. URL <https://www.trianglebiosystems.com/index.html> (Accessed 3.29.19).
- Tyler, D.J., 2018. Electrodes for the neural interface. *Neuromodulation*. Elsevier, pp. 239–274. <https://doi.org/10.1016/B978-0-12-805353-9.00020-6>.
- Tyler, D.J., Durand, D.M., 2003. Chronic response of the rat sciatic nerve to the flat interface nerve electrode. *Ann. Biomed. Eng.* 31, 633–642. <https://doi.org/10.1114/1.1569263>.
- Tyler, D.J., Durand, D.M., 2002. Functionally selective peripheral nerve stimulation with a flat interface nerve electrode. *IEEE Trans. Neural Syst. Rehabil. Eng.* 10, 294–303. <https://doi.org/10.1109/TNSRE.2002.806840>.
- Tyler, D.J., Durand, D.M., 1997a. Alteration of neural geometry for selective nerve stimulation. In: Proceedings of the 19th Annual International Conference of the IEEE Engineering in Medicine and Biology Society. “Magnificent Milestones and Emerging Opportunities in Medical Engineering” (Cat. No.97CH36136). Presented at the 19th Annual International Conference of the IEEE Engineering in Medicine and Biology Society. “Magnificent Milestones and Emerging Opportunities in Medical Engineering”. IEEE, Chicago, IL, USA. pp. 2002–2003. <https://doi.org/10.1109/IEMBS.1997.758736>.
- Tyler, D.J., Durand, D.M., 1997b. A slowly penetrating interfascicular nerve electrode for selective activation of peripheral nerves. *IEEE Trans. Rehabil. Eng.* 5, 51–61. <https://doi.org/10.1109/86.559349>.
- Tyler, D.J., Peterson, E.J., Brill, N., White, K., 2011. Increased selectivity of clinical peripheral nerve interfaces. In: 2011 5th International IEEE/EMBS Conference on Neural Engineering. Presented at the 5th International IEEE/EMBS Conference on Neural Engineering (NER 2011). IEEE, Cancun. pp. 257–260. <https://doi.org/10.1109/NER.2011.5910536>.
- Valle, G., Mazzoni, A., Iberite, F., D’Anna, E., Strauss, I., Granata, G., Controzzi, M., Clemente, F., Rognini, G., Cipriani, C., Stieglitz, T., Petrini, F.M., Rossini, P.M., Micera, S., 2018a. Biomimetic intraneural sensory feedback enhances sensation naturalness, tactile sensitivity, and manual dexterity in a bidirectional prosthesis. *Neuron* 100 <https://doi.org/10.1016/j.neuron.2018.08.033>. 37–45.e7.
- Valle, G., Petrini, F.M., Strauss, I., Iberite, F., D’Anna, E., Granata, G., Controzzi, M., Cipriani, C., Stieglitz, T., Rossini, P.M., Mazzoni, A., Raspopovic, S., Micera, S., 2018b. Comparison of linear frequency and amplitude modulation for intraneural sensory feedback in bidirectional hand prostheses. *Sci. Rep.* 8. <https://doi.org/10.1038/s41598-018-34910-w>.
- Varejão, A.S.P., Meek, M.F., Ferreira, A.J.A., Patrício, J.A.B., Cabrita, A.M.S., 2001. Functional evaluation of peripheral nerve regeneration in the rat: walking track analysis. *J. Neurosci. Methods* 108, 1–9. [https://doi.org/10.1016/S0165-0270\(01\)00378-8](https://doi.org/10.1016/S0165-0270(01)00378-8).
- Vasudevan, S., Kumsa, D., Takmakov, P., Welle, C.G., Hammer, D.X., 2016. Real time imaging of peripheral nerve vasculature using optical coherence angiography. In: Madsen, S.J., Yang, V.X.D., Jansen, E.D., Luo, Q., Mohanty, S.K., Thakor, N.V. (Eds.), Presented at the SPIE BiOS. San Francisco, California, United States. pp. 96901D. <https://doi.org/10.1117/12.2213160>.
- Vasudevan, S., Patel, K., Welle, C., 2017. Rodent model for assessing the long term safety and performance of peripheral nerve recording electrodes. *J. Neural Eng.* 14, 016008. <https://doi.org/10.1088/1741-2552/14/1/016008>.
- Vasudevan, S., Vo, J., Shafer, B., Nam, A.S., Vakoc, B.J., Hammer, D.X., 2019. Toward optical coherence tomography angiography-based biomarkers to assess the safety of peripheral nerve electrostimulation. *J. Neural Eng.* <https://doi.org/10.1088/1741-2552/ab1405>.
- Veltink, P.H., van Alsté, J.A., Boom, H.B.K., 1989. Multielectrode intrafascicular and extraneural stimulation. *Med. Biol. Eng. Comput.* 27, 19–24. <https://doi.org/10.1007/BF02442165>.
- Veraart, C., Grill, W.M., Mortimer, J.T., 1993. Selective control of muscle activation with a multipolar nerve cuff electrode. *IEEE Trans. Biomed. Eng.* 40, 640–653. <https://doi.org/10.1109/10.237694>.
- Veraart, C., Raftopoulos, C., Mortimer, J.T., Delbeke, J., Pins, D., Michaux, G., Vanlierde, A., Parrini, S., Wanet-Defalque, M.-C., 1998. Visual sensations produced by optic nerve stimulation using an implanted self-sizing spiral cuff electrode. *Brain Res.* 813, 181–186. [https://doi.org/10.1016/S0006-8993\(98\)00977-9](https://doi.org/10.1016/S0006-8993(98)00977-9).
- Vijayaraghavan, S., Huq, R., Hausman, M.R., 2014. Methods of peripheral nerve tissue preparation for second harmonic generation imaging of collagen fibers. *Methods* 66, 246–255. <https://doi.org/10.1016/j.ymeth.2013.08.012>.
- Vince, V., Brelen, M.E., Delbeke, J., Colin, I.M., 2005. Anti-TNF- $\alpha$  reduces the inflammatory reaction associated with cuff electrode implantation around the sciatic nerve. *J. Neuroimmunol.* 165, 121–128. <https://doi.org/10.1016/j.jneuroim.2005.04.019>.
- VNS Therapy System Epilepsy Physician’s Manual (US), 2018.
- VNS Therapy, 2019. LivaNova. [WWW Document]URL <https://us.livanova.cyberonics.com/healthcare-professionals/>.
- Vuckovic, A., Tosato, M., Struijk, J.J., 2008. A comparative study of three techniques for diameter selective fiber activation in the vagal nerve: anodal block, depolarizing prepulses and slowly rising pulses. *J. Neural Eng.* 5, 275–286. <https://doi.org/10.1088/1741-2560/5/3/002>.
- Wadhwa, R., Lagenaur, C.F., Cui, X.T., 2006. Electrochemically controlled release of dexamethasone from conducting polymer polypyrrole coated electrode. *J. Control. Release* 110, 531–541. <https://doi.org/10.1016/j.jconrel.2005.10.027>.
- Wark, H.A.C., Sharma, R., Mathews, K.S., Fernandez, E., Yoo, J., Christensen, B., Tresco, P., Rieth, L., Solzbacher, F., Normann, R.A., Tathireddy, P., 2013. A new high-density (25 electrodes/mm<sup>2</sup>) penetrating microelectrode array for recording and stimulating sub-millimeter neuroanatomical structures. *J. Neural Eng.* 10, 045003. <https://doi.org/10.1088/1741-2560/10/4/045003>.
- Waters, R.L., McNeal, D., Perry, J., 1975. Experimental correction of footprint by electrical stimulation of the peroneal nerve. *J. Bone Joint Surg. Am.* 57, 1047–1054.
- Weber, D.J., Stein, R.B., Everaert, D.G., Prochazka, A., 2007. Limb-state feedback from ensembles of simultaneously recorded dorsal root ganglion neurons. *J. Neural Eng.* 4, S168–S180. <https://doi.org/10.1088/1741-2560/4/3/S04>.
- Weinberg, S.L., 1993. Helical Nerve Electrode. US5251634. .
- Wellman, S.M., Eles, J.R., Ludwig, K.A., Seymour, J.P., Michelson, N.J., McFadden, W.E., Vazquez, A.L., Kozai, T.D.Y., 2018. A materials roadmap to functional neural interface design. *Adv. Funct. Mater.* 28, 1701269. <https://doi.org/10.1002/adfm.201701269>.
- Wells, M., Goldstein, L., 2010. The polony phantom: a cost-effective aid for teaching emergency ultrasound procedures. *Int. J. Emerg. Med.* 3, 115. <https://doi.org/10.1007/s12245-009-0156-1>.
- Weremfo, A., Carter, P., Hibbert, D.B., Zhao, C., 2015. Investigating the interfacial properties of electrochemically roughened platinum electrodes for neural stimulation. *Langmuir* 31, 2593–2599. <https://doi.org/10.1021/la504876n>.
- White, R.L., Gross, T.J., 1974. An evaluation of the resistance to electrolysis of metals for use in biostimulation microprobes. *IEEE Trans. Biomed. Eng. BME-21*, 487–490. <https://doi.org/10.1109/TBME.1974.3243399>.
- Wieringa, P.A., Wiertz, R.W.F., de Weerd, E., Rutten, W.L.C., 2010a. Bifurcating microchannels as a scaffold to induce separation of regenerating neurites. *J. Neural Eng.* 7, 016001. <https://doi.org/10.1088/1741-2560/7/1/016001>.
- Wieringa, P.A., Wiertz, R.W.F., de Weerd, E.L., Rutten, W.L.C., 2010b. In vitro verification of a 3-D regenerative neural interface design: examination of neurite growth and electrical properties within a bifurcating microchannel structure. *Proc. IEEE* 98, 389–397. <https://doi.org/10.1109/JPROC.2009.2038950>.
- Wodlinger, B., Durand, D., 2010. Peripheral nerve signal recording and processing for artificial limb control. 2010 Annual International Conference of the IEEE Engineering in Medicine and Biology. Presented at the 2010 Annual International Conference of the IEEE Engineering in Medicine and Biology 6206–6209. <https://doi.org/10.1109/IEMBS.2010.5627735>.
- Wodlinger, B., Durand, D.M., 2009. Localization and recovery of peripheral neural sources with beamforming algorithms. *IEEE Trans. Neural Syst. Rehabil. Eng.* 17, 461–468. <https://doi.org/10.1109/TNSRE.2009.2034072>.
- Wodlinger, B., Dweiri, Y., Durand, D.M., 2015. Biochips. Implantable Biomedical Microsystems. Elsevier, pp. 203–214. <https://doi.org/10.1016/B978-0-323-26208-8.00009-1>.
- Woloszko, J., Cahalan, P.T., Hendriks, M., 1998. Biocompatible Medical Lead. US5741319. .
- Wright, J., Macefield, V.G., van Schaik, A., Tapson, J.C., 2016. A review of control strategies in closed-loop neuroprosthetic systems. *Front. Neurosci.* 10. <https://doi.org/10.3389/fnins.2016.00312>.
- Wurth, S., Capogrosso, S., Gandar, J., Federici, G., Kinany, N., Cutrone, A., Piersigilli, A., Pavlova, N., Guiet, R., Taverni, G., Rigosa, J., Shkrobatova, P., Navarro, X., Barraud, Q., Courtine, G., Micera, S., 2017. Long-term usability and bio-integration of polyimide-based intra-neural stimulating electrodes. *Biomaterials* 122, 114–129. <https://doi.org/10.1016/j.biomaterials.2017.01.014>.
- Xiang, Z., Yen, S.-C., Sheshadri, S., Wang, J., Lee, S., Liu, Y.-H., Liao, L.-D., Thakor, N.V., Lee, C., 2016. Progress of flexible electronics in neural interfacing - a self-adaptive non-invasive neural ribbon electrode for small nerves recording. *Adv. Mater.* 28, 4472–4479. <https://doi.org/10.1002/adma.201503423>.
- Yaghoubi, F., Shafer, B., Asgari, S., Vasudevan, S., 2018. An experimental model for assessing long-term safety and efficacy of vagus nerve stimulation, in: neuroscience meeting planner. In: Presented at the Society for Neuroscience. San Diego, CA. p. 589.21.
- Yim, S., Oh, Y.-E., Choi, W., Park, H., Jeong, J., Ihn, Y., Hwang, D., Oh, S.-R., Kim, J., Kim, K., 2018. Preliminary results of a handheld nerve electrode insertion device. In: 2018 IEEE International Conference on Robotics and Automation (ICRA). Presented at the 2018 IEEE International Conference on Robotics and Automation (ICRA). IEEE, Brisbane, QLD. pp. 1504–1510. <https://doi.org/10.1109/ICRA.2018.8460882>.
- Yizhar, O., Fenno, L.E., Davidson, T.J., Mogri, M., Deisseroth, K., 2011. Optogenetics in neural systems. *Neuron* 71, 9–34. <https://doi.org/10.1016/j.neuron.2011.06.004>.
- Yoshida, K., Farina, D., Akay, M., Jensen, W., 2010. Multichannel intraneural and intramuscular techniques for multiunit recording and use in active prostheses. *Proc. IEEE* 98, 432–449. <https://doi.org/10.1109/JPROC.2009.2038613>.
- Yoshida, K., Hennings, K., Kammer, S., 2006. Acute performance of the thin-film longitudinal intra-fascicular electrode. In: The First IEEE/RAS-EMBS International Conference on Biomedical Robotics and Biomechatronics, 2006. BioRob 2006. Presented at the The First IEEE/RAS-EMBS International Conference on Biomedical Robotics and Biomechatronics, 2006. BioRob 2006. IEEE, Pisa, Italy. pp. 296–300. <https://doi.org/10.1109/BIOROB.2006.1639102>.
- Yoshida, K., Pellinen, D., Pivin, D., Rousche, P., Kipke, D., 2000. Development of the thin-film longitudinal intra-fascicular electrode. In: Proceedings of the 5th Annual Conference of the International Functional Electrical Stimulation Society. Presented at the International Functional Electrical Stimulation Society. Denmark. pp. 4.
- Yu, H., Xiong, W., Zhang, H., Wang, W., Li, Z., 2014. A parylene self-locking cuff electrode for peripheral nerve stimulation and recording. *J. Microelectromech. Syst.* 23, 1025–1035. <https://doi.org/10.1109/JMEMS.2014.2333733>.
- Yuste, R. (Ed.), 2011. Imaging: a Laboratory Manual. Cold Spring Harbor Laboratory Press, Cold Spring Harbor, N.Y.
- Zabara, J., 1985. Peripheral control of hypersynchronous discharge in epilepsy. *Electroencephalogr. Clin. Neurophysiol.* 61, S162. [https://doi.org/10.1016/0013-4694\(85\)90626-1](https://doi.org/10.1016/0013-4694(85)90626-1).

- Zanos, T.P., 2019. Recording and decoding of vagal neural signals related to changes in physiological parameters and biomarkers of disease. *Cold Spring Harb. Perspect. Med.*, a034157. <https://doi.org/10.1101/cshperspect.a034157>.
- Zariffa, J., Nagai, M.K., Schuettler, M., Stieglitz, T., Daskalakis, Z.J., Popovic, M.R., 2011. Use of an experimentally derived leadfield in the peripheral nerve pathway discrimination problem. *IEEE Trans. Neural Syst. Rehabil. Eng.* 19, 147–156. <https://doi.org/10.1109/TNSRE.2010.2091429>.
- Zhong, Y., Bellamkonda, R.V., 2007. Dexamethasone-coated neural probes elicit attenuated inflammatory response and neuronal loss compared to uncoated neural probes. *Brain Res.* 1148, 15–27. <https://doi.org/10.1016/j.brainres.2007.02.024>.
- Zitnik, R.J., 2011. Treatment of chronic inflammatory diseases with implantable medical devices. *Ann. Rheum. Dis.* 70, i67–i70. <https://doi.org/10.1136/ard.2010.138677>.